Alma Mater Studiorum · Università di Bologna

DOTTORATO DI RICERCA IN GEOFISICA

Ciclo XXIV

GEO/10

KINEMATICS OF THE SICILY AND CALABRIA SUBDUCTION SYSTEM FROM ELASTIC BLOCK MODELING OF GPS DATA

Presentata da: Brunella Mastrolembo Ventura

Coordinatore dottorato:

Prof. Michele Dragoni

Relatore:

Prof. Paolo Baldi

Correlatore:

Dr. Enrico Serpelloni

Esame finale anno 2012

Acknowledgments

I would like to thank all the people who supported me during these last three years of my Phd. A big thanks to my tutor prof. Paolo Baldi and to my cotutor Dr. Enrico Serpelloni for teaching me most of what I know now about the research and geophysics. The second thanks is for the prof. Roland Burgmann and his research group for making my seven months at the University of California, Berkeley, wonderful with their availability and kindness. The last thanks is for the Istituto Nazionale di Geofisica e Vulcanologia that hosted me and for all friends I met there who brightened up every day of these years.

Contents

Introduction

The Mediterranean region originated from the interaction among Eurasian, African and Arabian plates. This region is seismically active, and is currently undergoing rather rapid deformation. Although the large-scale geodynamic regime is dominated by the 100 Myr long convergent motion between Africa and Eurasia, the regional-scale kinematics reveals a very complex pattern, where contrasting tectonic styles compressive, extensional, strike-slip regimes coexist in close association. Subduction occurs next to back-arc extensional basins in the Calabrian-Tyrrhenian and Hellenic-Aegean systems. Transcurrent motion along the Northern and Eastern Anatolian faults marks the escape of the Anatolian block towards the west. Seismicity is widespread in the region, although it is not restricted to narrow seismogenic boundaries, but is generally rather diffuse (e.g., *Serpelloni et al.*, 2007; *Pondrelli et al.*, 2004; *Vannucci et al.*, 2004). The understanding of the kinematics governing this complex region is further complicated by the slow velocities that characterize it. Infact, except the Anatolian-Aegean block, moving at a rate of a few cm/yr, the central Mediterranean is characterized by average velocities < 5 mm/yr.

The aim of this work is to constraint the rates and styles of contemporary crustal deformation and to study the kinematics of plates and microplates in the central Mediterranean area and, at smaller scale, elastic strain accumulation across active faults in the Sicily and Calabria regions.

The Sicily and Calabria regions (Southern Italy) are among the most seismically active areas of the Mediterranean basin (*Serpelloni et al.*, 2007). The highest seismic moment rates align along the Calabro-Peloritani arc, a tectonically complex segment of the central Mediterranean plate boundary zone, whose Neogene to Quaternary evolution is generally interpreted in terms of slow relative Africa-Eurasia plate convergence and fast subduction and roll-back of the Ionian lithosphere beneath the Calabrian Arc, accompanied by fast back-arc extension in the Tyrrhenian Sea (*Malinverno & Ryan*, 1986; *Faccenna et al.*, 2004; *Gvirtzman & Nur*, 2001).

Global Positioning System (GPS) velocities, according to a large spectrum of geophysical and geological data, support the view that the present-day kinematics and geodynamics of the area significantly differ from the ones that governed its tectonic evolution. In particular, the rates and orientation of the present-day Nubia-Eurasia convergence along the Ionian-Calabrian segment are largely debated, and this uncertainty negatively impact our still incomplete knowledge of the kinematics and seismic potential of active faults in the region.

The rapid increase of continuous GPS stations in the study area, together with new integration of GPS surveys performed from early '90 in Sicily and Calabria, is going to add new fundamental constraints to our comprehension of this complex region, both in terms of plate kinematics and elastic strain accumulation across active faults, responsible for some of the largest earthquakes of the Mediterranean area. However, the still limited number of GPS stations, with respect to the known

tectonic complexity of the study region and the relatively short interval spanned by our GPS observations require integration with all the other available data.

The first part of this thesis is dedicated to the overview of the kinematic, tectonic and geodinamic frame of the study area. In particular, in the first chapter, I brefly describe the steps of the central Meditarranean evolution and then, on the basis of available focal mechanisms and seismological, geological and tomographic data, I provide a picture of the present-day tectonics of the central Mediterranean with the aim to define the boundary conditions within which to make our small-scale analysis.

I also present (chapter 2) a dense GPS velocity field at the plate boundary scale, which is obtained by combining GPS surveys, performed during the 1993-2010 time interval, and continuous observations collected in the 1993-2011 time span at about 700 stations operating in the Eurasian-Nubian region. GPS velocities depict the Eurasian and Nubian plates as two tectonically stable domains charaterized by rigid block behavior while velocity gradients are found crossing the central Mediterranean region.

NE-Sicily is confirmed as the area displaying the largest velocity gradients, and the region accommodates a clear change in the regional kinematics. However, the way the observed velocity gradients are presently accommodated by faulting and the number of faults that may take up this deformation is presently unclear, but very important for the evaluation of the associated seismic hazard. We focus our attention on studying of two active structures, that are probably accumulating strain during the interseismic phase, the Messina Straits and the Crati Valley Faults. We explore this question by first examining very simple dislocation models that try to explain the local Messina Straits and Crati Basin velocities in the context of elastic deformation about single locked normal faults. Following the dislocation theory of *Okada*, (1985), we model the analyzed structures as rectangular uniform-slip dislocations embedded in an elastic, homogeneous and isotropic lithosphere and use a constrained, non-linear optimization algorithm (*Burgmann et al.*, 1997; *Arnadottir & Segall*, 1994), to solve for the best fit rectangular dislocation geometries.

Moreover, given the tectonic complexity of the study region, it is not clear at which level the measured velocity gradients across known active normal faults may be affected by additional elastic contributes due to unknown or offshore active faults. We explore this question by developing a regional elastic block model (*Meade & Hager*, 2005; *Meade & Loveless*, 2009), which accounts for both crustal block rotations and strain loading at block-bounding faults. The combined use of elastic dislocation and block model (described in detail in the chapter 3) has proved to be very effective for our purposes allowing us to frame the analyzed structures within the regional kinematics.

As said, geological and seismic data indicate a fragmentation of the central Mediterranean region in several microplates and GPS velocities suggest their independent motion from Eurasian and Nubian blocks. Many different hypotheses have been made in the previous works about the kinematic of microplates within the Africa-Eurasia collision zone (e.g., *D'Agostino et al., 2008*; *Calais et al.*, 2002;

Battaglia et al., 2004; *Oldow et al.*, 2002; *Serpelloni et al.*, 2007). However, because of the complexity of active deformation in the area and of the lack of any clear decoupling fracture marking the transition between the Adriatic-Nubia plates and of any interruption of lithological facies along the marginal belts (Apennines-Maghrebides and Dinarides-Hellenides) (*Mantovani et al.*, 1990), the issue is still debated and a general consensus has not yet been reached.

On the light of a new and bigger availability of GPS data we test some different kinematic hypothesis using the block model approach (chapter 5) as the proximity of some stations to the block boundaries needs to consider the effects of interseismic elastic strain accumulation (*Murray & Segall*, 2001). On the basis of focal mechanisms, and geological, seismological and GPS data we draw five different block models, making move independently, the Adriatic, Calabrian and Sicilian plates, and compare them by performing F-ratio tests (*Gordon et al.*, 1987) on the model χ^2_ν (chi square per degrees of freedom) while looking for the model that best fits the observed velocities.

In the last stage of this work (chapter 6), we further explore the geometry of the Calabrian Subduction interface within our preferred kinematic model. As fault locking depth and dip are strictly correlated in the generation of the upper crust deformation, we run suites of block model inversions by varying together dip and locking depth exploring ranges of geometries that minimize the misfit to the observed data. Before applying the described approach to the Calabrian Subduction zone we test it on some active structure lying on the Italian pensinsula: the Mattinata, Irpinia, Friuli and Southern Tyrrhenian Fault systems. Even if the χ^2_ν statistic has proved unable to provide precise informations about the optimal geometric parameters, however, at a first approximation, our results rather agree with the avaible information about the study structures. Almost no information is obtained by applying the same approach to the Slab interface probably due to the particular geography of the structure, extending offshore the eastern Calabrian coast and to the poor data coverage.

More constrains are needed and an important contribution to the Slab modeling could be given by the vertical GPS velocity field. Observed velocities show that uplift characterizes the whole Calabrian region with biggest rates along the eastern coast decreasing westward. Such a pattern is in agreement with the typical vertical velocity profile generated by a partially locked trhust fault plane (e.g., *Kanda & Simons*, 2010, *Savage*, 1983). We estimate the predicted vertical velocity field by performing forward model of elastic dislocations while varying the Slab interface locking depth from 10 to 40 km. We compare the inferred velocity fields with the observed one looking for the maximum resolved locking depth.

Chapter 1

Mediterranean Tectonic Setting

1.1 Introduction

The Mediterranean region marks the broad transition zone between the African-Arabian and Eurasian plates, and its current tectonic setting is the result of a complex evolution of the related collisional plate boundary system (*Faccenna et al.*, 2001). The central Mediterranean dispalys an assemblage of lithospheric blocks with different structural and kinematic features and a variety of geodynamic processes, including subduction, backarc spreading, rifting, thrusting, normal and strike-slip faulting, trapped between the relatively undeformable African and Eurasian plates, that are converging at about 6 mm/yr (fig. 1.6, A, *Serpelloni et al.*, 2007).

In the following sections, we first brefly describe the steps of the central Mediterranean evolution and then provide a more detailed description of tectonic regions whose kinematic analysis is of interest of this thesis. For a description of the Messina Straits and Crati Valley tectonic refer to chapter 4.

1.2 Geodynamic evolution of the Meditarranean region

The geodynamic evolution of the central Mediterranean during the past 10-20 Myr is dominated by the eastward migration of the Apennine-Calabrian subduction zone (the thick black line in fig. 1.2, A). This eastward motion does not correlate with the regional convergence between Africa and Europe, which is approximately N-S and 5-6 times slower (Fig. 1.2, B) (*Gvirtzman & Nur*, 2001). The presence of a back-arc-trench system also suggests that arc can be related to the retreat of subduction zone. *Malinverno & Ryan*, (1986) firts proposed that the Calabrian Arc (fig. 1.1) formed by trench retreat in correspondence of the narrow Ionian oceanic lithospere. According with their *arc migration model* descending slabs retreat laterally driven by sinking of the liyhosphere. When a retreating slab rolls back faster than the convergence rate, it pulls on the edge of the overriding plate, rifting it from the rest of the plate and eventually forming a backarc basin with a new oceanic floor.

Gvirtzman & Nur, (2001) use the arc migration model to interpret the central Mediterranean kinematic evolution. In this case, the eastward retreat of the Apennine-Calabrian subduction zone rifted the SW portion of Italy from Sardinia and Corsica and opened the Tyrrhenian Sea in between (fig.1.2, A). In the north, this motion stopped when the subducting oceanic lithosphere (blue in fig. 1.2, A) was consumed, and the SW portion of Italy collided with the Adriatic continental

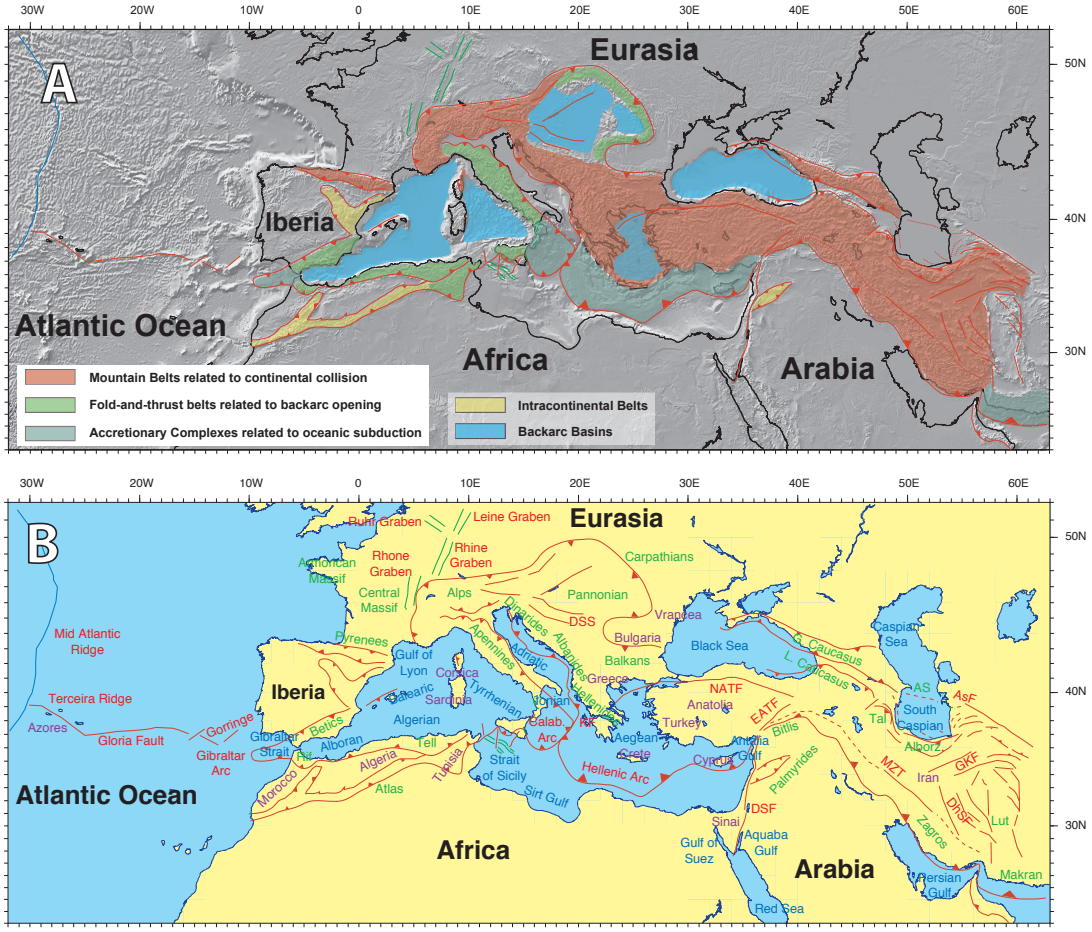

Figure 1.1: *(A) Schematic geological map of the Mediterranean region. The major tectonic structures of the Alpine orogen, thrust (with barbs) and strike-slip faults, are represented in red, whereas extensional faults are in green (topographic elevation, also used in the following figures, taken from ETOPO-2 global dataset). (B) Map of main toponyms and geological references. The structural map is the same as in fig. 1. NATF: North Anatolian Transform Fault; EATF: East Anatolian Transform Fault; G. and L. Caucasus: Greater and Lesser Caucasus, respectively; Tal: Talesh; AS: Apsheron Sill; MZT: Main Zagros Thrust; GKF: Great Kavir Fault; DhsF: Deh Sir Fault; DSF: Dead Sea Fault; AsF: Ashgabat Fault; KF: Kefallinia Fault. From* (Vannucci et al., 2004).

crust forming the Apennine Mountain belt. In the south, where oceanic lithosphere is still present today (the deep Ionian Basin) this process continues; the Ionian lithosphere subducts under Calabria, retreats southeastward, and extends the south Tyrrhenian Basin. A similar process also takes place on the other side of the Ionian Sea where the oceanic lithosphere subducts under Greece, retreats south-wards, and extends the Aegean Sea (fig 1.2, B).

Faccenna et al., (2004) note that, as the radius of curvature of western Mediter-

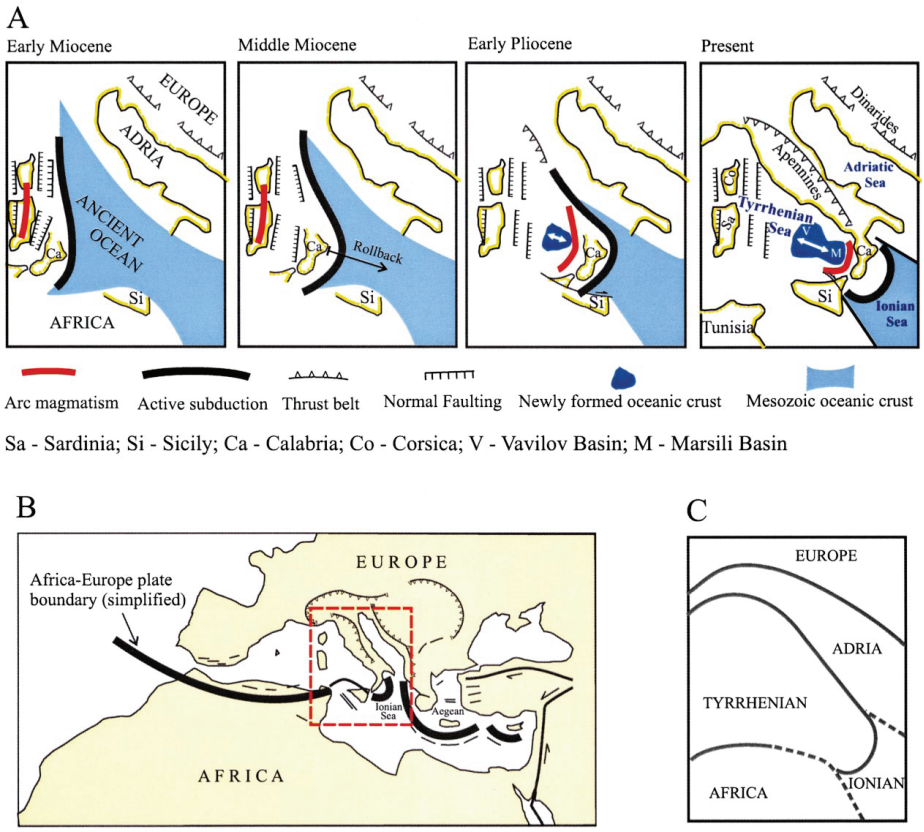

Figure 1.2: *(A) Schematic palinspastic reconstruction of the central Mediterranean since the Miocene. The eastward retreat of the Tyrrhenian-Apennines subduction system was associated with the closure of a Mesozoic basin and opening of the Tyrrhenian Sea. (B) Regional map showing the studied area (in red frame) within the Europe-Africa convergence zone. (C) Five plates and microplates in the studied area. From* (Gvirtzman & Nur, 2001).

ranean arcs is one order of magnitude smaller than other trench curvatures (10° on average), it is difficult to imagine that those structures can simply form as a consequence of slab bending. They use geological data, seismic tomography of the lithosphere-mantle and plate kinematics to formalize a geological consistent tectonic scenario at the scale of the upper mantle. From this reconstruction they conclude that the mechanism leading to the formation of the western Mediterranean arcs is similar, deriving from the fragmentation in narrow tongues of a single, wider subduction zone. They reconstruct the evolution of the western Mediterranean subduction zones (WMSZ) in four main steps from 35 Ma to present-day (fig 1.3).

Around 35 Ma, the WMSZ extended (NW dipping) for more than 1500 km from southern Iberia to the Ligurian region (figs. 1.1, B and 1.3, a). The trench terminated to the northeast in correspondence to the Ligurian region and to the southwest in correspondence with the Gibraltar region (fig. 1.3, a). At this time, the WMSZ was probably continuous and already well developed, reaching a depth of 300-

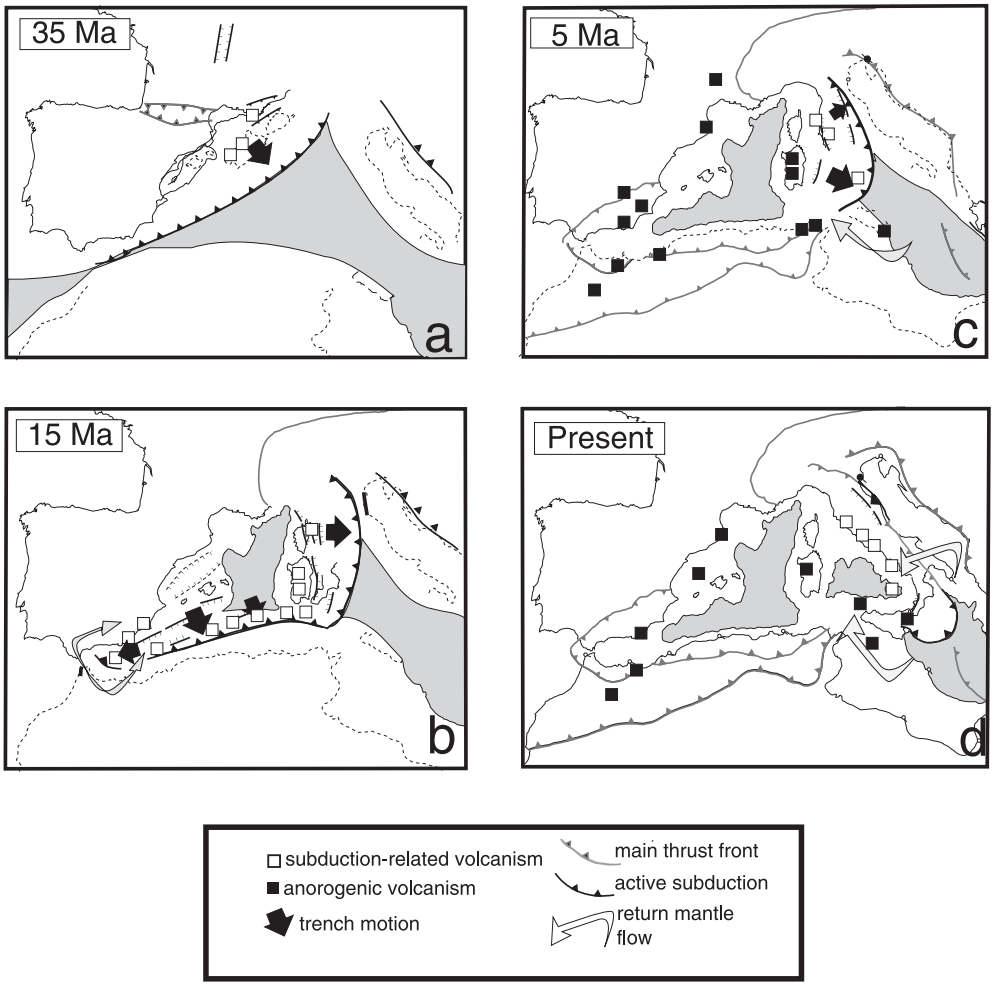

Figure 1.3: *Reconstruction of the evolution of the Mediterranean region in relative (Eurasia fixed) reference frame in four stages, from 35 Ma to present-day. Deep basin domains are marked in grey. The locations of the magmatic centers and their bearing with subduction process are marked with solid (anorogenic) and open (subduction-related) squares. From* (Faccenna et al., 2004).

400 km and dipping at rather shallow angle. The velocity of subduction decreased westward and this difference in subduction rate is attested to by the thermal gradient recorded by the metamorphic assemblages, which is lower in Calabria with respect to the Betics-Rif region.

At about 30 Ma, the back-arc extensional process started throughout the Mediterranean (*Jolivet & Faccenna*, 2000). It initiates in the northeastern sector, in the Liguro-Provencal area propagated southward to the Valencia and the Alboran basin. The velocity of subduction, mainly related to the slab retrograde motion, progressively increased, reaching its maximum in southern Sardinia (fig. 1.3, b), and produced the formation of a first smooth arc in front of the oceanic seaway.

Around 16-15 Ma (fig. 1.3, b), the retrograde migration of the western Mediterranean slab stopped. Back-arc extensional processes produced two triangular-shaped back-arc basins facing each other: the oceanic floored Liguro-Provencal basin and the smaller Valencia trough. Between 10 and 5 Ma (fig. 1.3, c), rifting migrated eastward within the Tyrrhenian domain and at present (fig. 1.3, d), the remnant of the once vigorous WMSZ is preserved only in the narrow tongue below Calabria and partly in the northern Apennine (*Selvaggi & Amato*, 1992)

1.3 Mediterranean seismological framework

In this region, seismicity is widely spread and rather frequent, as shown by fig. 1.4. Shallow earthquakes mark the boundaries of the main plates involved in this geodynamic arena (Africa, Eurasia, and Arabia) and also identify smaller regions with little or no deformation (e.g., Adriatic Sea, Ionian Sea, Central Tyrrhenian Sea and Balearic basin), surrounded by broad seismic belts, suggesting that there is more than just a three-plate game.

Events occurring at depths greater than 150 km mark those regions that are related to lithospheric subduction (fig. 1.4, B). In the southernmost part of the Tyrrhenian Sea a clear Wadati-Benioff zone can be recognized by the earthquakes distribution with depth, delineating the northwestward dipping Ionian slab, subducted beneath Calabria and the Tyrrhenian (*Chiarabba et al.*, 2005). The other clear deep seismicity in the Mediterranean is present south of the Kephallinia fault zone and delineates the northeastward gently dipping Hellenic subduction plane. Intermediate-depth seismicity (35-150 km) is present beneath the Gibraltar Arc and westernmost Alboran Sea.

Figure 1.5 shows the average moment tensors computed summing the earthquake moment tensors located within seismotectonically homogeneous boxes (*Vannucci et al.*, 2004). The resulting moment tensors give a synoptic view of the large-scale seismic deformation pattern. The extension that characterizes the Middle Atlantic Ridge passes to strike-slip towards Gibraltar, along the E-W plate boundary, and finally to compression where the convergent plate motion between Africa and Eurasia prevails. Extension is active along the Apennines and in the Aegean region, and coexists with adjacent compression that runs throughout the eastern coast of the Adriatic Sea up to the Hellenic Trench. The southern Tyrrhenian seismic belt displays a clear compressive tectonic regime, whereas eastern Sicily is characterized by strike-slip to extensional regimes. Further to the east, strike-slip deformation is dominant along the western and northern boundaries of the Arabian plate and in Anatolia. Compressional deformation again becomes predominant in the easternmost zones, extending from the Greater Caucasus to the Zagros.

Fig. 1.6, B shows the seismic flux, that is the seismic moment released per year and per unit area) computed on a regular $0.5^\circ \times 0.5^\circ$ grid, using all earthquakes with hypocentral depths < 35 km in the Mediterranean region. The map outlines some spatially continuous narrower regions (mainly displayed in yellow and orange, and

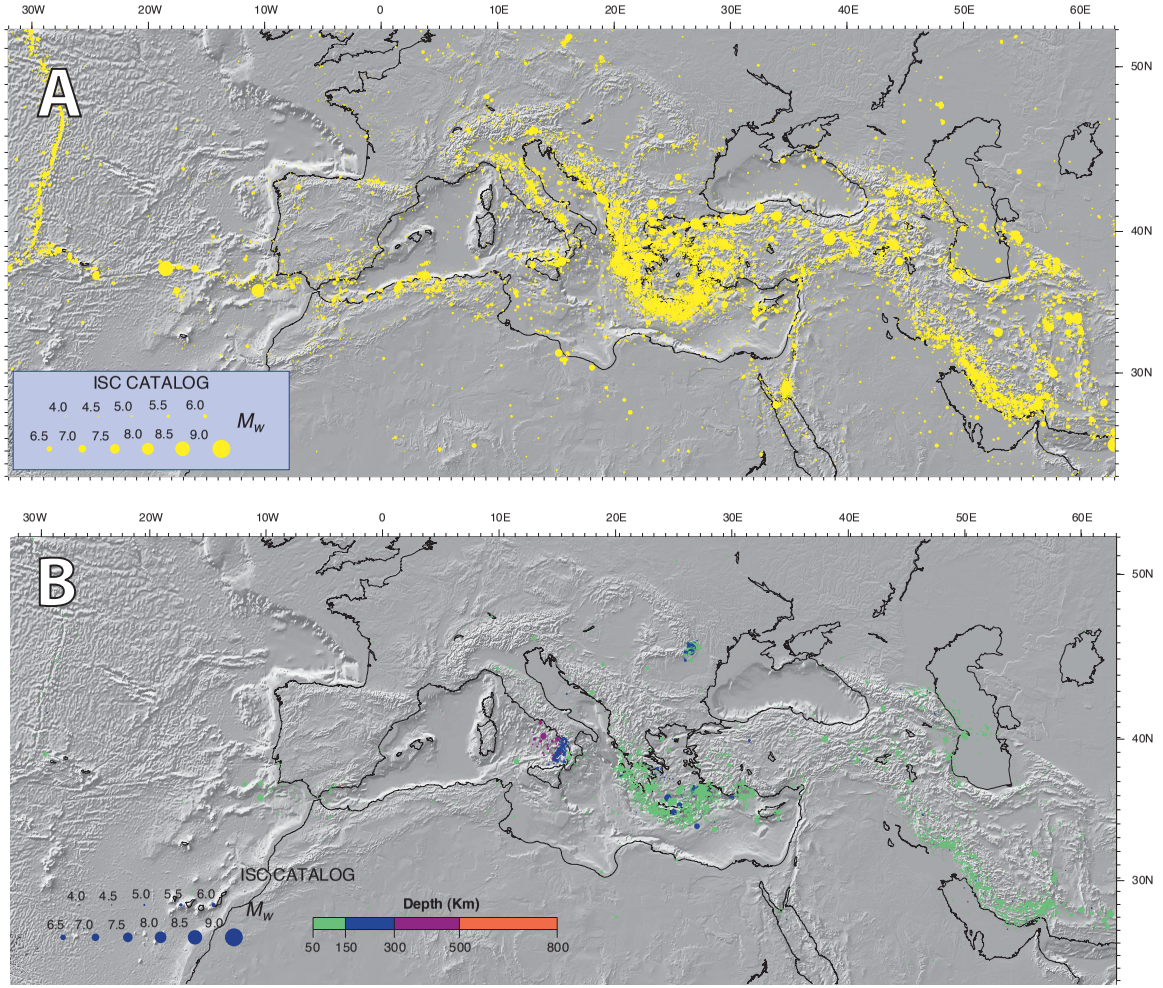

Figure 1.4: *(A) Instrumental seismicity of the Mediterranean region (from ISC Catalog) for depth interval 0-50 km. (B) Instrumental seismicity of the Mediterranean region (from ISC Catalog) for depth interval 50-800 km. From* (Vannucci et al., 2004)

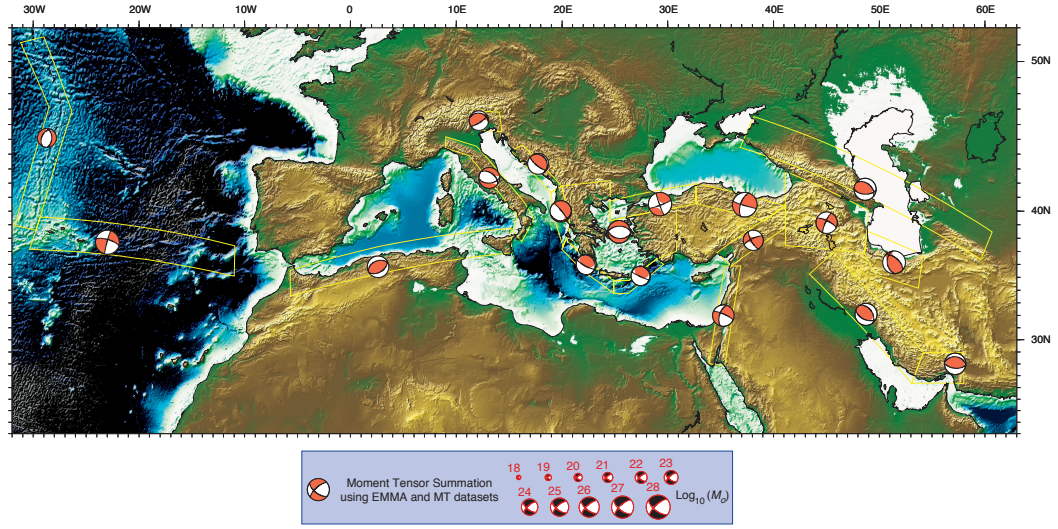

Figure 1.5: *Map of the Mediterranean region with boxes (in yellow) outlining the main deformation areas. The focal mechanism within each box represents the sum of moment tensors of earthquakes with depth < 50 km contained in the box. The focal mechanism plots are scaled with magnitude and located in the barycenter of the epicenters distribution weighted with magnitude. From* (Vannucci et al., 2004)

contoured) that provide a clearer picture of the seismically active segments of the Africa-Eurasia plate boundary. The roughly E-W trending seismic belts characterizing the main plate boundary zone (i.e. Terceira ridge, southwestern Iberia, northern Algeria and south- ern Tyrrhenian) appear to be interrupted by regions displaying a significantly lower seismic flux (e.g., the western segment of the Gloria Fault and the Strait of Sicily), or by differently oriented belts (e.g., the Rif-Alboran-Betics region and the Tunisia-Libya lineament).

The Western Mediterranean seismic flux distribution is complex, delineating a 'Z-shaped' seismic belt that includes the offshore southwestern Iberia, the Betics, the Alboran and the Rif-Tell belts (fig 1.6, B). Moving toward the Central Mediterranean, the seismic moment release is lower and the earthquake distribution is sparser (e.g., in the Tunisian shelf), or almost absent (e.g., in the Sardinia Channel and Strait of Sicily). A NW-SE oriented seismic belt runs from northern Tunisia to Libya, with the highest seismic flux values located west of the Sirt Gulf. In Sicily and Calabria, where moderate to large (Mw $>$ 5.5) magnitude events occur (up to the M = 7.0, 1908 Messina and the M = 7.3, 1905 Calabria earthquakes) the seismic flux shows larger values clustered along an E-W trending belt in northern Sicily and southern Tyrrhenian. Starting from Calabria, the orientation of the majorseismic belts changes, following the Apennines range along peninsular Italy and, on the eastern side of the Adriatic Sea, the NW-SE trending Dinaric-Albanides-Hellenides belts, where the largest seismic cluster of the Mediterranean is present. In the Cen-

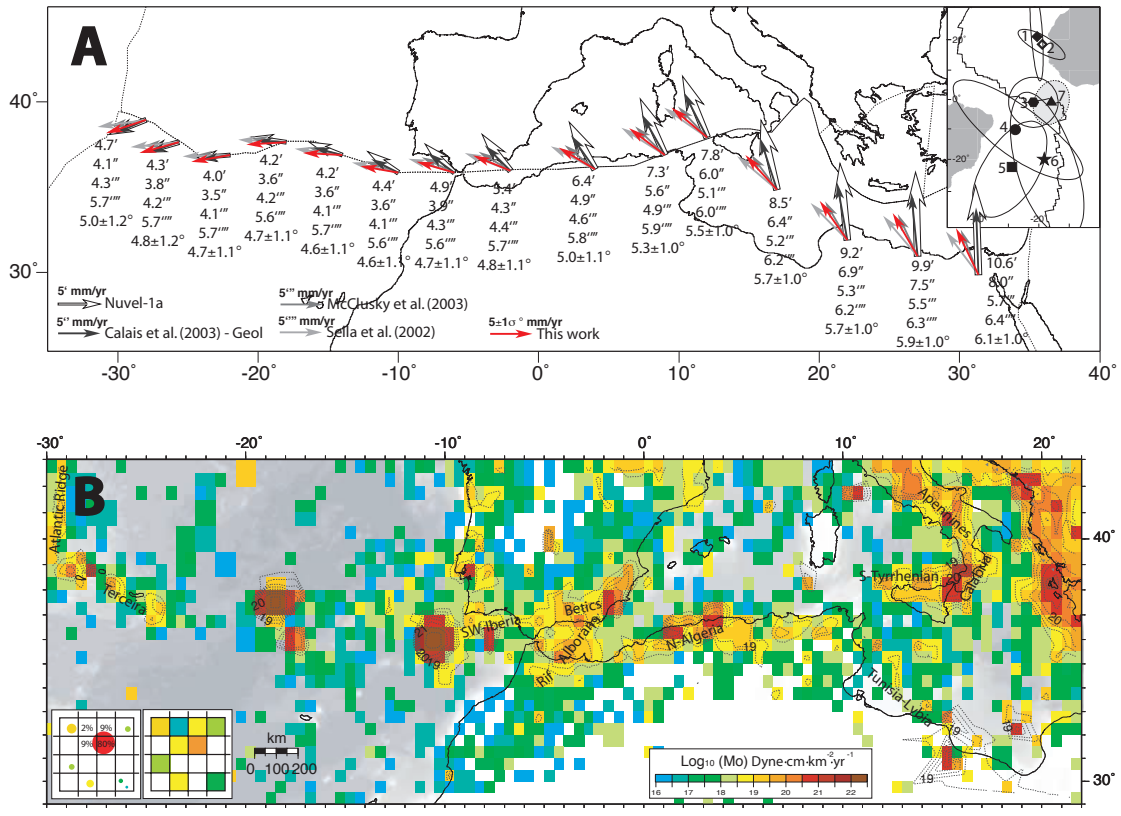

Figure 1.6: *(A): Africa-Eurasia kinematic boundary conditions predicted by geologically and some geodetically derived relative Euler poles, along as implified plate boundary (dashed line). (B): map of the seismic flux (i.e. the seismic moment released per year and per unit area) computed on a regular* $0.5° \times 0.5°$ *grid, using all earthquakes with hypocentral depths* < 35 *km. From* (Serpelloni et al., 2007).

tral Mediterranean, regions characterized by a significantly lower seismic moment release (i.e. the Ionian and southern Adriatic Seas) are surrounded by highly seismic belts (i.e. Apennines and Albanides-Hellenides). The external Calabrian wedge in the Ionian sea, in particular, is characterized by very low seismicity, although this offshore portion of the Calabrian subduction system may be deforming aseismically and, further to the North, locked or partially locked (*Gutscher et al.*, 2006).

1.4 Central Mediterranean tectonics

1.4.1 Sicily and surroundings

The Strait of Sicily, which interrupts the continuity of the Maghrebian fold-and-thrust belt between North Africa and Sicily, is characterised by a thinned crust (about 20 km) and by a system of NW-SE-trending extensional troughs originated

mainly during the Pliocene (*Argnani*, 1990). Seismicity is almost absent in the segment of fold-and-thrust belt that connects Tunisia to Sicily, and appears much reduced in the whole Strait of Sicily, when compared to the adjacent areas. Moderate magnitude seismicity is present in the Malta plateau and in the Sirt Gulf, on either side of the rifting (fig. 1.4). Focal mechanisms show consistently a strike-slip regime with P-axes that agree with Africa-Europe convergence (fig. 1.8; *DeMets et al.*, 1994; *Sella et al.*, 2002). This kind of foreland seismicity might avoid the rift zone because there heat flow is still high (*Argnani and Torelli*, 2001). The map of the seismic flux (fig. 1.6, B) confirms the presence of a NW-SE striking, rather diffuse, seismic belt, characterized by moderate to large events that display a clear kinematic coherence.

In the Southern Tyrrhenian Sea shallow seismicity is well clustered along an ∼E-W trending belt, running between longitude 11°E and 15°E (figs. 1.8 and 1.4), and displays seismotectonic features that are similar to those observed along the northern Algeria segment of the plate boundary. East of the central Aeolian islands (roughly corresponding to the Salina-Lipari-Vulcano lineament) shallow seismicity becomes almost absent and deep earthquakes (fig. 1.4) are present along an approximately continuous NE-SW striking and NW-ward dipping narrow Benioff plane, that can be followed down to about 600 km (*Wortel & Spakman*, 2000; *Piromallo & Morelli*, 2003; *Chiarabba et al.*, 2005).

Focal solutions of shallow earthquakes offshore northern Sicily are highly consistent, and outline a narrow compressive belt (fig. 1.8), with P-axes oriented from N-S to N20°W, in agreement with the motion of Sicily with respect to Eurasia, which differs from the motion of the Nubian plate (*Serpelloni et al.*, 2007). East of Alicudi, thrust mechanisms do not prevail (fig. 1.8), while extensional to strike-slip mechanisms occur along a nearly NNW-SSE alignment, which connects the central Aeolian Islands to Mount Etna, and continues toward the south along the eastern Sicily escarpment. The seismotectonic setting of this area is characterized by a transtensional to strike-slip regime, with T-axes E-W to N60°E oriented (*Serpelloni et al.*, 2007).

1.4.2 Calabrian Arc

The Calabrian Arc (fig. 1.1) is part of the eastward migrating Apennine subduction system and connects the NW trending Apennine with the E-W oriented Maghrebian thrust belt (*Patacca & Scandone*, 2004).

The Neogene and Quaternary evolution of the Calabrian Arc is controlled by the southeastward retreat of the Apennine-Calabrian subduction zone, that caused rifting and lithospheric thinning culminating in the opening of the Tyrrhenian Sea starting from the upper Miocene (*Malinverno and Ryan*, 1986; *Faccenna et al.*, 2001). Trench retreat was particularly fast over the Neogene and early Quaternary as indicated by rapid migration of the trench (*Faccenna et al.*, 2001). The episodic retreat of the subduction zone was accompanied by its progressive fragmentation (*Faccenna et al.*, 2005). The relict of this once large subduction zone is presently

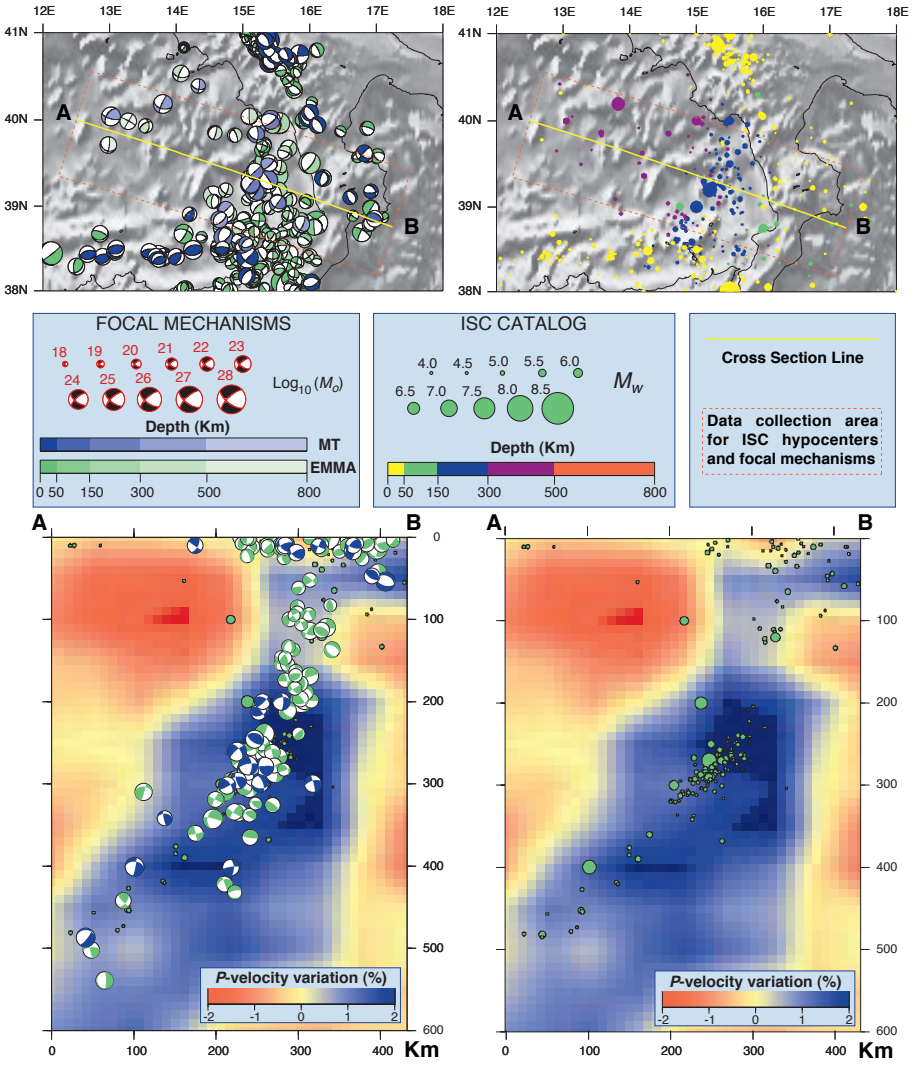

Figure 1.7: *Cross section of the Calabrian Arc: depth distribution of instrumental seismicity (from ISC Catalog) and focal mechanisms from EMMA database (green) and MT catalogs (blue). From* (Vannucci et al., 2004).

limited to an extremely narrow (< 200 km), deep (> 400 km) and steep (70°) NW dipping Wadati-Benioff zone (*Selvaggi & Chiarabba*, 1995).

Tomographic images illuminate the prosecution of this once continuous structure at depth toward both the Apennine and the Maghrebide chains (*Wortel & Spakman*, 2000; *Piromallo & Morelli*, 2003; *Faccenna et al.*, 2004). These tomographic images also show no direct linkage between the Calabrian and southern Apennine slabs (*Chiarabba et al.,* 2008) where the high-velocity anomaly is limited to a depth of 200 km (*Wortel & Spakman*, 2000). The present-day Wadati-Benioff zone lines up

with the deeper (> 4 km) portion of the Ionian abyssal plain, laterally bounded to the northeast and west by the Apulian and Hyblean platforms, respectively. The tomographic cross section in fig. 1.7 shows an almost continuous high-velocity body below Calabria, with a dip of $70° - 80°$ toward the NW and then turning horizontally in the transition zone. The estimated total length of the fast velocity zone, interpreted as subducted lithosphere, is about 1200-1400 km, measured from the base of the lithosphere and including its lowermost flat portion (*Faccenna et al.*, 2004). Focal mechanisms of deep events show mostly a down dip geometry (fig. 1.7).

Cifelli et al., (2007) speculate that slab retreat could be not sufficient alone to form tight arcs like those that characterize the Mediterranean region, and suggest that a progressive decrease in the width of the active trench should also be considered as an active mechanism to explain the timing and distribution of crustal rotations in the Calabrian Arc and its huge curvature. On the other hand, vertical axis rotations occurred during Miocene to Quaternary but were almost finished 1 Ma (*Mattei et al.*, 2007) as confirmed by GPS results showing no active back-arc extension in the Southern Tyrrhenian Sea (*D'Agostino et al.*, 2008).

The onshore Calabrian Arc has been affected by major uplift in the last 0.8 Ma, with rates close to 2.0 mm/yr (*Westaway*, 1993; *Bordoni & Valensise*, 1998). *Gvirtzman & Nur*, (2001), based on the unusually high elevation of Calabria, argue that the Tyrrhenian lithosphere is not pulled down by any force. To their opinion, Calabria is rebounding simply because it was released from the Ionian because the mantle flow is balancing the low pressure generated by slab motion.

The external part of the arc is represented by a subduction complex that reaches both the Ionian abyssal plain and the Mediterranean Ridge and is bordered by two major structural features, the Malta escarpment to the southwest and the Apulia escarpment to the northeast. The Calabrian Arc accretionary wedge developed due to the SE-NW Africa/Eurasia convergence, presently occurring at a very slow rate (5 mm/yr or even < 5 mm/yr), as reported by recent GPS studies (*Serpelloni et al.*, 2007; *D'Agostino et al.*, 2008; *Devoti et al.*, 2008). On the other hand, geodetic investigations of crustal motion in the central Mediterranean have shown significant deviations from the direction of relative motion between the Eurasia and Africa plates. It is evident that the dominance of compression driven by the Africa-Europe convergence, previously seen along North Africa and Sicily, no longer holds in Calabria. This discrepancy with major plate motion can be observed throughout the Apennines. It is only in the Eastern Alps that earthquake focal mechanisms start tracking major plate motion again.

Despite the very slow present-day plate convergence rates observed by GPS, subduction may still be active in the Calabrian Arc, and subduction rate will depend both on the convergence rate and the velocity of the subduction hinge (*Doglioni et al.*, 2006, 2007). GPS sites in Calabria (relative to Apulia) show systematic residuals directed toward the Ionian Sea, suggesting active crustal compression and an outward motion of the Calabrian Arc as a result of still active subduction that accounts for the shortening taken up in the accretionary wedge, eventually accommodated by

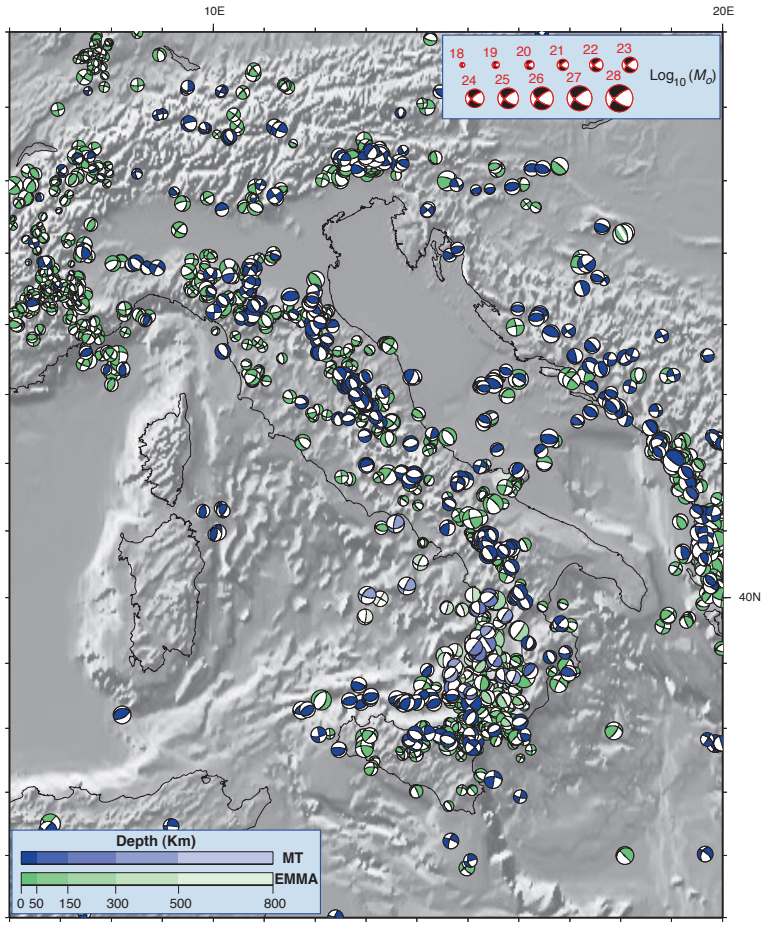

Figure 1.8: *Central Mediterranean. Focal mechanisms of earthquakes from MT catalogs (blue) and EMMA data-base (green). From* (Vannucci et al., 2004).

long-term slip on the subduction interface (*D'Agostino et al.*, 2008).

The lack of instrumentally recorded thrust earthquakes supports the hypotesis of a locked subduction fault plane. *Gutscher et al.*, (2006) investigate the source of the 1693 Catania earthquake (eastern Sicily) supposing that it occurred on the subduction fault plane. They use GPS and high-resolution seismic data and thermal modeling to calculate the limits of the seismogenic zone obtaining a locked fault plane with dimensions of 160×120 km. Tsunami modeling of the inferred subduction plane successfully reproduces the available historical observations confirming the goodness of the model.

The submerged portion of the Calabrian Arc consists of a northwestward thickening wedge of deformed sediments (*Cernobori et al.*, 1996; *Minelli & Faccenna*, 2010) overlying, in the most external portion, northwestward dipping sediments and the basement. This is structurally consistent with the presence of a SE-verging accretionary wedge.

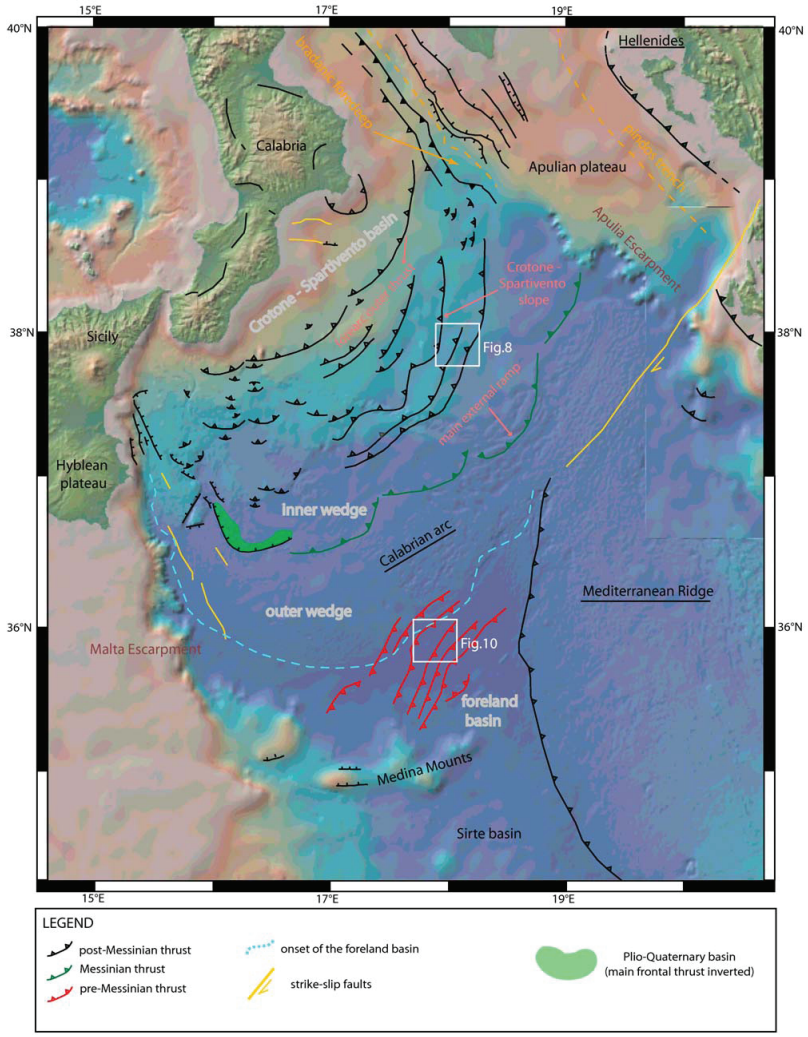

Figure 1.9: *Structural map of the Ionian offshore and of the Calabrian accretionary prism. Main thrust systems (fore-arc outer thrust, Crotone-Spartivento slope, main external ramp) bounding the four structural domains (Crotone-Spartivento fore-arc basin, inner accretionary wedge, outer accretionary wedge, and foreland basin) are labeled. From* (Minelli & Faccenna, 2010).

Following *Rossi & Sartori*, (1981), the wedge can be divided in four main tectonic domains, marked by different stratigraphies and styles and ages of deformation (fig. 1.9 and 1.10). 1. The Crotone-Spartivento basin is a subsiding, relatively undeformed, basin filled by Plio-Quaternary sediments. The basin deposits lie on top of either the crystalline basement or the inner accretionary wedge. The southern boundary of the basin is represented by the forearc outer thrust. 2. The inner accretionary wedge represents the inner portion of the wedge, composed of pre-Messinian sediments, accreted mainly during pre-Messinian time. It is separated from the

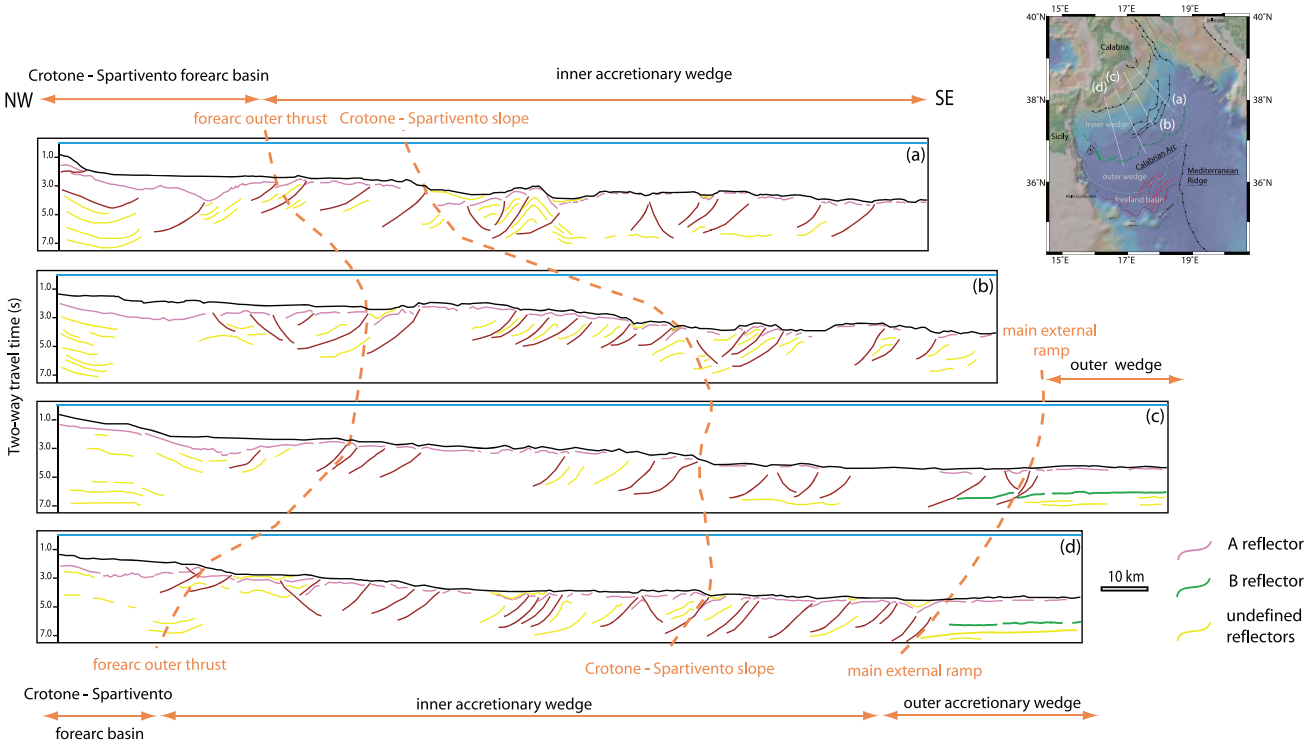

Figure 1.10: *View of four line drawings of the Calabrian accretionary wedge running NW-SE. Vertical scale in TWT (s). The main tectonic elements are indicated. Note a post-Messinian reactivation of internal thrusts and the Plio-Quaternary subsidence in the Crotone-Spartivento fore-arc basin. From* (Minelli & Faccenna, 2010).

outer accretionary wedge by the main external ramp. A major tectonic feature, the "Crotone-Spartivento slope" divides the inner wedge into two portions characterized by different topographic slopes. 3. The outer accretionary wedge represents the frontal part of the wedge, composed of deformed Messinian to Quaternary deposits. 4. Foreland basin represents the foreland basin of both the Calabrian Arc and the Mediterranean Ridge. The foreland basin shows compressive pre-Messinian structures.

Chapter 2

GPS data analysis

2.1 Data processing

Data from almost 800 continuous (CGPS) and epoch (EGPS) GPS stations operating in the EuroMediterranean and African regions from Jenuary 1994 to April 2011 are used in this thesis (figs. 2.2 and 2.3), about 700 of wich are processed at the Istituto Nazionale di Geofisica e Vulcanologia (INGV), Bologna office and then combined with over 100 published solutions from the Aegean region.

Final GPS station velocities are the result of a three-step approach, which includes: 1) the phase data processing, 2) the combination of solutions and 3) the time series analysis. In the first step, station coordinates are estimated using daily GPS phase observations, hourly atmospheric zenith delay, orbital and Earth orientation parameters by means of the GAMIT 10.33 software (*Herring et al.*, 2006), applying loose constraints to geodetic parameters and adopting standard procedures for the analysis of regional networks (e.g., *Serpelloni et al.*, 2006). Then applying the ocean-loading model FES2004 and using the IGS (International GNSS Service) absolute antenna phase center models for both satellites and ground-based antennas.

GPS data are divided into about 30 sub-networks, CGPS and EGPS sub-networks are processed independently, following the same procedures. A number of high quality CGPS sites are included in all solutions, and are used to tie together the daily loosely constrained solutions in the second step of our analysis. The common CGPS sites are chosen among the stations showing the highest data continuity through time, in order to ensure that a minimum number (always N>3) of sites are in common to all sub-network solutions.

In the second step all the daily loosely constrained solutions, for both CGPS and EGPS sub-networks, are combined with the global and regional solutions made available by SOPAC (http:// sopac.ucsd.edu), using the ST_FILTER program of the QOCA software (*Dong et al.*, 2002) to combine and simultaneously realize a global reference frame by applying generalized constraints (*Dong et al.*, 1998). Specifically, the reference frame is defined by minimizing the horizontal velocities of the 132 IGS-core stations (http://igscb.jpl.nasa.gov), while estimating a seven-parameter transformation with respect to the IGS05 realization of the ITRF2005 NNR frame (*Altamimi et al.*, 2007). In order to account for offsets observed in the time series of some IGS-core sites (due to earthquakes or changes in the receiver/antenna configuration that could contaminate the combined solution), they estimate the offset parameters of the IGS-core sites in a preliminary ST_FILTER run of the IGS daily solutions only, and then use the estimated values to correct the reference frame

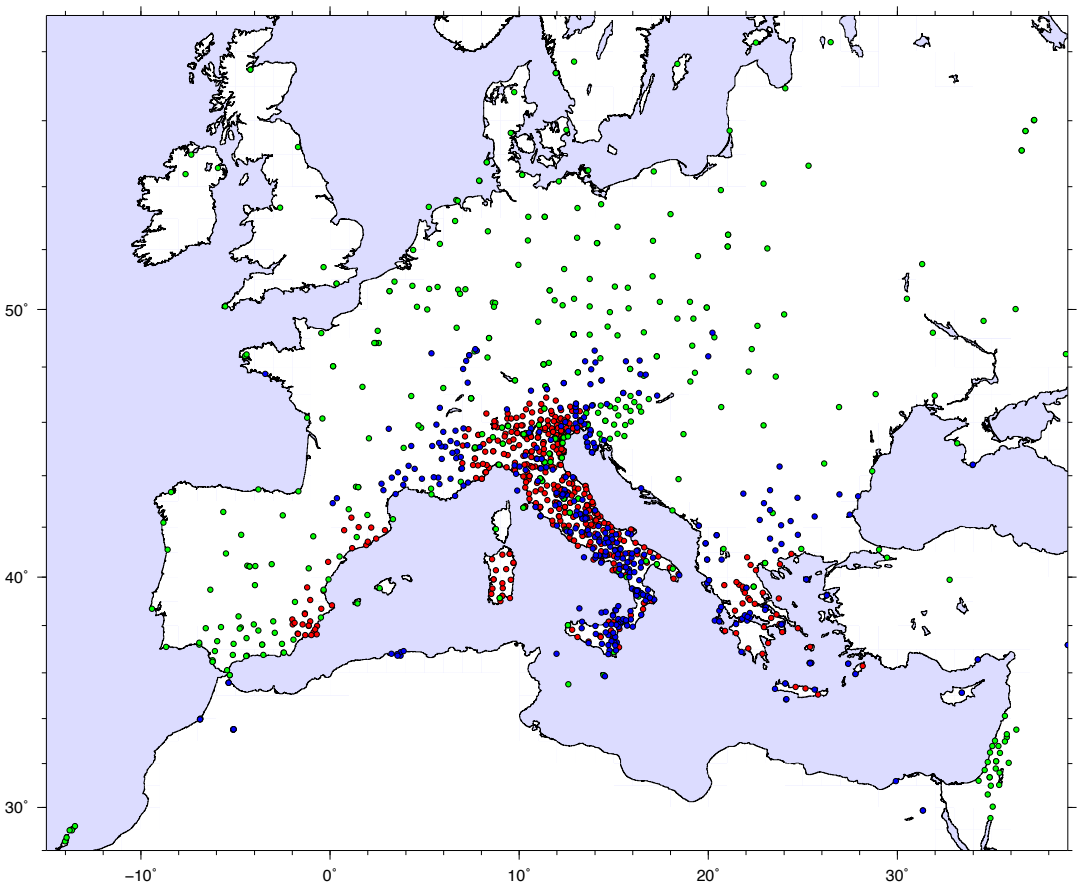

Figure 2.1: *GPS stations in the EuroMediterranean region clustered by type. Blue: geophysical stations, red: topographic stations and green: geodetic stations.*

jumps in the final combination and reference frame realization. Reference frame stability through time is ensured by the presence of at least 40 IGS-core sites that are continuously present in SOPAC solutions from 1994 to present-days.

In the third step the position time series are analyzed in order to estimate absolute IGS05 velocities and uncertainties for both CGPS and EGPS stations. In particular, for the CGPS stations they estimate a constant velocity term together with annual and semi-annual seasonal terms and, if present, offsets at specific epochs. For the EGPS stations only the constant velocity term is estimated. Realistic velocity uncertainties are evaluated adopting a white-plus-colored noise model following the maximum likelihood estimation approach implemented in the CATS software (*Williams et al.*, 2004), and the procedures described in *Williams*, (2003). In particular, for CGPS stations they adopt a white + flicker noise model, whereas for EGPS stations they adopt an error model that combines white + random walk noise using a value of 1 mm/yr$^{0.5}$ for the random walk component (*Langbein & Johnson*,

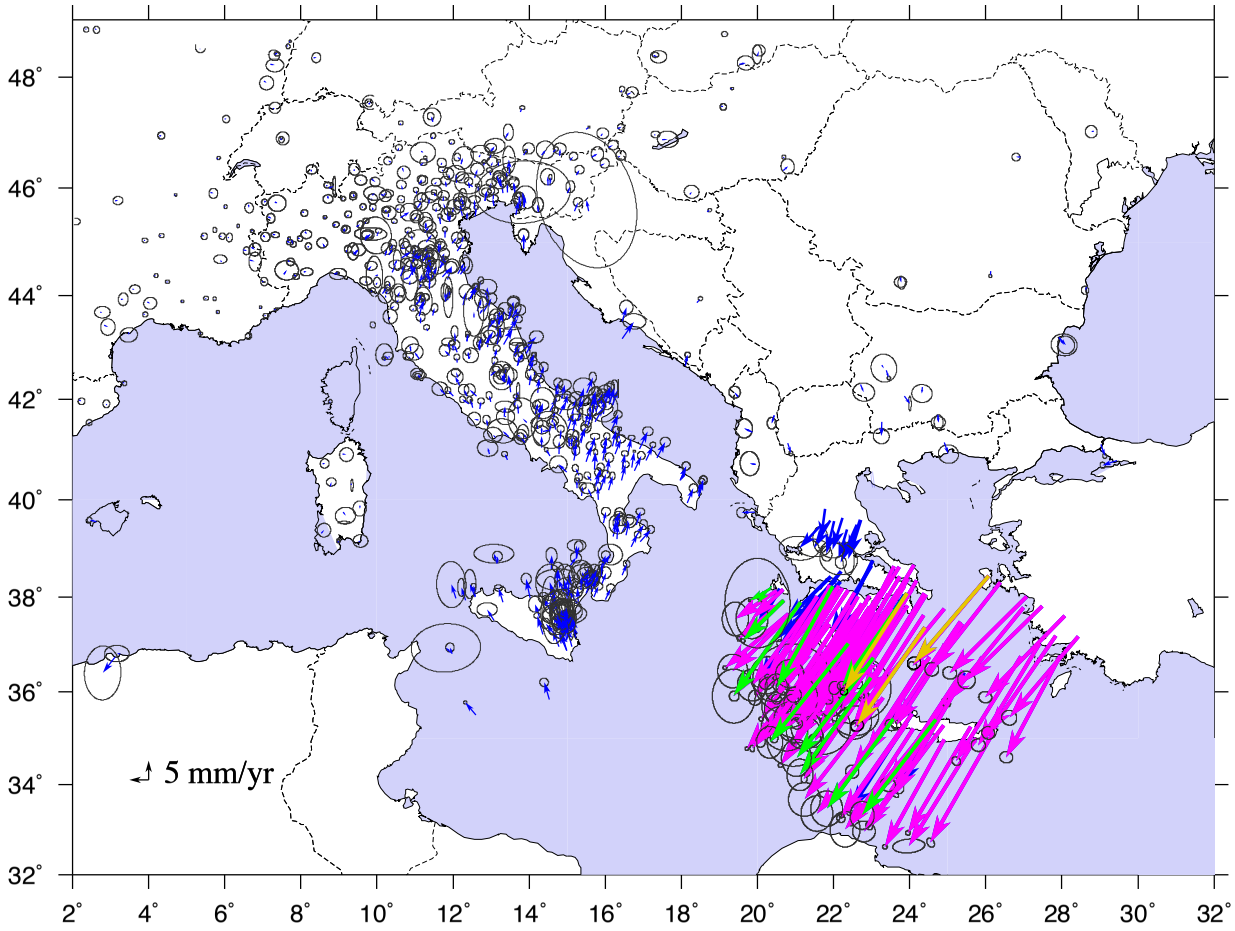

Figure 2.2: *Eurasia fixed horizontal GPS velocity vectors and 95% confidence error ellipses. Blue arrows represent some of the 700 GPS station velocities processed at the INGV lying in the center Mediterranean. Colored arrows are the aligned published velocities. Magenta:* Floyd et al., (2010), *green:* Hollenstein et al., (2008), *dark yellow:* Reilinger et al., (2006).

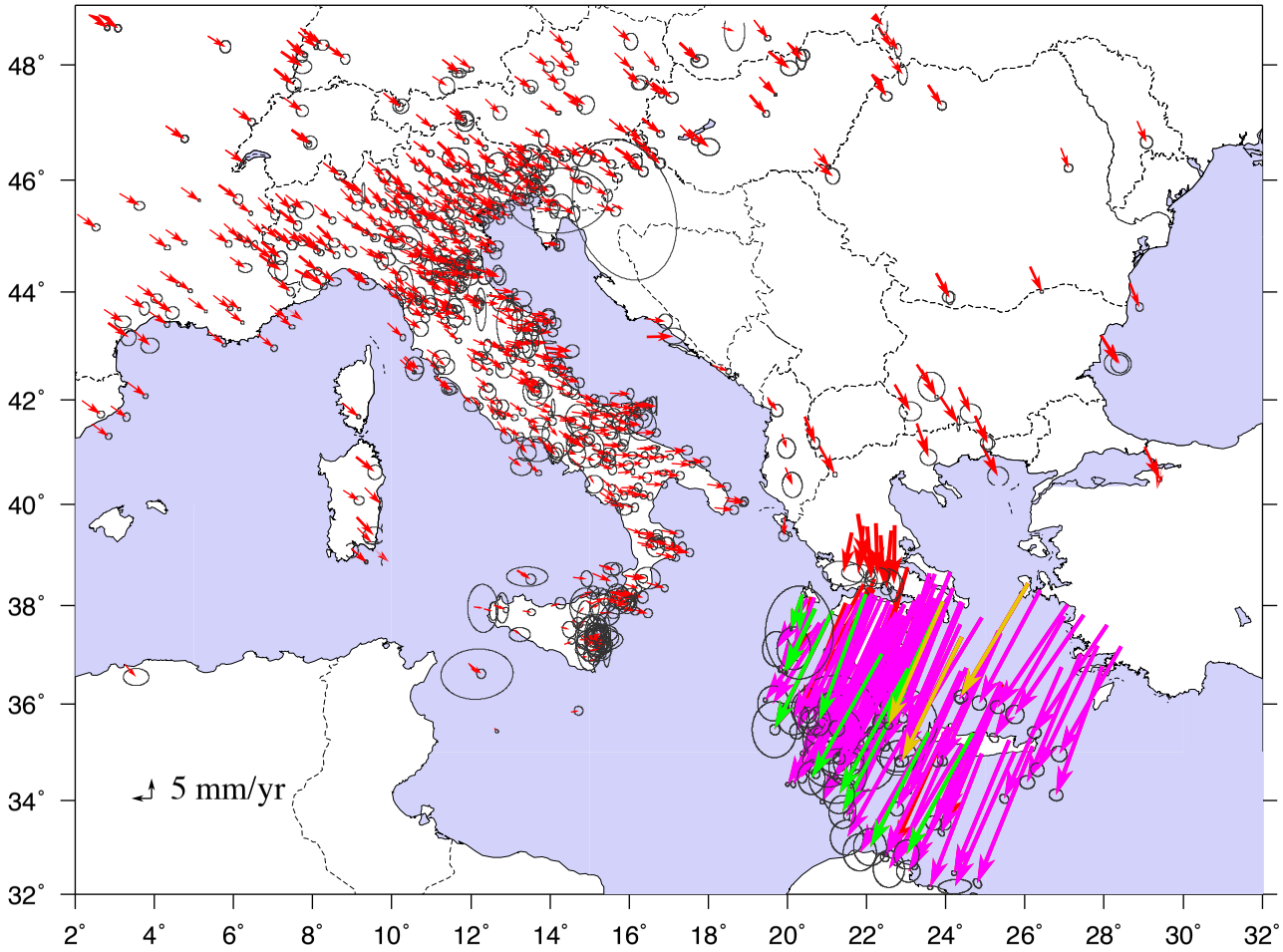

Figure 2.3: *Nubia fixed horizontal GPS velocity vectors and 95% confidence error ellipses. Blue arrows represent some of the 700 GPS station velocities processed at the INGV lying in the center Mediterranean. Colored arrows are the aligned published velocities. Magenta:* Floyd et al., (2010), *green:* Hollenstein et al., (2008), *dark yellow:* Reilinger et al., (2006).

Figure 2.4: *Map of the Eurasian (black squares) and Nubian (grey squares) continuous GPS site locations used to define the respective reference frames and location of estimated Nubia-Eurasia pole of rotation (black star with grey* 95% *confidence error ellipse). Also shown are the earthquake epicenters (from the Harvard CMT catalog). The poles of rotation from Nuvel-1* (DeMets et al.), 1994)*, NUV1A, and previous GPS studies are shown with their* 95% *confidence ellipses. GDVEL10:* DeMets et al., (2010)*; DAG08:* D'Agostino et al., (2008)*; SER07:* Serpelloni et al., (2007)*; CA03GPS:* Calais et al., (2003)*; MC03:* McClusky et al., (2003)*; REV02:* Sella et al., (2002)*. From* (Serpelloni et al., 2010)*.*

1997; *Dixon et al.*, 2000) (see next paragraph for a more detailed explanation).

Velocities and uncertainties of CGPS stations located on tectonically stable domains of the Eurasian and Nubian plates are used in order to estimate their Euler rotation vectors with respect to the IGS05 frame. Fig. 2.4 shows the location of the estimated Nubia-Eurasia pole with respect to previously published values.

In addition to the about 700 GPS velocities analyzed at the INGV we integrate over 100 GPS-station velocities from published work in the Aegean region (*Hollenstein et al.*, 2008; *Reilinger et al.*, 2006, *Floyd et al.*, 2010). In order to align the published velocities to the original solution, a seven-parameter Helmert transformation is performed to minimize the root-mean-square (RMS) differences between the velocities of common stations to the networks.

For collocated sites with velocities from multiple sources we used a single velocity

for the site based on the following priorities: 1) GPS velocity was derived from the time series with the most observations, typically the most recent publication. 2) GPS velocity with the smallest formal uncertainties. All velocities from the combined solution are plotted and colored by source in figure 2.2. All GPS velocities from the above-mentioned references were incorporated in our combined velocity solution, however some stations were excluded prior to the block model inversion. Sites were excluded for one of three reasons: We exclude 1) sites outside our area of interest and 2) redundant velocity estimates for collocated sites with a preferred velocity (see above).

2.2 Error analysis of GPS position time series

2.2.1 Noise modeling

GPS time series are affected by noise coming from different sources. Several geodetic data sets have provided evidence for error sources that introduce large temporal correlations into the data. One common statistical model for many types of geophysical signal (which may contribute to the noise) may be described as a power-law process. The one-dimensional time- or space-domain behaviour of this stochastic process is such that its power spectrum has the form (*Williams*, 2003,a):

$$P_x(f) = P_0\Big(\frac{f}{f_0}\Big)^k \tag{2.1}$$

where f è is the spatial or temporal frequency, P_0 and f_0 are normalising constants, and k is the spectral index.

Geophysical phenomena and noise with fractional spectral indices in the range $[-3, 1]$ are termed *fractal random walk* while indices in the range $[-1, 1]$ are termed *fractal withe noise*. Noise processes with $-1 < k < 1$ are stationary, while processes with k larger than 1 are non-stationary, that is its statistical properties (eg. mean and variance) are not invariant in time (*Mao et al.*, 1999). For $k = 0$ we have classic *withe noise* (WN), for $k = -2$ we have *classic brownian noise* (or *random walk noise*, RWN) and for $k = -1$ *flicker noise* (FN). The latter charaterize a wide variety of dynamical processes as the earth oscillation around its own axis. All processes with $k \neq 0$ are called *colored noise*(CN) and are correlated in time and space (*Mao et al.*, 1999).

It is important to understand the noise content of GPS position data so that realistic uncertainties can be assigned to parameters estimated from them. The assumption that the noise is purely white leads, for example, to grossly under-estimated site rate uncertainties. *Zhang et al.*, (1997) concluded that rate uncertainties were 3-6 times greater when the preferred white plus flicker noise model was used instead of the white noise only model. Likewise, *Mao et al.*, (1999) concluded that their rate uncertainties were underestimated by as much as an order or magnitude if they neglected the correlated noise. The estimate of the standard error in rate is dependent upon several parameters of power law noise including the amplitude,

spectral index, and sampling interval (*Williams*, 2003a). It is clear that the assumed noise type greatly affects the resulting rate uncertainty, and so an important part of deriving crustal motion models from GPS data is to classify and quantify the noise components.

Previous works focused their analysis on two noise models WN+FN and WN+RWN and, using maximum likelihood estimation (MLE) with integer spectral indices, most of them found that the noise in the data was best described as a combination of white noise and flicker noise (*Mao et al.*, 1999; *Zhang et al.*, 1997; *Williams et al.*, 2004).

Several studies also acknowledge the importance of random walk noise in GPS data. This noise is correlated with the geodetic monuments instability due to disturbances from the soils and weather that displace geodetic monuments with respect to the deeper crust and can be as high as 3 $mm/yr^{1/2}$. Whether or not the random walk noise is detectable depends on the length of the time series, the sampling frequency, and the relative amplitudes of the other noise components. It is clear that this kind of noise particulary affects time series from EGPS stations. For this reason, EGPS velocity uncertainties are evaluated adopting an error model that combines white + random walk noise.

2.2.2 Velocities uncertainties estimation

Velocity uncertainties are evaluated using the approach described in *Mao et al.*, (1999). Following this approach, uncertainties for each velocity component (north, east, up) are estimated as sum of the contributions of individual noise sources according to:

$$\sigma_r^2 = \Big(\frac{12\sigma_w^2}{gT^3} + \frac{a\sigma_f^2}{g^bT^2} + \frac{\sigma_{rw}^2}{T}\Big) \tag{2.2}$$

where g is the number of measurements per year, T is the total time span, σ_w and σ_f are the magnitudes of white and flicker noise in mm, σ_{rw} is thewalk noise in mm/yr$^{-1/2}$ and a and b are empirical constants.

The standard error of a rate σ_r can be expressed, for pure withe noise as:

$$(\sigma_r)_w^2 = \frac{12\sigma_w^2}{NT^2} = \frac{12\sigma_w^2}{f_sT^3} \qquad N >> 1 \tag{2.3}$$

and for random walk noise as:

$$(\sigma_r)_{rw}^2 = \frac{\sigma_{rw}^2}{T} \qquad N >> 1 \tag{2.4}$$

where f_s is the sampling frequency and σ_w and σ_{rw} are the standard deviations of white and random walk noise. There is no exact analytical expression for flicker noise.

2.3 GPS velocity field

GPS data in the Mediterranean area depict the presence of some clear different velocity domains. Looking at the velocity fields in figs. 2.2 and 2.3 we can observe that, while velocities of a few mm/yr, rotating from NNW-ward to NNE-ward, charaterize the Italian Pensinsula and surroundings, the Aegean region is moving significantly faster, at a rate of a few centimeters per year, due to the west-ward extrusion of the Anatolia-Aegean block. GPS velocities depict the Eurasian and Nubian plates as two tectonically stable domains charaterized by rigid block behavior while velocity gradients are found crossing the central Mediterranean region. The Corsica-Sardinia block is not moving w.r.t. Eurasia, while to the East, residual velocities charaterize the Italian pensinsula both, w.r.t. Eurasian and Nubian plates. An extentional velocity gradient of about 2-3 mm/yr is observed across the Appenine chain.

2.3.1 Calabrian Arc

Observing the GPS velocities running from the Corsica-Sardinia block to the Calabrian arc, we can infer that there are no evidences of active extension in the Tyrrhenian basin. On the contrary, a NW-SE shortening of a few mm/yr is likely to be accommodated there (2.2). The whole NW-SE extension affecting the Calabrian arc is of the order of $\sim$ 3.0 mm/yr, $\sim$ 2.0 mm/yr of which are accommodated on land. All these observations suggest that the rollback in the Tyrrhenian-Calabrian system is almost stopped or significantly slowed down. However, the particular geography of the region (i.e. the distribution of land and seas), the few GPS stations in Calabria and the lack of stations in the Ionian Sea, leave some uncertainties. In particular, the kinematics of the Ionian basin is a key information missing to define the kinematics of the Ionian-Calabria-Tyrrhenian subduction system, since the absence of GPS stations (no islands are present here) and the few focal solutions in the Calabrian wedge do not provide a well defined pattern of deformation. The SE-ward displacements of Calabrian stations with respect to Nubia (fig. 2.6), occurring at rates of $\sim$ 6/7 mm/yr, and the lack of instrumentally recorded thrust earthquakes in the external Calabrian Arc may suggest that convergence is still occurring and that the subduction fault plane may be presently locked (e.g. *Gutscher et al.*, 2006). Alternatively, the Ionian basin may be presently moving independently, or partially independently, from the Nubian plate, with important implication for the study of the kinematics and geodynamics of the Central Mediterranean.

2.3.2 Sicily and surroundings

Figs. 2.5 and 2.6 illustrates some first-order features of the regional GPS velocity field, showing a smooth transition between two clearly distinguishable velocity domains in Sicily and Calabria, as already highlighted by *D'Agostino & Selvaggi*, (2004), *Serpelloni et al.*, (2007) and *D'Agostino et al.*, (2008). GPS velocities in the Sicily domain are in general agreement with the NW-ward motion of the Nubian

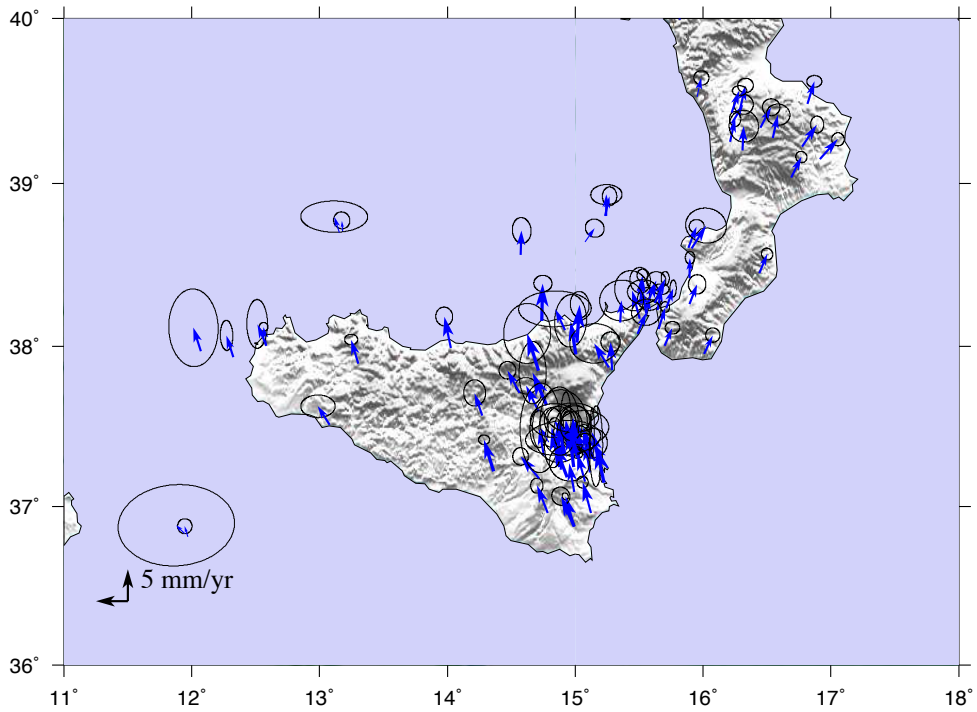

Figure 2.5: *Eurasia fixed horizontal GPS velocity vectors and 95% confidence error ellipses for the Sicily and Calabria region.*

plate with respect to Eurasia, although, residual motion of stations in Sicily and the Pelagian area (i.e., LAMP and MALT) (please, refer to figure fig. 4.3 for the station names) with respect to Nubia suggest that this region is moving independently from both Nubia and Eurasia. A few stations in eastern Sicily (i.e., EIIV and ESLN) show E-ward oriented velocities that may be related to local deformation of Etna volcano (*Lundgren et al.*, 2004; *Bonforte & Puglisi*, 2006). As these velocities are not representative of the regional microplate kinematics, they have been excluded from the analysis of the velocity gradient field. In northern Sicily, more rapid northward motion of some stations is observed north of the Kumeta-Alcantara lineament. NE-Sicily GPS velocities rotate clockwise, moving to a NE-ward direction that is about normal to the predicted Nubian plate motion. A clear velocity gradient is also observed moving from the Iblean region (south Sicily) to the northern coast of Sicily with velocities increasing of about 2 mm/yr both, w.r.t. Eurasian or Nubian plate. At a more local scale, our new GPS velocity solution outlines a fan-like pattern of the velocity vectors across the Messina Straits, where velocities undergo a clockwise rotation of about 30°, from north to south.

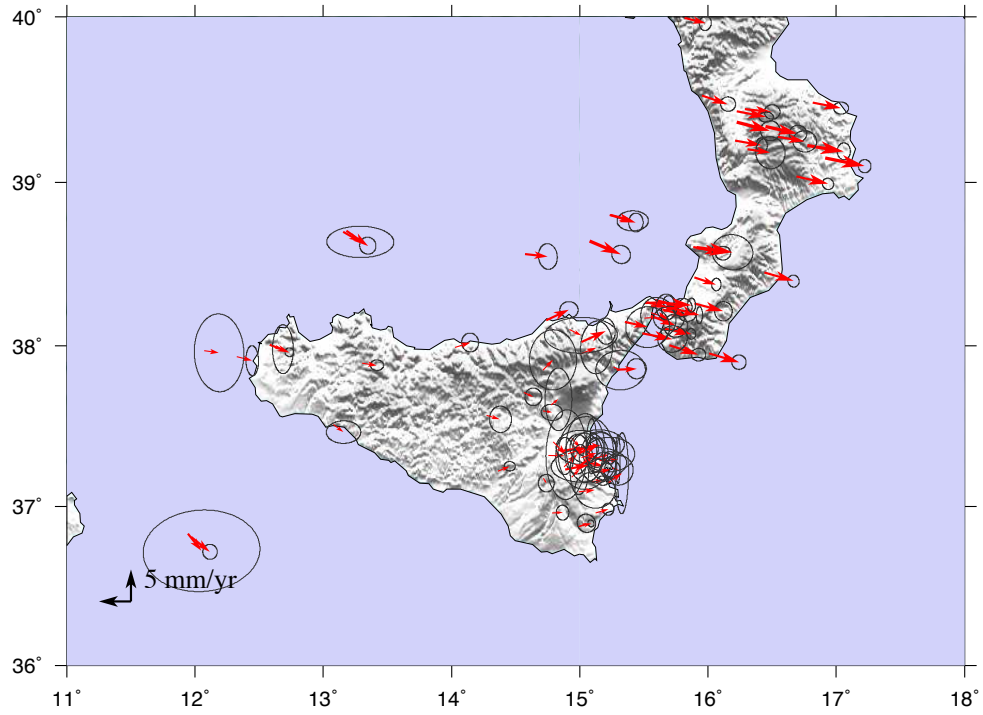

Figure 2.6: *Nubia fixed horizontal GPS velocity vectors and 95% confidence error ellipses for the Sicily and Calabria region.*

2.4 Strain rate field

Fig. 2.7 shows the strain rate field estimated from the velocity data and uncertainties through weighted least squares on a regular $0.2° \times 0.2°$ grid (*Shen et al.*, 2007). The contribution of each station in the least squares inversion is scaled by a Gaussian function $\exp(-\Delta R^2/D^2)$, where ΔR is the distance between a geodetic station and the grid point being evaluated and D is a smoothing distance that is optimally determined, within a priori defined bounds, through balancing the trade-off between the formal strain rate uncertainty estimate and the total weight assigned to the data (*Shen et al.*, 2007). The re-weighting determines the degree of smoothing around a given spot and the uncertainties of the strain estimates, while the optimal D value can be considered as an indicator of how local or regional the strain rate tensor inverted at each grid point is. Strain rates in the study region are computed with D values of about 20 km, making the estimates a local measurement of the deformation across it.

Higher deformation rates occur in the Peloritani-Messina and Central Aeolian area. The SE Tyrrhenian is characterized by fast (up to $\sim$ 200 nanostrains/yr) shortening, which rotates from N-S to SW-NE direction across the Salina-Lipari-Vulcano tectonic lineament. Fast shortening rates in the Central Aeolian Islands have been

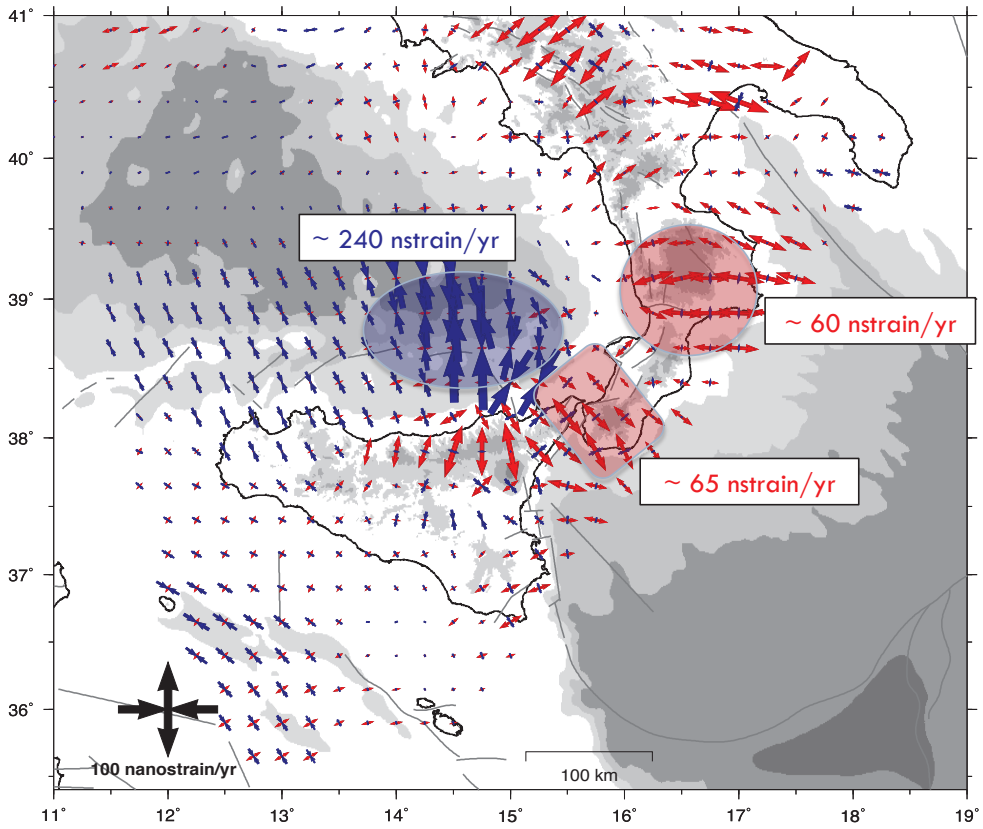

Figure 2.7: *Geodetic strain rate field computed over a regular* $0.2° \times 0.2°$ *grid. Red and blue arrows show extensional and compressional strain rates, respectively. Grey crosses display* 1σ *uncertainties. Slightly modified from* (Serpelloni et al., 2010).

associated with the interplay between convergence of the Sicily and Tyrrhenian domains and volcano-tectonic deformation (*Mattia et al.*, 2008; *Serpelloni et al.*, 2007), whereas the NE-SW oriented shortening has been related to an actively deforming sub-marine anticline between Cape Milazzo and the Aeolian Is. (*Argnani et al.*, 2007). The inferred continuation of the contraction to the north of the islands is from the high D value and smoothing, but is not fully constrained by data since no GPS sites (i.e., islands) are available for some distance to the N.

Rapid NW-SE oriented extensional deformation rates (up to $\sim$ 65 nanostrains/yr) characterize the Peloritani and Messina Straits, about normal to its coastlines. The almost purely extensional deformation regime observed across the Messina-Peloritani region is consistent with the dominant extensional faulting here. Significant extensional deformation, but at lower rates, is also inferred along the Tyrrhenian side of the Calabrian Arc and, on-land Sicily, along a EW oriented belt that corresponds to the distributed extensional tectonic belt along the Kumeta-Alcantara

lineament. On the contrary, no significant strain is observed across the Apennines thrust belt.

Moving to the northern Calabria, extensional deformation rates E-W oriented and with maximum magnitude of ∼60 nanostrain/yr charaterizes the Crati Basin and Sila Massif area where seismological and geolocical data reveal the presece of normal fault systems. Extension continues all along the Appenine chain with rates comparable to those obteined in Calabria.

Chapter 3

Modeling the earthquake cycle

3.1 Introduction

As noted, the aim of this work is to study the interseismic strain accumulation across active structures in the Sicily and Calabria region. Most of the previous works, about this region (i.e. *Mattia et al.*, 2009) or other seismic areas around the world (e.g., *Burgmann et al.*, 2005; *Murray et al.*, 2001; *Bettinelli et al.*, 2006; *Vergne et al.*, 2001) do that by using an **elastic dislocation model** that solves for the best fit rectangular dislocation geometry and fault slip-rates assuming that all the observed velocity gradients are due to single normal faults accumulating elastic strain, then not taking into account the regional kinematics. However, our observed intersismic velocity gradients are likely to be affected by the strain accumulation associated with other nearby faults surrounding the area. Unfortunately, our knowledge of the geometry and kinematics of these faults is quite incomplete (*Argnani et al.*, 2007; *Billi et al.*, 2006; *D'Agostino & Selvaggi*, 2004) also because most of them are located offshore, and/or poorly covered by GPS networks. On the other hand, however, we can't neglect the impact of elastic strain fields from these faults. For this reason we use a combined approach of elastic dislocation and **block modeling**. The latter, infact, combining block rotaion and elastic strain accumulation on the faults, allows us to take into account, in our models, the regional kinematics. The following paragraphs briefly describe the theory behind this approach: the seismic cycle and the used models.

3.2 Seismic cycle

The seismic cycle theory, conceptually introduced for the first time in 1910, by Reid and known as 'elastic rebound' assumes that the crust gradually stores elastic stress that is released suddenly during an earthquake. Depending on the different geological features and on the variable conditions of temperature and pressure with depth the earth's crust can, to a first approximation, be separated into two layers: the upper crust caraterized by elastic reology and seismic behavior and the lower crust caraterized by viscous reology and aseismic creeping. The behavior of these two portions of crust is variable during the whole seismic cycle that consists of three main phases: **inter**seismic, **co**seismic and **post**seismic.

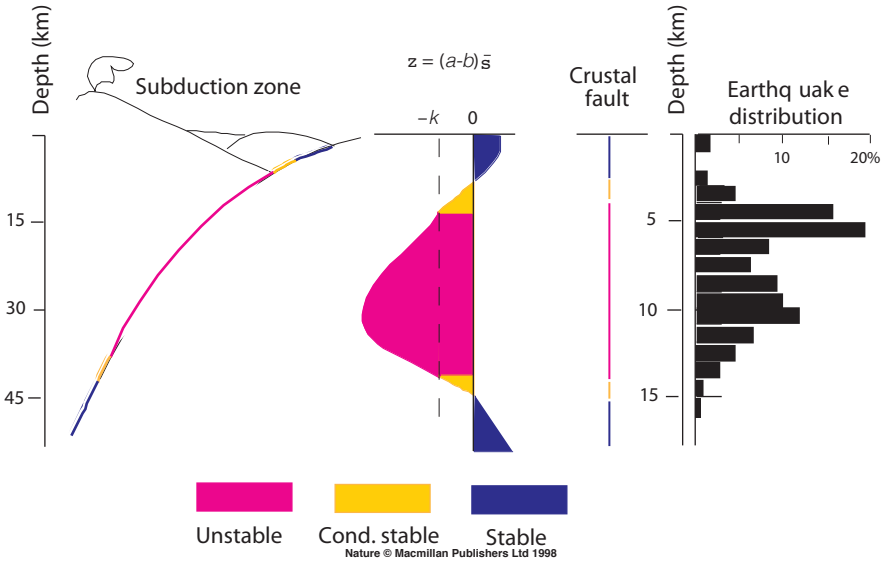

Figure 3.1: *A synoptic model for stability as a function of depth for crustal faults and subduction zones. The histogram of the depth distribution of earthquakes (right) is for a section of the San Andreas fault near Parkfield, California. From* (Scholz et al., 1998)

3.2.1 Reology and stability regimes of a fault plane

Fault planes are charaterized by variable stability conditions with depth (fig. 3.1). Stability regimes have the following consequences for earthquakes: earthquakes can nucleate only in those regions of a fault that lie within the unstable regime. They may propagate indefinitely into conditionally stable regions, provided that their dynamic stresses continue to produce a large enough velocity jump. If earthquakes propagate into a stable region a negative stress drop will occur, resulting in a large energy sink that will rapidly stop the propagation of the earthquake (*Sholz*, 1998). Faults are not simply frictional contacts of bare rock surfaces: they are usually lined with wear detritus, which, being poorly consolidated at shallow depths, favor the creation of stable regions. A stable regime is found also at large depth because of the onset of plasticity at a critical temperature. The regions between these two stability transitions are unstable, indicated by red in fig. 3.1, and yellow indicates the regions of conditional stability. Thus, the red regions define the seismogenic zone, the depth range over which earthquakes may nucleate, as indicated by their hypocentral depths, an example of which is given on the right of fig. 3.1.

For crustal faults, the upper transition depth is typically observed to be at 3-4 km, but may be absent at faults on which there has been little slip and hence little or no gouge developed. The lower transition occurs at 15-20 km, corresponding to the onset of plasticity of quartz at about 300°C. The depth at which this occurs depends on the local thermal gradient (*Scholz*, 1998).

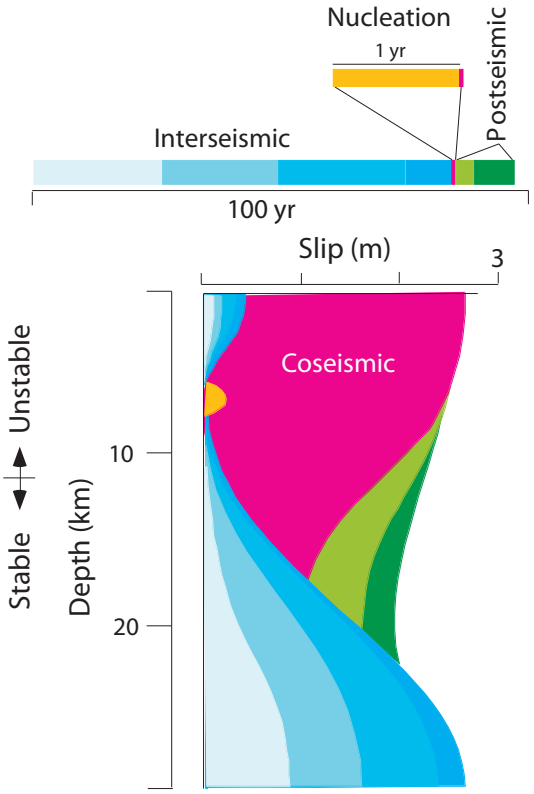

Figure 3.2: *Slip as a function of depth over the seismic cycle of a strike-slip fault, using a frictional model containing a transition from unstable to stable friction at 11 km depth (typical value for the S. Andreas fault). From* Scholz et al., (1998)

3.2.2 Seismic phases

As noted above, seismically coupled faults are typified by infrequent large events, separated by long quiescent interseismic periods in which the stresses relaxed by the preceding earthquake are restored. The **interseismic** phase is, by definition, the period between two main events. During this phase, which makes up most of the cycle, the upper crust is locked and deforms under the pressure of the plates relative motion while the lower crust, slips steadly along its own length into the asthenospere at the plate convergence rate (blue sector in fig. 3.2). What we observe on the surface is a velocity gradient across the fault track. The figure 3.3 shows a sketch for a strike-slip fault and a subduction zone.

The **coseismic** phase coincides with the earthquake (see fig. 3.3, left, phase (c)). Just before the earthquake a pre-seismic phase, known as nucleation, occurs (orange in fig. 3.2); in this phase, slip accelerates until the instability results in the coseismic motions (red). Thus, when the amount of strain accumulated during the interseismic phase exceeds the frictional forces that are preventing slip the locked portion of the fault ruptures and rocks on either side of the fault slide rapidly as

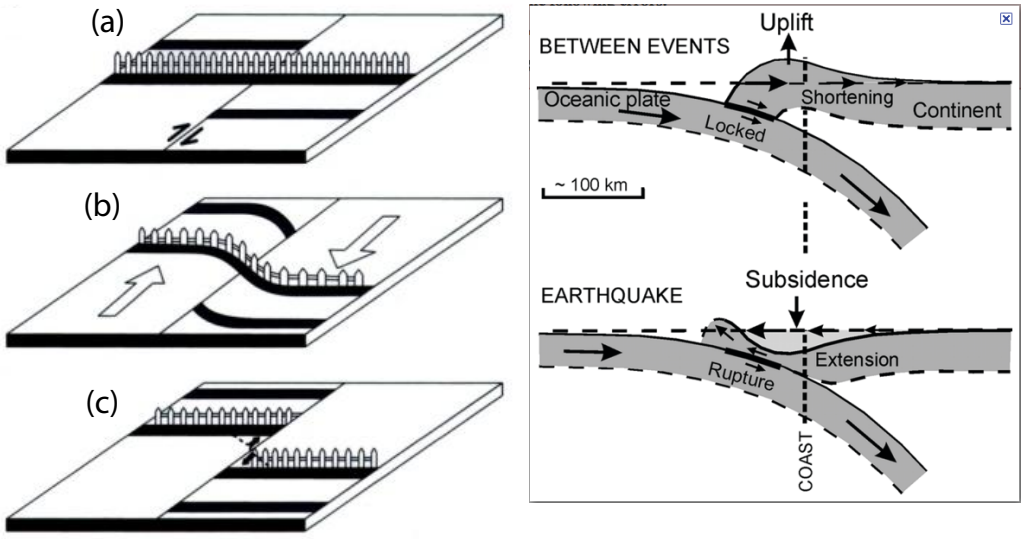

Figure 3.3: *Schemes of the elastic rebound model for a strike-slip fault (left) and a subducion zone (right). Left: during the interseismic phase the fault is locked so that features across it (such as a fence) that were linear at time (a), are slowly deformed with time (b). Finally the strain becomes so great that the fault breaks in an earthquake (coseismic phase) offsetting the features (c). Right: sketch of interseismic strain accumulation (upper) and coseismic strain release (lower) in a subduction zone. Between two big events the shallower portion of the plate interface is locked and deforms due to relative plate motion, while the lower portion of the plate slips at the plate convergence rate.*

the pent-up strain is relieved.

Even if most idealized models of earthquake deformation cycle, assume that, inter-earthquake strain accumulation is perfectly balanced by coseismic strain release, however, some geodetic mesurements, along with geological indicators and paleomagnetic measurements suggest significant deviations from this behavior (fig. 3.4). Depending on which phase of the cycle is dominant, permanent deformation features can mimic either the coseismic or interseismic movement patterns.

The **postseismic** phase (green in fig. 3.2) corresponds to a period of minutes to years after an earthquake when the crust and fault both "adjust" to the modified state of crustal stress caused by an earthquake. During this period, at least two distinct processes give rise to additional movement of the crust. One consists of additional slip, usually minor, along the fault. Some of this additional slip is due to earthquake aftershocks on the ruptured fault. After large earthquakes, deeper regions of the crust "flow" in response to changes in crustal stress caused by the preceding earthquake, much like water flows away from areas of high pressure.

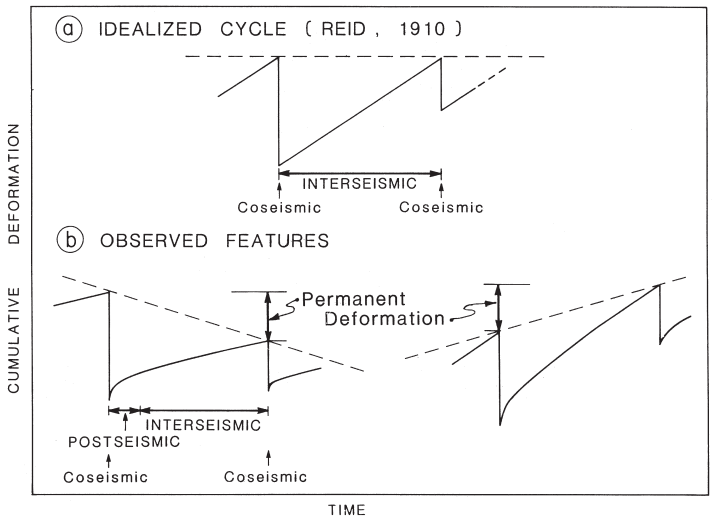

Figure 3.4: *The earthquake deformation cycle for a) an idealized linear strain build-up model, and b) the case where inter-earthquake straining is not perfectly balanced by coseismic strain release. From* Thatcher, (1993).

3.3 Kinematic models of observed interseismic deformation

Several classes of quantitative models have been used to interpret deformation measured by geodesy. We can divide these models into four categories: continuum, microplate, fault/earthquake cycle, and block models (*Meade & Loveless*, 2009). Description and comparisons of these models made in previous papers (e.g. *Allmendinger et al.*, 2009; *Meade & Loveless*, 2009) have shown that the first three are predicated on unrealistic assumptions and overlook important components of the deformation. Continuum and microplate models have been considered to lie at opposite ends of a spectrum of crustal deformation hypotheses (*Thatcher*, 1995), with the latter assuming that geodetically observed velocities result from the rotation of a finite number of crustal micorplates (*Tatcher*, 2007). The continuum limit approximates a pervasively fractured upper crust with deformation accommodated on an infinite number of faults. Therefore, continuum models do not provide information regarding slip rates on specific geologic structures. In constrast, earthquake cycle models (*Savage & Burford*, 1973; *Savage*, 1983), which are commonly used to model inter-, co-, and/or post-seismic deformation around individual or small groups of structures, assume that geodetically observed velocity fields result from the elastic behavior of the upper crust and viscoelastic behavior of the lower crust/upper mantle. The mechanical concept underlying these models is that, during the interseismic part of the seismic cycle, either localized slip (*Savage and Burford*, 1973) or viscoelastic relaxation below the seismogenic layer exert a stress on the elastic upper crust and causes it to deform.

Block theory combines microplate and earthquake cycle models, describing in-

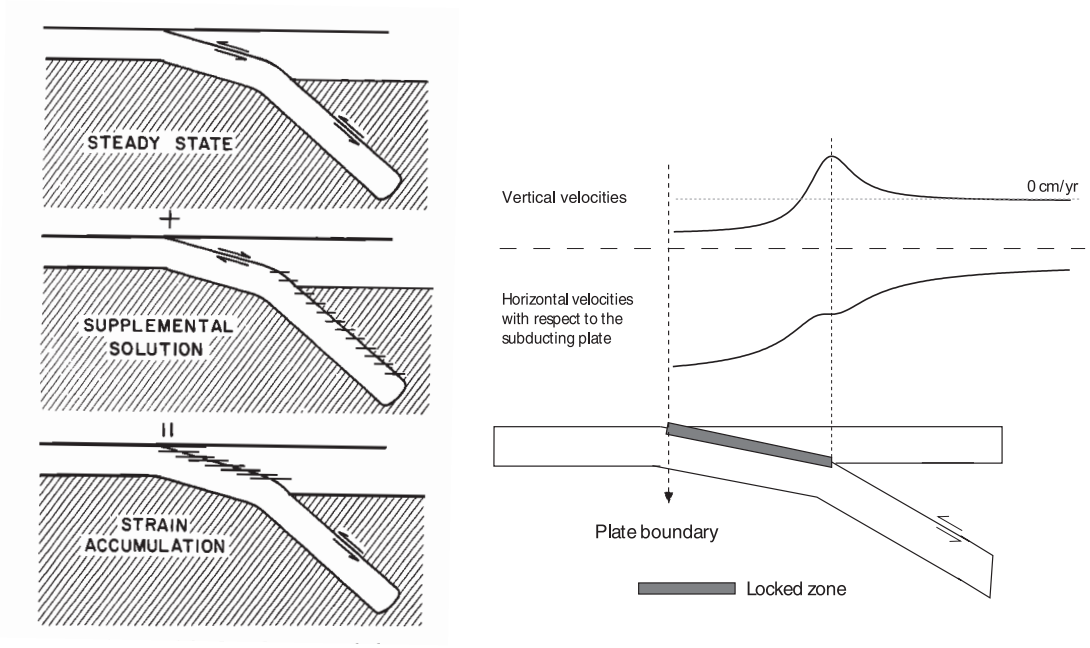

Figure 3.5: *Left: superposition model of strain accumulation at a subduction zone. The asthenosphere is indicated by shading. A locked (no slip) condition at an interface is indicated by short horizontal bars crossing the interface. From* Savage, (1983). *Right: vertical (upper) and horizontal (middle) velocity model on a transect perpendicular to the trench, born by the (lower) locked zone (from* Bergeot et al., (2009)*).*

terseismic geodetic velocities as the summed effects of crustal block rotation and the earthquake cycle processes that occur on the faults defining block boundaries (*Meade & Hager*, 2005; *Meade & Loveless*, 2009). By integrating seismic cycle models with microplate rotations, block models provide information about relative motion across discrete structures as well as the smooth velocity gradients produced by the accumulation of elastic strain on these structures.

3.3.1 Back slip model

The strain accumulation and release on a fault plane is described in *Savage*, (1983) simply as a perturbation of steady state motion. In steady state motion the fault plane slides uniformly along its length at the plate convergence rate. In the cited work, the author describes, in particular, the behavior of a subduction interface where the strain accumulation is generated by locking (no-slip condition) the main thrust zone (fig. 3.5, left). This locking is represented simply by adding a supplemental solution that imposes normal slip at the plate convergence rate upon the main thrust zone. In addition to steady normal slip, the supplemental solution must provide occasional abrupt thrust events to recover the accumulated normal slip. These events represent the major, shallow, thrust earthquakes that occur at the subduction zone. The superposition of the supplemental and steady state solu-

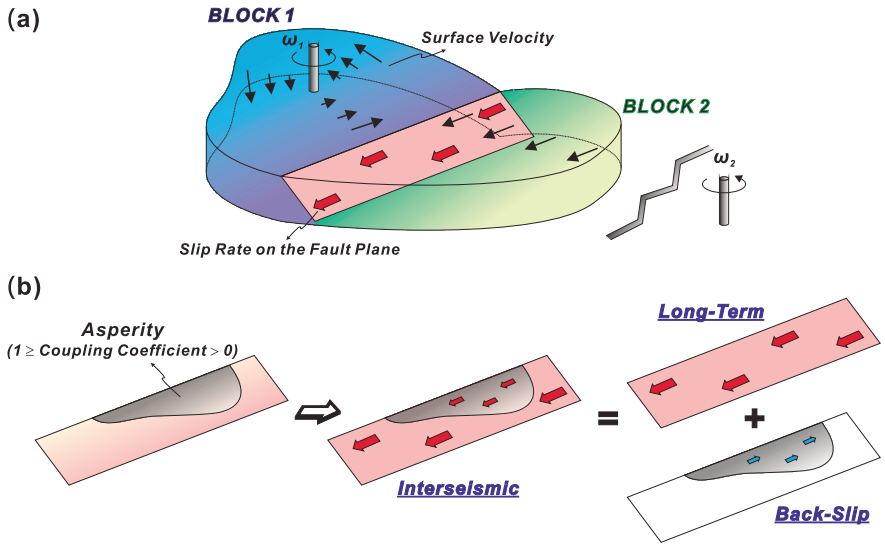

Figure 3.6: *Sketch of a 3D block model. (a) Relationship of the Euler pole location and block motion. The black thick arrows indicate the directions and magnitudes of the surface velocities in tectonic blocks. The pink plane (fault plane) is the interface between two blocks; ω means rotation rate. Red arrows denote the slip rates along the fault plane and the slip rates are derived from the velocity difference between two blocks. (b) Relationship between the longterm slip rate, back-clip rate (slip rate deficit) and interseismic slip rate. Red arrows denote the slip rates along the fault plane, and the blue arrows are the back slip rates on the asperity. From* Ching et al., (2011).

tion then gives a complete representation of the earthquake cycle.

Note that this is not to say that normal slip actually occurs on the main thrust zone. On the contrary, the normal slip from the supplemental solution is cancelled by the reverse slip from the steady state subduction solution so that a no-slip condition obtains on the main thrust zone except at the time of abrupt thrust events in the supplemental solution.

Figure 3.5, (right) shows the vertical and horizontal velocity gradient perpendicular to the trench. The model predicts shorthening all along a horizontal transect normal to the trench on the overriding plate, with an inflexion point marking the downdip edge of the locked zone. On the vertical component, the downdip edge of the locked zone corresponds to a maximum uplift while the region close to the trench subsides.

3.3.2 Elastic Block Model

Block theory is a method for decomposing a geodetically observed velocity field into block motion, elastic, and homogeneous intrablock deformation components. In the *Meade and Loveless*, (2009), formulation of this model they describe the east, north, and up components of the observed interseismic velocity $\mathbf{v}_I$ as a sum of three tectonic processes: block rotation, elastic strain accumulation, and internal block deformation (fig. 3.6)

$$\mathbf{v}_I = \mathbf{v}_B + \mathbf{v}_E + \mathbf{v}_\varepsilon \tag{3.1}$$

Following the back slip model theory described above, as the block model approach shapes the steady state motion (that is the secular motion) as blocks rotation, the locking on the main thrust zone is obtained assuming reverse slip on it (fig. 3.5). Using this approach thus we model the upper portion of the fault interface.

Unlike the early block models, wich estimated block motions and fault slip rates indipendently, in this model motion due to multiple rotating blocks is supplemented by elastic deformation due to fault slip at block boundaries without the *a priori* assumption that one effect or the other dominates the observed velocity field. The model uses spherical geometry with locally optimal coordinate transformations, triangular dislocation elements, and linear estimator to simultaneously solve for block motions, kinematically consistent fault-slip rates, and effective elastic coupling coefficients.

In this work we use the block model approach assuming: (1) planar geometry for all the block bounding faults, and (2) rigid block rotation (no intraplate strain). Latter assumption is made to avoid that the mismodeled component of the velocity field is parametrized as internal strain even when is not.

An example of rotational and elastic components of a gridded velocity field estimated by using the block model code of *Brendan & Loveless*, (2009) is shown in figure 3.7. A simple microplates model for the central Mediterranean is used. The three maps show the velocities estimated assuming full locking for all the block bounding faults except a synthetic fault system parametrized by three 60° ∼N-ward dipping, ∼E-W striking and 30 km locked segments. Red and blue arrows in fig. 3.7 represent the rigid blocks rotatational and the elastic components of the deformation field on the fault system, respectively. Violet arrows in fig. 3.8 depict the model horizontal velocity field (elastic + rotational component). Except those really close to the fault, the modeled velocities agree rather well with the observed ones (yellow arrows).

As noted the block model approach allows us to investigate strain accumulation and slip-rates related to a single fault while taking into account for the block rotation and the elastic strain contribution from other nearby faults. We use the block model just with the aim to test if the velocity gradient across some investigated active structures in the study area may be significantly modified by the elastic strain contribution from other fault systems. The spatial extent of surface interseismic strain of a block-bounding fault depends on its degree of coupling, which can be

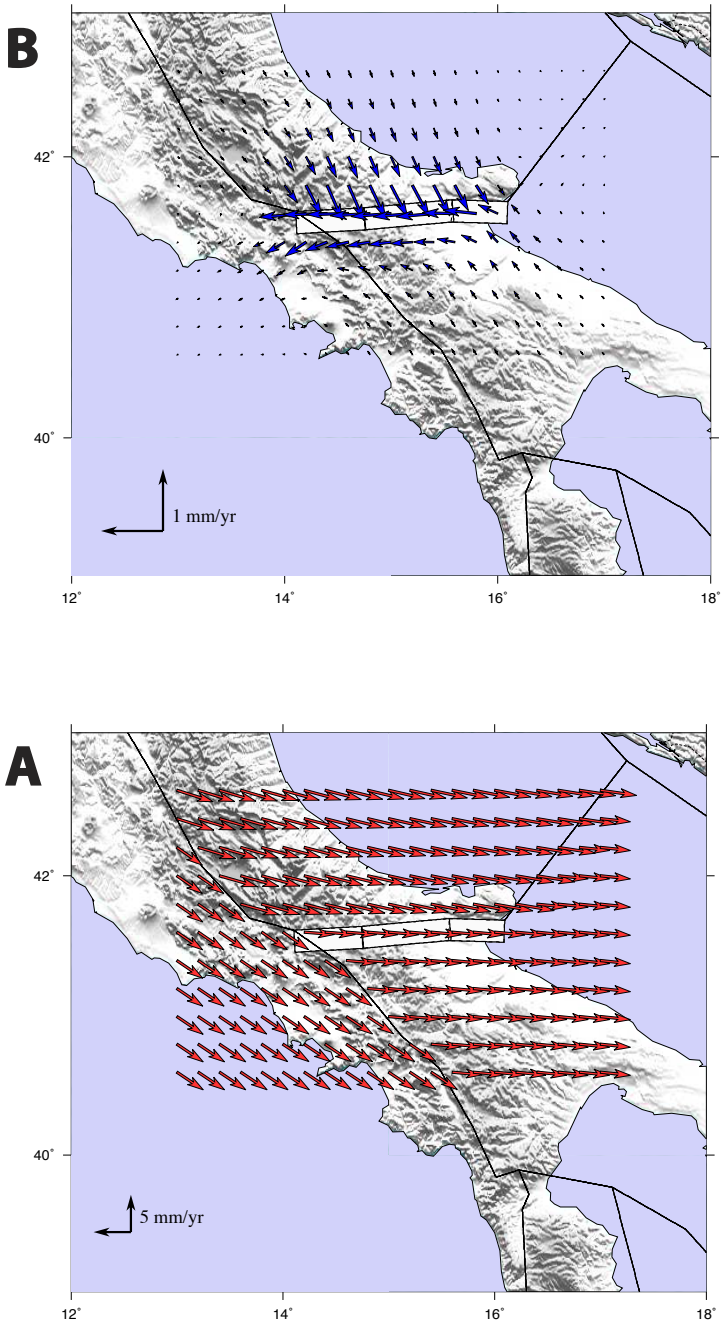

Figure 3.7: *Elastic (A) and rotational (B) components of the velocity field expected from a microplates model that assumes rigid block rotation with all the faults vertical and fully locked except a synthetic fault system parametrized by three segments* 60° *N-ward dipping and 30 km depth locked.*

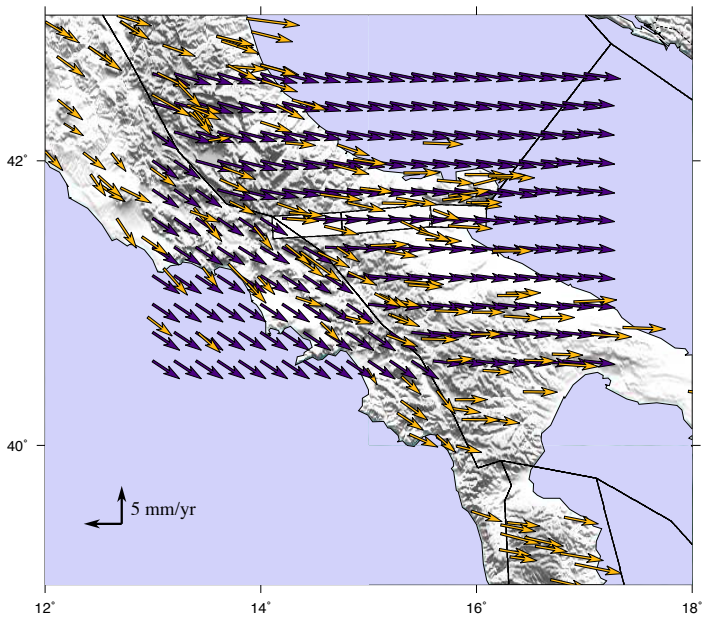

Figure 3.8: *Model horizontal velocity field (violet) and Nubia fixed observed velocities (dark yellow). Microplates model as in fig. 3.7.*

parameterized by changing the width of its locked portion. Increasing the locking width, infact, increases the magnitude and reach of elastic deformation associated with the fault. Figures 3.9 show magnitude and reach of the horizontal elastic deformation-rate expected by varying the width of a 30° dipping Calabrian slab interface, from 10 to 40 km, while assuming all the other faults vertical and fully locked. We can see that the region affected by the elastic deformation widens with increasing slab locking depth. Fault systems in eastern Sicily and Western Calabria are affected by an horizontal deformation rate smaller than 0.5 mm/yr and of ~ 2 mm/yr, at the minimun and maximum locking width, respectively. As the study area is caraterized by mean velocities of a few mm/yr a contribution of 1-2 mm/yr may represent a significant portion of the observed velocity gradients. It is clear that neglect any elastic contributions from nearby faults may lead to erroneous conclusions about the kinematics of the analyzed structures.

3.3.3 Dislocation model of a buried fault

Interseismic deformation near active faults is often modeled by using the theory of elastic dislocation (*Okada*, 1992). This deformation resulting from the elastic deformation on the brittle crust in response to plate dispacement away from the fault zone and ductile shear at depth. Fig. 3.11 shows a scketch of the crust layering and of the interseismic behavior of fault plane regions. Synthetic interseismic velocity

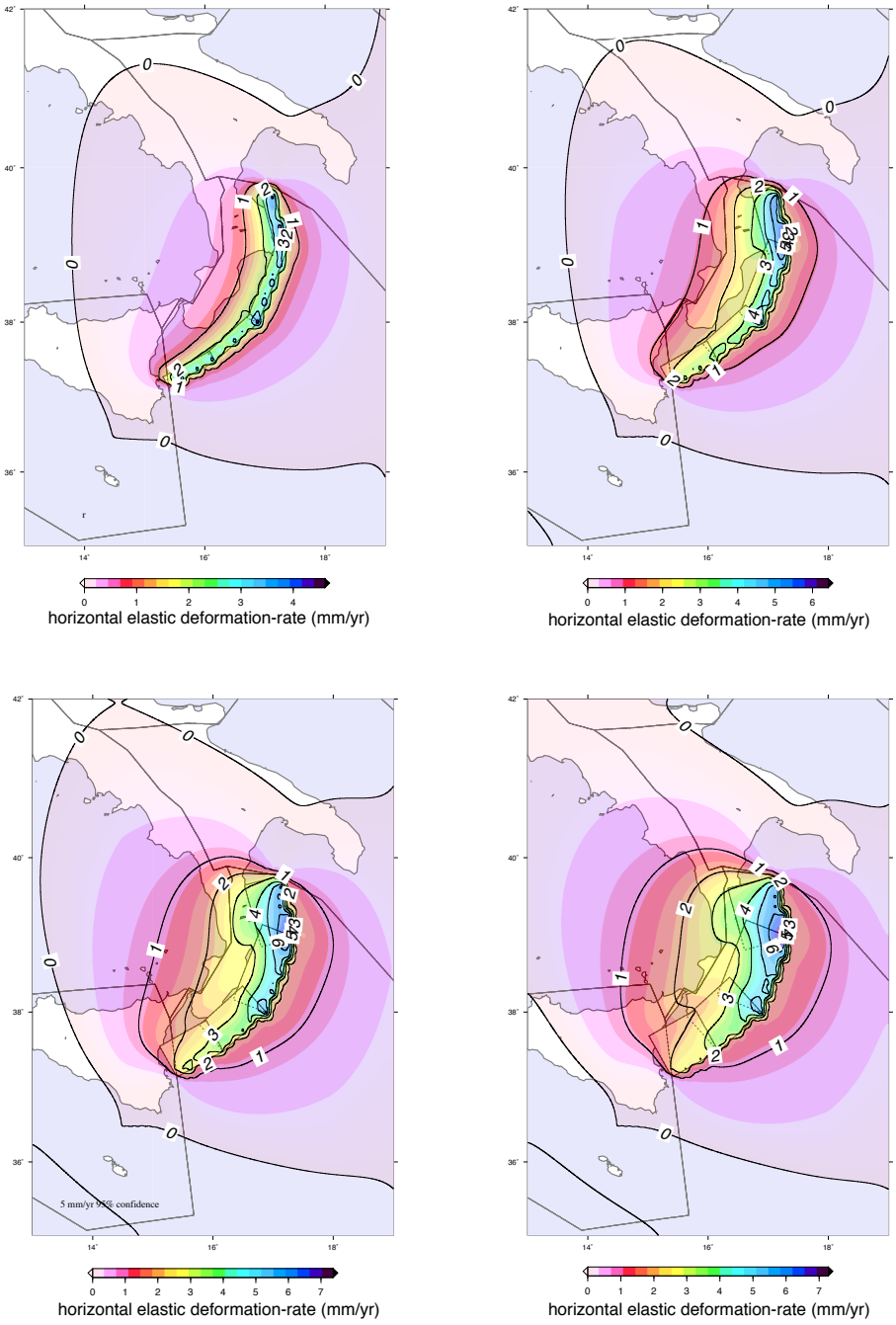

Figure 3.9: *Horizontal elastic deformation-rate expected by varying the width of a 30° dipping Calabrian slab interface, from 10 to 40 km (up left to bottom right). All the other block bounding faults are assumed to be vertical and fully locked.*

gradients at varying fault parameters are also shown.

In this work we use the dislocation model approach and a constrained, non-linear optimization algorithm to solve for best fit dislocation geometries (for a detailed description of the algorithm see Appendix A). Although this modelling approach is questionable, it has been shown to be a reasonable approximation when compared to mechanical models that account for the variations with depth of rheological properties, as well as to the effect of erosion and sedimentation on crustal deformation (*Vergne et al.*, 2001). *Okada*, (1992) models the plate interface as a rectangular, uniform-slip dislocations embedded in an elastic, homogeneous and isotropic half-space. The fault plane geometry is parametrized by length, depth, width, dip, strike, and fault edge location (fig. 3.10).

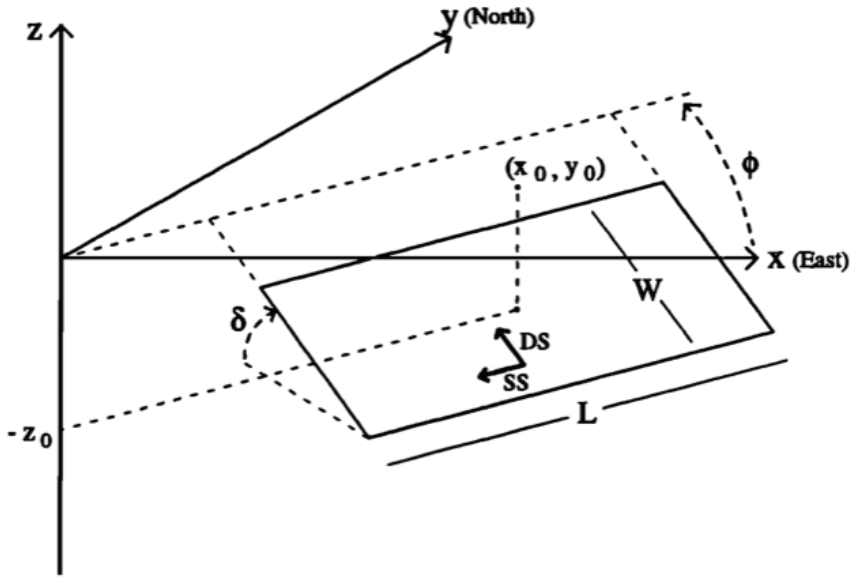

Figure 3.10: *Dislocation model parameters: length along strike L, width along dip W, depth to center z_0, dip δ, strike ϕ, location of center (x_0, y_0), right lateral strike slip SS, and reverse dip slip DS. From* (Arnadottir & Segall, 1994).

3.4 Block and dislocation model

3.4.1 Two equivalent approaches

Summarizing wath already said (par. 3.3.2), the seismic cycle model of *Savage*, (1983) considers two terms, namely a steady state term equivalent to stable sliding along the whole thrust fault from the surface to its down-dip extension, and a cyclic term representing the stick slip behaviour of the seismogenic portion of the fault (fig. 3.5, left).

Some authors adopt the back-slip model, and later on introduce a steady-state

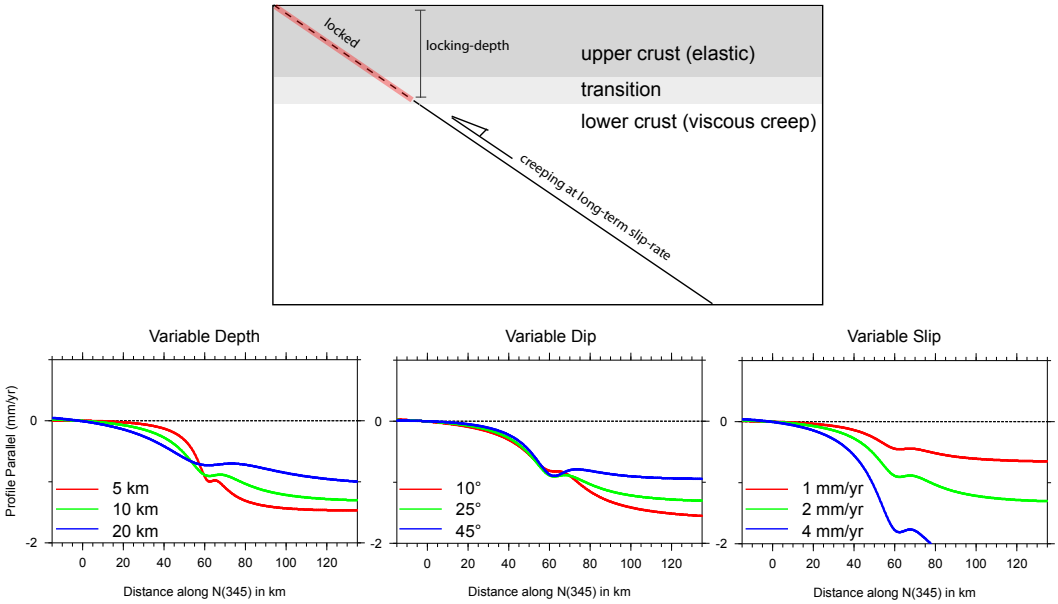

Figure 3.11: *Conceptual model of interseismic deformation and model velocity gradients at varying fault plane parameters. Dislocation model of interseismic deformation assumes that the brittle crust is deformed by continuous aseismic creep, presumably occurring at rates comparable to the long term geologic slip-rates, of the fault plane in the lower crust. Velocity gradients are obtained by varying each parameter while keeping fixed the others.*

term to account for accumulation of permanent deformation. This approach, then, is similar to modelling directly the creeping portion of the thrust fault at depth using a deeply buried dislocation. A shortcoming of this approach is that the steady-state term does not exactly balance the back-slip term because the two terms have different mechanical bases: ductile flow and elasto-brittle deformation over long time-scales (steady state), and elastic deformation without a failure criterion for the back-slip term.

Fig. 3.12 shows the comparison of velocity profiles from four different approaches used by *Vergne et al.*, (2001) to model the interseismic deformation accros a major intracontinental thrust faults, the Main Himalayan Thrust. They conclude that except where the fault emerges, the four approaches yield about the same horizontal velocities (fig. 3.12). It should be noted, that the back slip plus stady state term also provides a correct fit to the horizontal velocities except where the fault reaches the surface (fig. 3.12). This shows that, for a perfectly locked seismogenic zone, the only meaningful parameters in the back slip and buried slip models are the position of the point at the deep end of the locked portion of the fault and the local dip angle of the zone of aseismic shear. The geometry of the back slip dislocation does not need to follow that of the seismogenic portion of the fault.

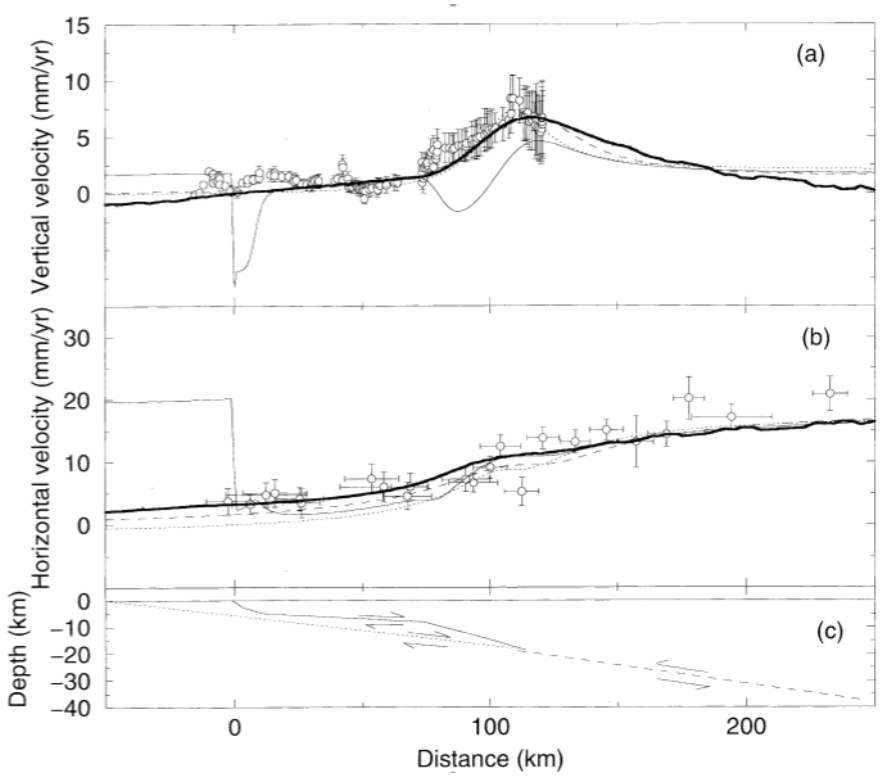

Figure 3.12: *Comparison between measured and calculated interseismic velocities computed from the finite element model (thick line), the deeply buried creeping dislocation model (dashed line), the back-slip model (solid line), and the back-slip model proposed by* Gahalaut & Chander, (1997), (1999) *(dotted line). (a) Vertical velocities relative to the southernmost point in the Indo-Gangetic plain, derived from levelling data (*Jackson & Bilham, 1994*). (b) Horizontal velocities with respect to India derived from GPS measurements (*Larson et al., 1999*). (c) Fault geometry used in the dislocation model. From* Vergne et al., (2001).

3.4.2 Strengths of a combined approach

As said previously, in our work we use an approach based on the combination of elastic *block* and *dislocation* models. Both models have some lack or limitation but, from some point of view they are complementary so that using them together make a really robust method for our pourposes. The table 3.1 shows a schematic overview of strengths and weaknesses of the two models we try to summarize below.

The main goal of this work is to study active structures that are accumulating strain during the interseismic phase and investigate possible contributions from the other nearby structures. This means that we need models that allow us to invert the observed velocity gradients to estimate the fault planes geometric parameters while tacking into account for the other structures.

The dislocation model approach I use has the advantage to realize a constrained

	BLOCK MODEL	DISLOCATION MODEL
PROS	• Takes into account for regional kinematics • Model of offshore strucures	• Geometric parameters estimation
CONS	• A priori block geometry • No geometric parameters estimation	• No regional kinematics • Need for data coverage

Table 3.1: *Schematic overview of strengths and weakness of elastic dislocation and block models. Table wants to point out the strength of their combined use.*

inversion for the fault plane geometric parameters, but it assumes that all the observed velocity gradient is due to individual or small group of structures, neglecting the regional kinematics. Moreover, the area under study is a narrow strip of land surrounded by the sea and then some of the active structures we want to study lie offshore. The use of model optimization techniques in half-space dislocation models requires a certain number of GPS stations sampling details of the velocity gradient across the active fault under investigation. Consequently, this model approach cannot be used to study offshore faults or areas of poor geodetic coverage.

Conversely, the block model approach, invert the observed velocity field, assuming that is a sum of block rotation and strain loading at block-bounding faults. Then, the main advantage is the possibility to analyze the strain accumulation related to a single structure in the frame of regional kinematics. On the other hand, it allows us to estimate the block rotation parameters (Euler poles and rotation rates) taking into account for the fault strain accumulation component. This is required, since some GPS stations we use lie close to the block boundaries and so their velocities are affected by an elastic strain component. Moreover, as this approach doesn't need a data coverage across the investigated fault, we can also model offshore structures. However, as noted, block model, doesn't invert for geometric parameters and so needs to define an a priori block geometry.

3.5 Modeling of subduction zones

Spatially, subduction zones are characterized by a first-order cross-fore-arc seismotectonic segmentation into shortened domains near the trench (accretionary prism, splay faults, outer arc high) and the coast overlying largely aseismic parts of the subduction megathrust interface at depth (*Rosenau & Oncken*, 2009). These shortened domains generally bound a tectonically stable shelf region including forearc basins which correlate with the areas of large slip during megathrust earthquakes (e.g. *Song & Simons*, 2003; *Wells et al.*, 2003).

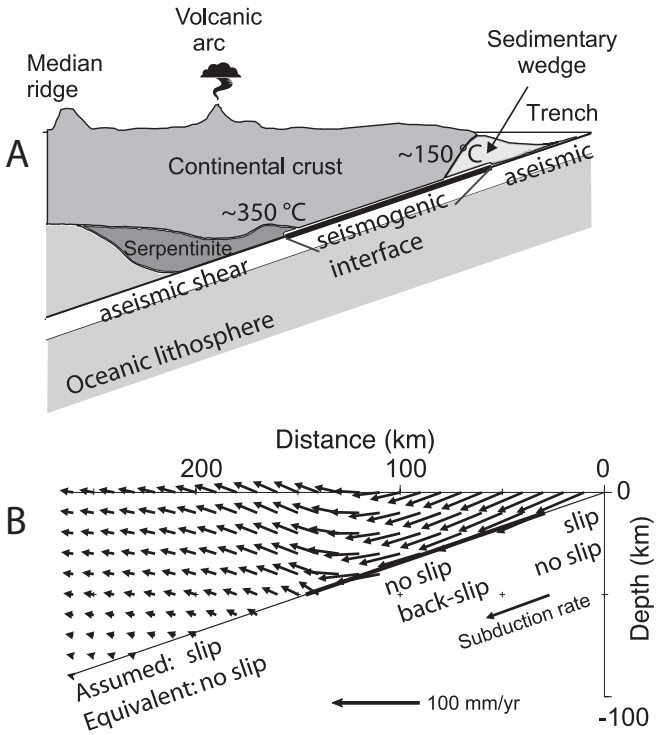

Figure 3.13: *(A) Example of schematic cross section of the first-order geometry and factors of subduction zone locking at the Kamchatka subduction zone. (B) Dislocation solution for velocities within the overhanging wall relative to the plate interior. Identical deformation fields result from the assumed (slip on plate interface adjacent to locked portion) and equivalent back slip model scenarios. Variations in the locking width and degree of kinematic coupling result in changes in the predicted surface velocity field. Thus inversions of surface GPS velocities can be used to invert for the optimal subsurface locking pattern across and along a subduction zone. From* (Burgmann et al., 2005).

Subduction zones release 90% of the total global seismic moment, and thus constitute much of the Earth's seismic potential. To better determine the seismic potential of a specific subduction zone, the spatial and temporal distribution of elastic strain accumulation and release along the plate boundary underthrust must be understood. The simplest description of subduction thrusts involves an interseismically locked depth interval (from 5-10 km to 30-70 km in depth) of the plate boundary interface that is bounded both updip and downdip by portions of the fault zone that deform aseismically (figs. 3.13, A and 3.1) (*Burgmann et al.*, 2005). The width of the seismogenic zone, measured perpendicular to strike, varies widely both along and between the world's subduction zones (*Pacheco et al.*, 1993; *Tichelaar & Ruff*, 1993).

Geodetic measurements of surface velocities allow for direct estimation of the pattern of nonslipping and creeping fault segments during the period of geodetic

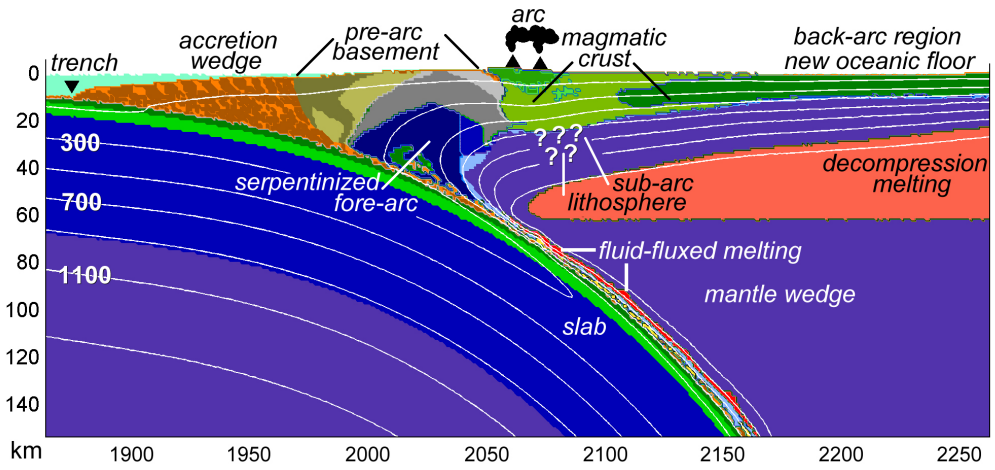

Figure 3.14: *Scketch of main subduction zone features. Model of a typical thermal structure of a subduction zone is also shown.*

observations (fig. 3.13, B). GPS measurements of interseismic deformation along subduction zones throughout the world reveal that some plate interface faults are for the most part locked, others appear only partially locked , while some appear to be accommodating convergence by steady aseismic slip only.

A number of factors have been suggested that control the extent of the seismogenic portion of the subduction thrust, which may vary in space and time. The updip aseismic zone has been related to material properties in the shallow, unconsolidated accretionary prism that contains stable-sliding clay minerals. The transition in behavior of clay minerals appears to be sensitive to temperature (*Oleskevich et al.*, 1999), and thus the upper aseismic zone is predicted to be wider for older and colder downgoing oceanic crust. The downdip transition to aseismic deformation also appears to be temperature controlled, indicating a transition to aseismic slip at 350°C and ultimately to viscous flow at higher temperatures that allow for crystal-plastic flow of rocks in the subduction zone. However, the lower transition might also be related to the juxtaposition of the plate interface with stable-sliding hydrated mantle material of the forearc. *Oleskevich et al*,. (1999) suggest that the lower transition depth is defined by the 350°C isotherm or the crustal thickness of the overriding plate, whichever comes first; however exceptions to this pattern have been noted (*Simoes et al.*, 2004). In addition to temperature-related phenomena, the plate convergence rate and/or the absolute velocity of the upper plate, the size and composition of the accretionary wedge, and the existence of heterogeneous features (such as seamounts) on the down-going plate may lead to differences in effective stresses, temperature, permeability, and fault morphology that may favor seismic stick slip or stable aseismic slip.

Comparison of the source areas of large historic subduction earthquakes and

nonslipping fault areas deduced from geodetic data suggests that asperities on the subduction interface are persistently locked interseismically, slip in large stick-slip events and are surrounded by areas of stable sliding. Thus the subduction thrust system appears to be a spatially heterogeneous system (*Pacheco et al.*, 1993) that may potentially evolve over time.

Subducting slabs provide the main driving force for plate motion and flow in the Earth's mantle, and geodynamic, seismic and geo-chemical studies offer insight into slab dynamics and subduction- induced flow. *Schellart et al.*, (2007) show that slab width controls two first-order features of plate tectonics, the curvature of subduction zones and their tendency to retreat backwards with time. Using three-dimensional numerical simulations of free subduction, they show that trench migration rate is inversely related to slab width and depends on proximity to a lateral slab edge.

Gvirtzman & Nur, (2001) argue that the width of the slab is the major factor controlling the rate of mantle flow into the corner between subducting and overriding plates. On the other hand whether or not the downward force induced by the sinking slab depresses the overriding lithosphere depends on the rate of mantle flow. Infact, when the slab is narrow the mantle flow around its edges effectively reduces the suction between the two plates and thus allows the slab to roll back relatively fast (for example, the Tyrrhenian, and the Aegean Seas), while, when the slab is wide, as for example, in the Andes, the suction force keeps it relatively stable.

Chapter 4

Strain accumulation across the Messina Straits and Crati Valley from a combined approach of elastic dislocation and block modeling[1]

4.1 Introduction

We use dislocation modeling to investigate the rate and nature of interseismic strain accumulation in the area affected by the 1908 Mw 7.1 Messina earthquake (eastern Sicily) and across the Crati Basin and the Sila Massif (northern Calabria).

The investigated region is among the most seismically hazardous sectors of the Mediterranean plate boundary, and few is known, or is still largely debated, about the present day kinematics and geometry of active seismogenic faults there. Our data confirm a change in the velocity trends between Sicily and Calabria, moving from NNW-ward to NE-ward with respect to Eurasia, and details a fan-like pattern across the Messina Straits where ∼3 mm/yr NW-SE extension are accommodated. In northern Calabria, where GPS stations move NE-ward, ∼2 mm/yr about E-W extension are accommodated across the Crati Valley and Sila Massif.

Half space dislocation models of the horizontal and vertical GPS velocities are used, together with model optimization algorithms, to infer the kinematics (i.e, slip-rates) and geometric parameters of the two fault zones taken into consideration. The observed velocity gradients across the Messina Straits and Crati Valley can be rather well explained by elastic strain accumulation due to slip below the seismogenic layer of ∼SE-ward and ∼E-ward dipping normal faults, respectively, with slip-rates that are of the same order of magnitude than, even if higher, than the ones constrained by geological and paleoseismological data.

Given the tectonic and geodynamic complexity of the study region, active fault systems in Sicily and Calabria must be analyzed in the framework of the complex

[1]Partially published in Earth and Planetary Science Letters: Serpelloni, E., R. Burgmann, M. Anzidei, P. Baldi, B. Mastrolembo Ventura, and E. Boschi (2010), Strain accumulation across the Messina Straits and kinematics of Sicily and Calabria from GPS data and dislocation modeling, Earth Planet. Sci. Lett., 298, 347-360, doi:10.1016/j. epsl.2010.08.005.

central Mediterranean microplates kinematics. By developing a regional elastic block model that accounts for both crustal block rotations and strain loading at block-bounding faults, we investigate if the measured velocity gradient across the two fault segments may be significantly affected by the elastic strain contribution from other nearby faults. We find that this longer wavelength signal can be presently super-imposed on the observed velocity gradients in NE-Sicily and Calabria, and the inferred slip rates on the Messina and Northern Calabria faults are impacted by elastic strain from Calabria.

4.2 Messina Strait Fault

4.2.1 Geological and tectonic setting

The Straits of Messina is one of the most tectonically active areas of the Mediterranean characterized by flight of uplifted marine terraces on both, the Sicilian and Calabrian side. The December 28, 1908 Messina Earthquake has been ranked as one of the most destructive events of the last centuries, and costed the highest toll in life in Italy's history of seismicity. The damages produced by ground shaking were aggravated by the effects of a remarkable tsunami, with up to 11 m of run-up height, that followed the earthquake. Despite such catastrophic effects the location of the causative fault is not fully assessed. Inverse modelling of seismograms and geodetic levelling, and geological studies have produced a variety of results in terms of position, direction, length and dip of the fault (fig. 4.1), with the most recent solutions proposing long, E-dipping faults trending about N-S (e.g., *Amoruso*, 2002; *Pino*, 2009, and references therein). At present, the most accepted seismogenic source for the 1908 earthquake is a 40 km-long, blind fault dipping 30° to the ESE which is thought to accounts for the topography of the Messina Straits. However data collected during the 'Taormina-2006' survey open some interesting questions concerning the position, direction and extent of active faults within the Messina Straits, where it is difficult to find a single fault that is long enough to account for the M_w 7.1, 1908 Messina earthquake. Moreover, the trend of the observed faults, though consistent with faults onshore Calabria, is different from the trend of many of the faults proposed on the basis of inversion of seismological and geodetic data.

Argnani, 2011 suggest the hypothesis of a system of interconnected faults partly exploiting preexisting fault planes. This interpretation leaves the possibility to have more than a fault active at the same time an event that has been inferred for the 1908 earthquake. At present it is difficult to say whether the observed active faults are just the surface expression of a single, deeper and blind seismogenic fault, as suggested by seismological arguments, or if they truly represent the complex response of an area that suffered a great deal of geological deformation and where more than one fault can be active at the same time.

The Messina Straits is located in the Calabro-Peloritani Arc (fig. 4.2), which lies along a segment of the Central Mediterranean plate boundary zone. Over the Neogene and Quaternary the evolution of this zone is interpreted in terms of slow

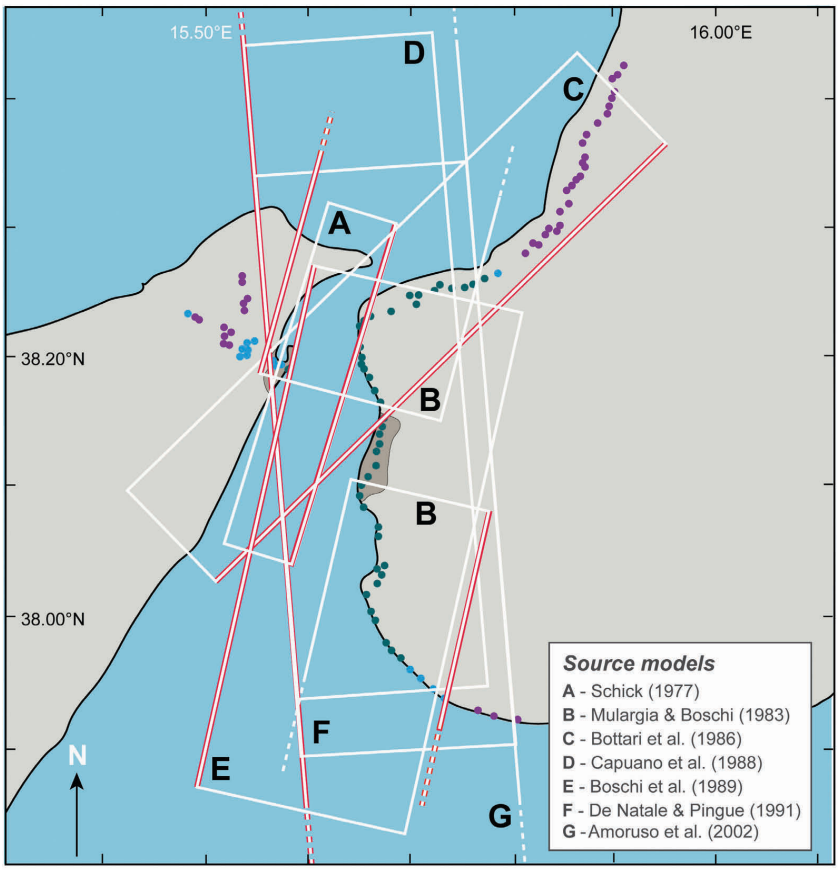

Figure 4.1: *Surface projection of the published fault planes for the 1908 earthquake. A red line marks the intersection of the fault plane with the surface (cut-off line) and hence shows the direction of dip of the fault (but notice that all faults are explicitly or implicitly assumed to be blind). From* (Pino et al, 2009)

relative Africa-Eurasia plate convergence and fast subduction and roll-back of the Ionian lithosphere beneath the Calabrian Arc, accompanied by fast back-arc extension in the Tyrrhenian Sea (*Faccenna et al.*, 2001; *Rosenbaum et al.*, 2002; *Malinverno & Ryan*, 1986).

The NE-Sicily and Calabria region is characterized by some of the highest rates of seismic moment release along the Nubia-Eurasia plate boundary (*Serpelloni et al.*, 2007). Deep and intermediate seismicity is mainly distributed E of the central Aeolian Is. (Lipari and Vulcano), while it is almost absent W of them (fig. 4.2). On the contrary, shallow seismicity ($h < 30$ km) is clustered mainly along a narrow EW stripe, offshore northern Sicily up to central Aeolian Is. and along a roughly NNW-SSE lineament moving southward from Aeolian Is. East of the central Aeolian Is., shallow seismicity is more sparse and rare, distributed within the accretionary

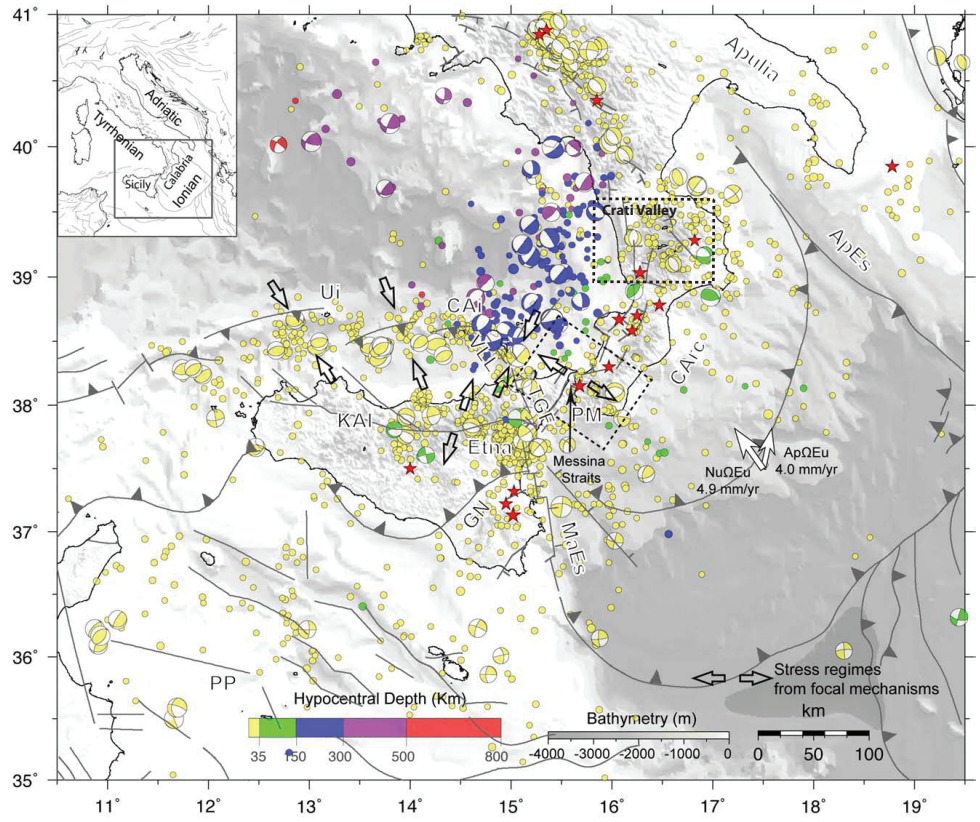

Figure 4.2: *Tectonic map of the Sicily and Calabria area. Grey lines show major fault systems (modified from the Geodynamic Map of the Mediterranean, compiled in the frame of the Commission for the Geological Map of the World, http://ccgm.free.fr). Earthquake focal mechanisms are taken from Harvard-CMT, INGV-RCMT and ETH-RMT catalogues. Instrumental seismicity is taken from* Chiarabba et al. (2005)*, for the 1981-2002 interval, and from the INGV seismic bulletin (http://iside.rm.ingv.it) for the 2002-2009 time interval. Red stars show historical earthquakes with $M \geq 6.5$ from the CPTI04 catalogue (available at http://emidius.mi.ingv.it/CPTI04). Stress regimes are taken from* Neri et al. (2003)*. Ui = Ustica Island, CAi = Central Aeolian Islands, VLL: Vulcano-Lipari lineament; TGF: Tindari-Giardini Fault system; KAl: = Kumeta-Alcantara Fault system, PM=Peloritani-Messina area, CArc=Calabrian Arc, MaEs=Malta Escarpment, PP=Pelagian Plateau, ApEs=Apulian Escarpment, GN=Gela Nappe, CV = Crati Valley. White arrows show competing kinematic boundary conditions for the Ioian Sea, after* D'Agostino et al., (2008)

wedge and along the Apennines (*Pondrelli et al.*, 2004).

Focal solutions of shallow earthquakes offshore northern Sicily outline a narrow E-W compressive belt (fig. 4.2), consistent also with geologic data (*Pepe et al.*, 2005). East of the central Aeolian area extensional to strike-slip mechanisms occur along a NNW-SSE seismic lineament that runs from the central Aeolian Islands to Mount Etna and continues S-ward along the eastern Sicily escarpment (*Pondrelli et*

al., 2004; *Serpelloni et al.*, 2007). Shallow extensional seismicity also characterizes the Mt. Etna area, and a diffuse belt running ESE-WNW in northern Sicily (KAl in fig. 4.2). The transition zone between these two domains approximately corresponds to the western lateral termination of the Ionian slab at depth of 100-200 km (*Faccenna et al.*, 2004), and to the Vulcano-Tindari-Giardini Fault system at shallow depths (*Argnani*, 2009; *Billi et al.*, 2006). The active tectonics inferred from focal mechanisms in Calabria is less well defined. However, extensional tectonics and regional uplift characterized the onshore Calabrian Arc during the last 0.8 Ma (*Westaway*, 1993), and strong historical normal-faulting earthquakes indicate that extension is the dominant style of faulting along its Tyrrhenian side.

GPS and seismological data (*D'Agostino et al.*, 2008; *Hollenstein et al.*, 2003; *Pondrelli et al.*, 2004; *Serpelloni et al.*, 2005; *Serpelloni et al.*, 2007) consistently locate the Messina Straits at the boundary between two different kinematic and tectonic domains, depicting NE-Sicily and Calabria as a key region for understanding of active geodynamic processes in the central Mediterranean. However, the general kinematic framework of the area continues to be debated.

4.2.2 Messina Straits Fault dislocation model

Fig. 4.3 illustrates some first-order features of the regional GPS velocity field, showing a smooth transition between two clearly distinguishable velocity domains in Sicily and Calabria, as already highlighted by *D'Agostino & Selvaggi*, (2004), *Serpelloni et al.*, (2007) and *D'Agostino et al.*, (2008).

At a local scale, across the Messina Strait, our GPS velocity solution outlines a fan-like pattern of the velocity vectors that undergo a clockwise rotation of about 30°, from north to south (fig. 4.3, insert). Moreover, ∼3 mm/yr NW-SE extension are accommodated across the Straits.

The way the observed velocity gradient (fig. 4.4) is presently accommodated by faulting and the number of faults that may take up this deformation is presently unclear, but very important for the evaluation of the associated seismic hazard. We explore this question by first examining very simple dislocation models that try to explain the local Messina Straits velocities in the context of elastic deformation about single locked normal faults.

The horizontal GPS velocities allow us to develop first-order models of the deformation using elastic dislocation theory, assuming that the observed velocity gradient across the Messina Straits, results from the elastic deformation of the brittle crust in response to plate displacement away from the fault zone and ductile shear at depth. The model explicitly assumes aseismic creep beneath a given depth (i.e., the fault locking depth) at rates that should be comparable with the long-term tectonic loading (*Savage & Burford*, 1970) [2].

We use rectangular (*Okada*, 1985), uniform-slip dislocations embedded in an elastic, homogeneous and isotropic half-space and a constrained, non-linear optimization algorithm (*Burgmann et al.*, 1997), to solve for the best fit rectangular

[2] Cf Par. 3.3.3

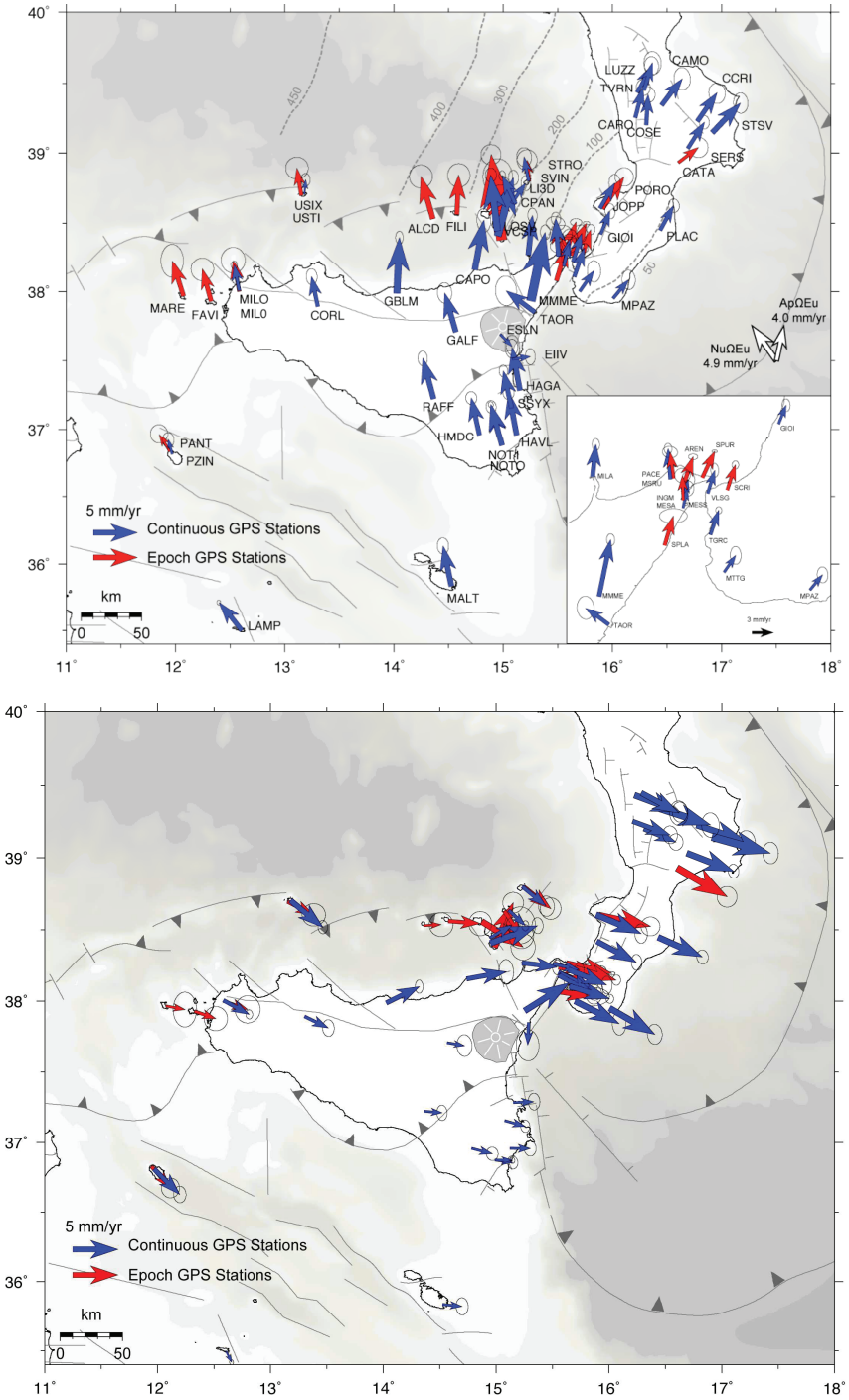

Figure 4.3: *GPS velocity field with respect to fixed Eurasian (top) and Nubian (bottom) frames. Error ellipses are at the 95% confidence level.*

dislocation geometry (parameterized by length, depth, width, dip, strike, and fault

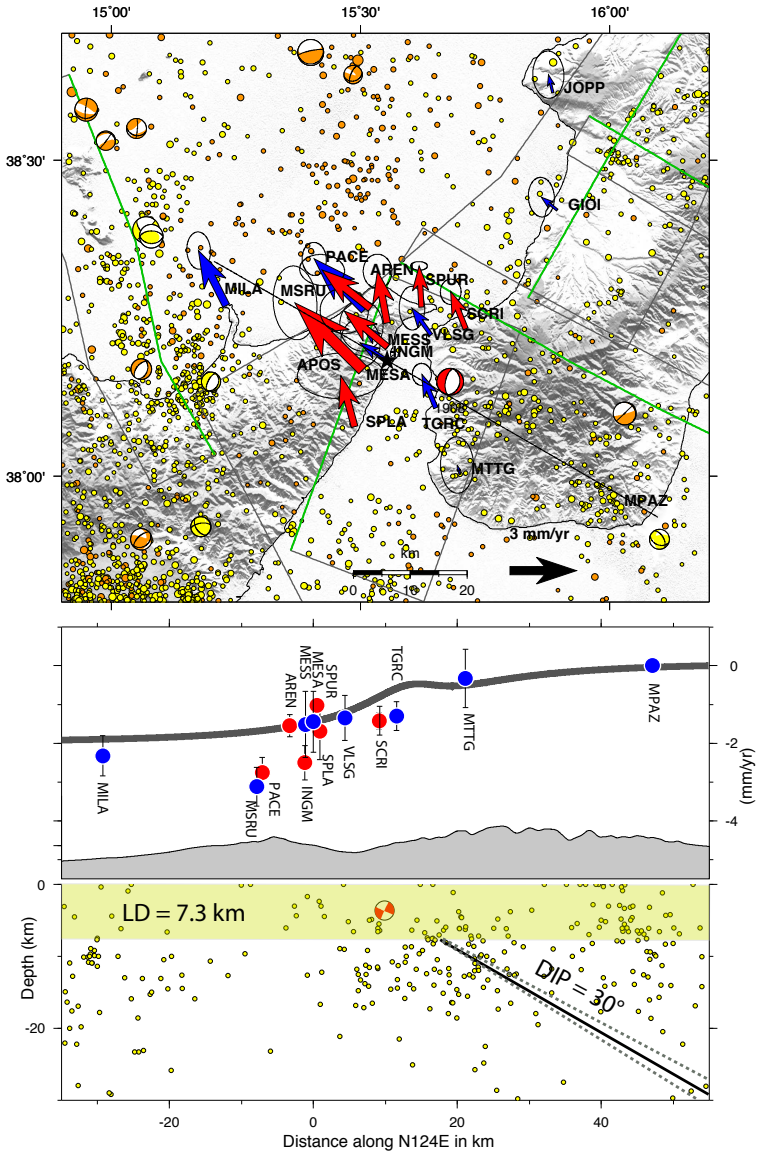

Figure 4.4: *top: horizontal observed velocities (w.r.t. station MPAZ, red and blu arrows show EGPS and CPGS stations, respectively) with 95% confidece elipses. Seismicity from the CSI-1.1 earthquake catalog* (Chiarabba et al., [2005]) *is also reported (yellow circle: seismicity within 0-30 km depth, orange circle: deeper seismicity). The dotted lines show the upper edge of the modeled dislocations at the locking depth, the grey boxes show active faults from the DISS database. Bottom: cross sections (N120° E) showing the modeled velocity gradient from optimal fault parameters (grey lines) and observed velocity values (red and blu circles, with uncertanties, show EGPS and CGPS stations, respectively). The fault dip angle is also shown with 95% confidence level lower and upper bounds computed using the bootstrap percentile method.*

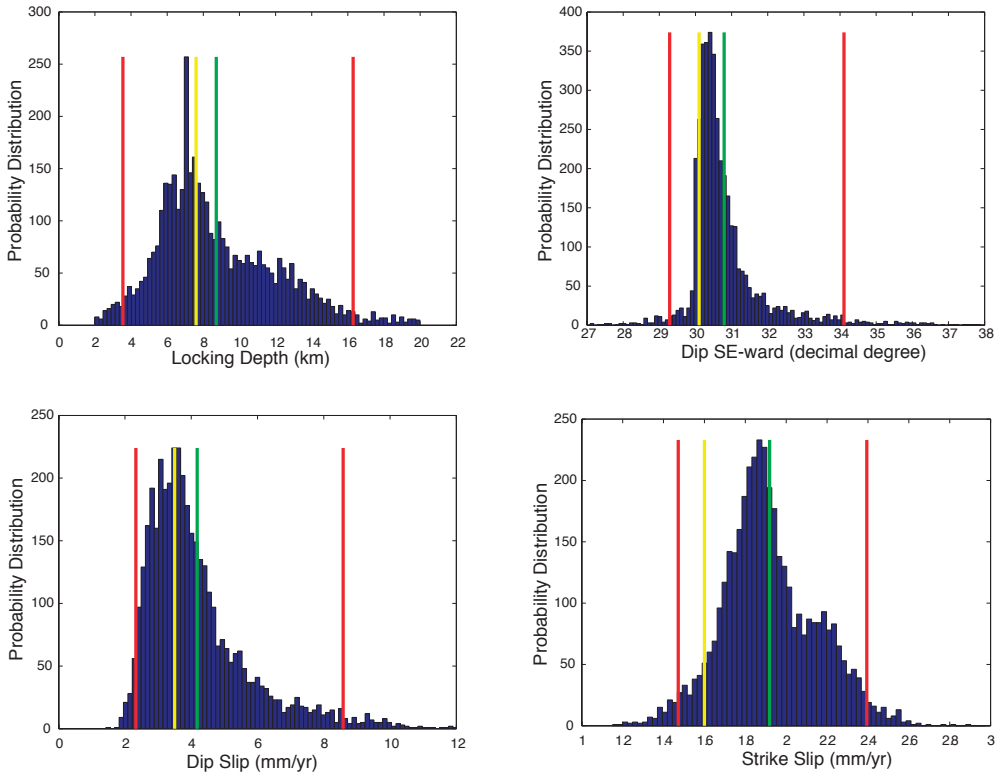

Figure 4.5: *Histograms of modeled Messina Straits fault parameters from 5000 bootstrap resamples of the data. Red lines mark values of 95% confidence level lower and upper bounds computed using the bootstrap percentile method. Green and yellow lines mark mean and optimal values of every parameter. The same parameters are listed in the table .*

edge location) and fault slip-rates (both dip-slip and strike-slip components). For a complete mathematical description of non-linear optmization algorithm see Appendix A

Our inversions aim to find model parameters that minimize the weighted residual sum of squares $WRSS = (d_{obs} - d_{mod})T \times cov - 1 \times (d_{obs} - d_{mod})$, where d_{obs} and d_{mod} are the observed and modeled motions, respectively and cov is the data covariance matrix. We use 14 stations (fig. 4.4) across the Straits and assume quasi-2D model geometry (i.e., we constrain the faults length and width to very large values). On the basis of the computed strain rate field shown in the fig. 2.7 we constrain the fault strikes to be perpendicular to the maximum extensional strain (i.e., ∼N34°E) and explore all other parameters.

To estimate the individual confidence intervals associated with the inverted model parameters, we employ a bootstrap method (*Arnadottir & Segall*, 1994), which establishes confidence intervals by randomly resampling from the data, with replacement, and running the parameter optimization n-times. Figure 4.5 displays histograms of the inverted model parameters obtained from 5000 random bootstrap

	LD (km)	**D SE-ward** (°)	**SS** (mm/yr)	**DS** (mm/yr)
Optimal model	7.6	30.1	1.6	3.5
Bootstrap	$8.8^{-5.1}_{+7.5}$	$30.08^{-1.5}_{+3.3}$	$1.9^{-0.4}_{+0.5}$	$4.1^{-1.8}_{+4.4}$

Table 4.1: *The upper row shows the values of optimally inverted model parameters estimated with the non-linear inversion algorithm. LD = locking depth, D= dip, SS = strike slip, DS = dip slip. The bottom row shows the mean values, obtained by running inversion with 5000 bootstrap re-samples of the original data, with 95% confidence level interval, estimated using the bootstrap percentile method* (Arnadottir & Segall, 1994).

resamples, together with the corresponding mean values and uncertainties. The optimal model fault geometries and slip-rates are reported in table 4.1 together with 95% confidence intervals estimated using the bootstrap percentile method.

We find that to first-order, the observed velocity gradient across the Straits can be explained by a single $30.1^{-0.7^\circ}_{+1.1}$ SE-dipping normal fault, locked at $7.6^{-2.9}_{+4.6}$ depth, and a dip-slip-rate of $-3.5^{-1.3}_{+2.0}$ mm/yr and a right-lateral slip-rate of $1.6^{-0.2}_{+0.3}$ mm/yr. Figure 4.4 shows observed velocities relative to station MPAZ, and the velocity profile across the Messina Straits, including the modeled velocity gradients from the inverted fault parameters. While observed CGPS velocities are well matched by the model velocity gradient, velocities of EGPS stations on the Sicilian side of the Messina network display larger residuals. MSRU and PACE, in particular, for which horizontal velocities are rather well constrained, display the largest residuals on a strike-perpendicular direction.

4.2.3 Elastic Block model

In the previous section we modeled the velocity gradient across the Messina Straits assuming it is due to single normal fault accumulating elastic strain. However, the area is surrounded by other active fault zones that are likely to be interseismically accumulating elastic deformation, among which the Tindari-Giardini fault system to the W, the Calabrian normal fault system to the NE and the Calabria subduction interface to the SE, are the most important ones (fig. 4.6, B). Unfortunately, our knowledge of the geometry and kinematics of these faults is quite incomplete (*Argnani et al.*, 2007; *Billi et al.*, 2006; *D'Agostino & Selvaggi*, 2004; *Ferranti et al.*, 2007; *Gutscher et al.*, 2006). As they are located offshore, and/or poorly covered by GPS networks, it is not possible to develop any optimal geometry and kinematic inversions outside investigated areas. However, we find that it is important to evaluate the impact of elastic strain fields from these faults on the inferred slip-rates of the Messina fault, especially from the far-reaching strain of the potentially seismogenic Calabrian subduction thrust.

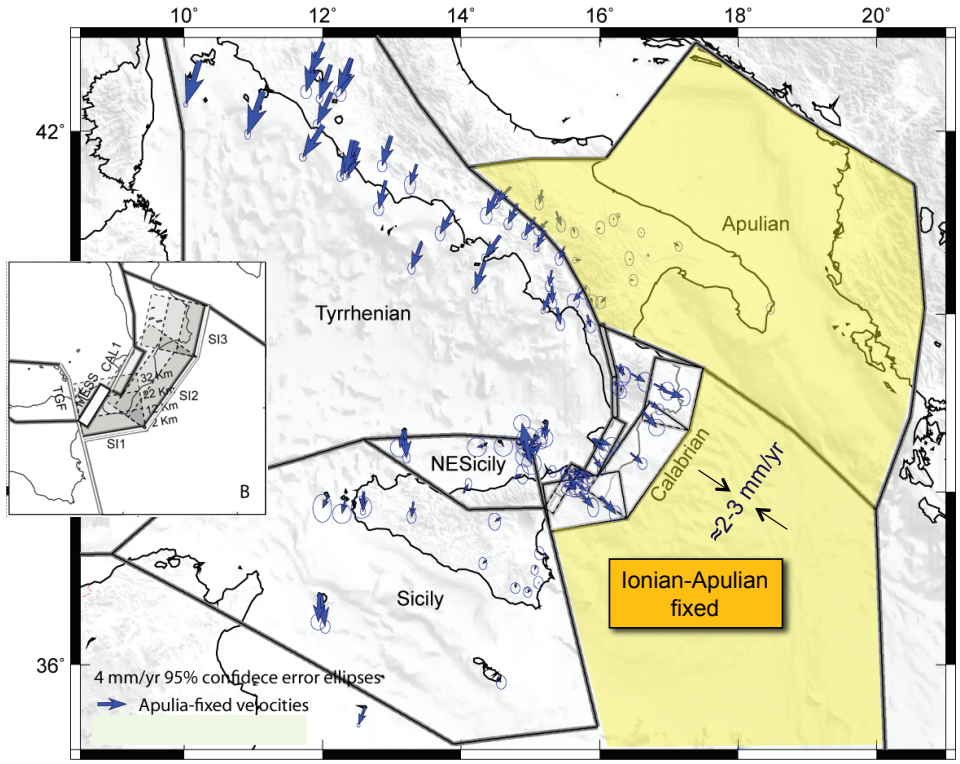

Figure 4.6: *Block model geometry and horizontal GPS velocities (with 95% confidence ellipses) rotated into the Apulia-fixed reference frame. Convergence rate across the Ionian-Calabrian subduction interface assuming the Ionian litosphere belonging to the Apulian plate is also shown. (B) Fault systems investigated in this work, keeping fixed the geometry of the Messina Fault (MESS) at the values obtained from the local dislocation model (tables 4.1). For the western Calabrian normal Fault system (CAL1) and the Tindari-Giardini Fault system (TGF) the locking depth varies from 0 to 20 km, whereas for the Calabrian subduction interface (Sl1, Sl2, and Sl3) the locking depth varies from 0 to 40 km.*

To test if the velocity gradient across the Messina Straits may be significantly modified by the elastic strain contribution from these three fault systems we use an elastic block-modeling approach that accounts for both crustal block rotations and strain accumulation at block-bounding faults (*Meade & Hager*, 2005). The spatial extent of surface interseismic strain of a block-bounding fault depends on its degree of coupling, which is parameterized by changing the width of its locked portion. Increasing the locking width increases the magnitude and reach of elastic deformation associated with the fault, which changes the optimal block rotation parameters and fault slip-rates in the optimal model. For each investigated fault system, we run suites of model inversions using different values of the locking depth, and evaluate the trade-off curves between the model reduced χ^2 and the faults slip-rates (the dip-slip component) as a function of increasing values of assumed locking depth.

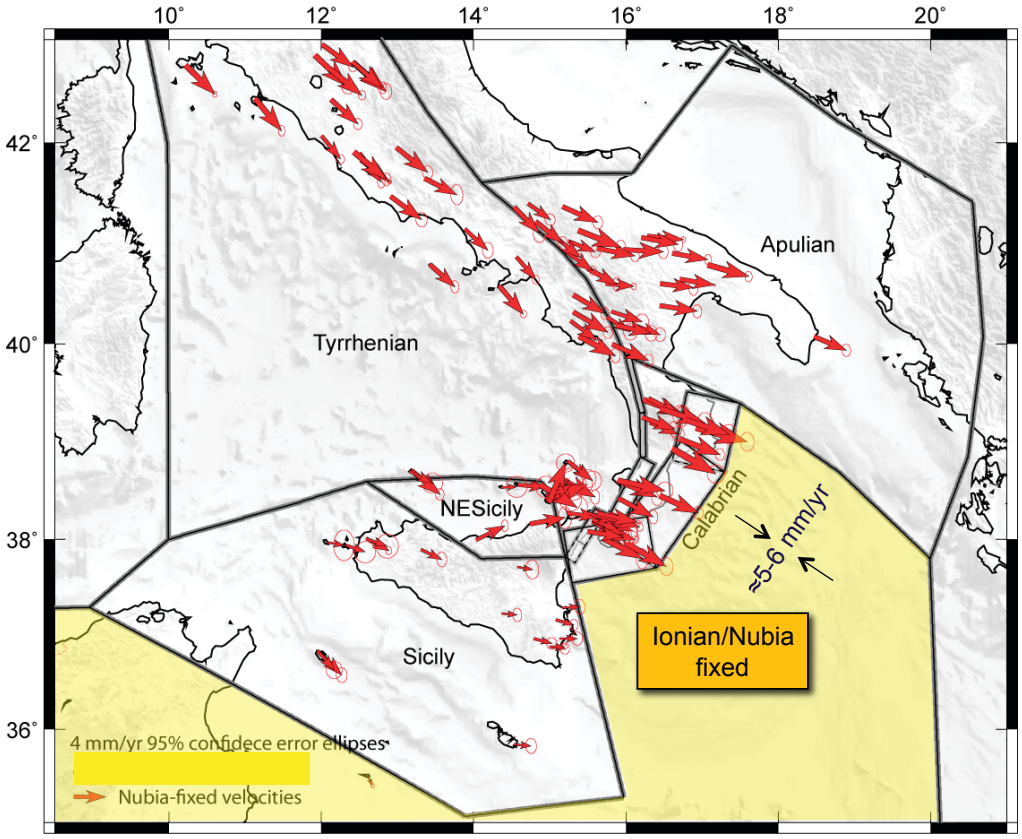

Figure 4.7: *Block model geometry and horizontal GPS velocities (with 95% confidence ellipses) rotated into the Nubia-fixed reference frame. The Ionian plate is assumed moving with Nubia. Ionian-Calabrian convergence rate is shown.*

Importantly, the convergence rates across the Ionian-Calabrian subduction interface differ by a factor of two depending on which plate the Ionian oceanic lithosphere belongs to. The SE-ward displacements of the Calabrian stations with respect to the Ionian block occur at rates of ∼5 mm/yr and ∼2.5 mm/yr with respect to Nubia or to the Ionian-Apulian plate, respectively (see figs. 4.6 and 4.7). Therefore, it is of fundamental importance for the evaluation of the seismic potential of the Calabrian region to understand how this convergence is eventually accommodated along the subduction interface, and if its deformation signal may be overprinted on the measured velocity gradient across the Messina Straits. An Ionian-fixed velocity field is the appropriate reference frame realization for our objective, allowing us to implement a relatively simple block geometry while accounting for the two end-member kinematic boundary conditions along the Ionian-Calabria plate contact. This is realized by implementing two different experiments (figs. 4.6 and 4.7), the first one considering the Ionian block as part of Nubia (i.e., using Nubia-fixed velocities), and the second one considering the Ionian block as part of the Apulian microplate (i.e., using Apulia-fixed velocities).

We use seismicity, fault maps (fig. 4.2), fault databases (*Basili et al.*, 2008, *Meletti et al.*, 2008) and other indicators of active deformation along the central Mediterranean Africa-Eurasia plate boundary (*Serpelloni et al.*, 2007) to define the model geometry (i.e., numbers of blocks, strike, dip and locking depths of block-bounding faults). We consider a relatively simple block configuration, where Sicily, Calabria, the Tyrrhenian lithosphere and the southern Adriatic region (i.e., Apulia) behave as independent blocks with respect to the Ionian lithosphere, used as the reference micro plate (fig. 4.6). A more detailed analysis of the microplate settings and kinematics of the study area is beyond the scope of this first part of the work, then we adopt the same block geometry (i.e., the same number of inverted parameters) with both experiments. In order to represent the Ionian-Apulian microplate, as proposed by *D'Agostino et al.*, (2008), when running the models with Apulia-fixed velocities we constrain the southern Adriatic block to not rotate with respect to the Ionian block.

We use vertical planar dislocations and a regional locking depth of 10 km, consistent with average depths to the base of crustal seismicity (*Chiarabba et al.*, 2005) and values reported in the **Database of Individual Seismogenic Sources (DISS)**[3], for all block-bounding faults, except for the Messina and Calabrian normal faults and the NW-ward dipping subduction interface (fig 4.6, B). For the Messina Straits fault we use the geometry (i.e., strike, dip and locking depth) derived from our local inversion (table 4.1). For the western Calabria normal fault system we adopt the geometry reported in the DISS database. The subduction interface is parameterized by three 20° NW-dipping planes, whose first-order representation has been obtained from the analysis of cross sections of instrumental seismicity across the Calabrian Arc, and geological and geophysical data (*Cernobori et al.*, [1996]) together with general constraints from slab geometry. Importantly, as we effectively model the shear zone down-dip of a zone assumed to be fully locked, we cannot address to what degree shallow, distributed or localized accretionary-wedge deformation occurs interseismically.

Figure 4.8 shows that changing the degree of coupling of the Tindari-Giardini Fault system (A and A') does not significantly affect the slip-rates of the Messina fault, and the impact on the reduced model χ^2 is minimal for both kinematic boundary conditions. Changing the degree of coupling of the western Calabria normal fault system (B and B' in fig. 4.8) also has little impact on the model χ^2; however, slip-rates of the Messina fault increase by about 1 mm/yr for both kinematic boundary conditions, as the imposed locking width changes from 0 to 20 km on the western Calabria normal faults. On the contrary, we find that changing the locking width of the subduction interface (C and C' in fig. 4.8) has a large impact on the model χ^2 statistics and on the Messina fault slip-rates for both kinematic boundary conditions.

Inferred dip-slip-rates on the Messina fault are strongly impacted by the assumed locking width of the Calabrian subduction thrust. Assuming that the Ionian litho-

[3] http://diss.rm.ingv.it/dissNet/

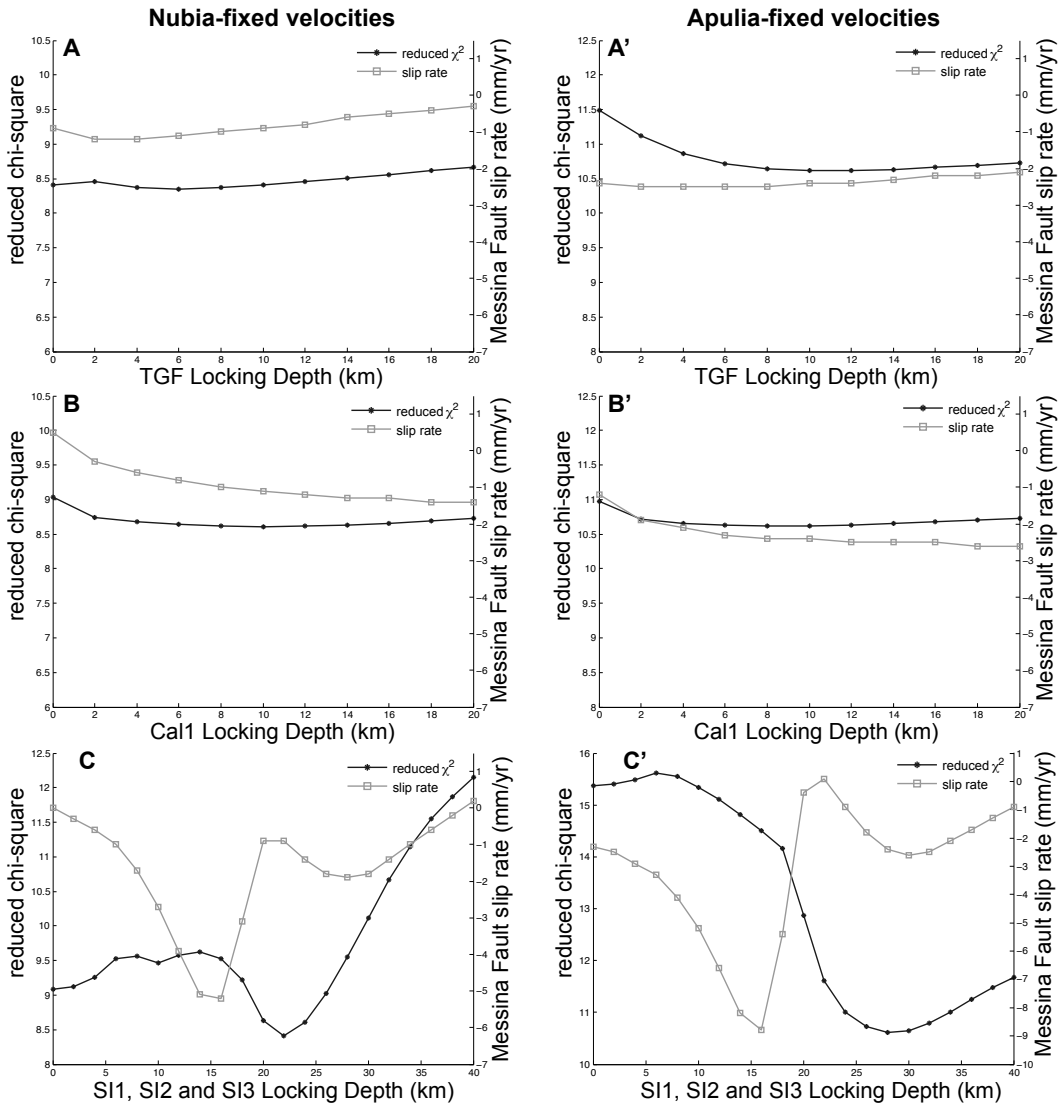

Figure 4.8: *Plots of the variation in the reduced chi-square values (black lines) and Messina Fault dip slip-rates (grey lines; negative values correspond to extension) obtained from the block-modeling by varying the locking depths of the Tindari-Giardini Fault system from 0 to 20 km, the western Calabria normal fault system from 0 to 20 km, and the Calabrian subduction interface from 0 to 40 km. (Left) Results obtained using Nubia-fixed velocities (fig. 4.7). (Right) Results obtained using Apulia-fixed velocities (see fig. 4.6).*

sphere is moving with the Nubian plate, the optimal Messina dip-slip rate varies between ∼0 and -5 mm/yr as the subduction interface locking width is changed (fig. 4.8). The slip-rate corresponding to the model χ^2 minima (reached for a 22 km locking depth, or 64 km down-dip width) is ∼-1 mm/yr, whereas a subduction in-

terface locked to only 16 km results in a -5 mm/yr value. Assuming that the Ionian lithosphere is moving together with the Apulian microplate, the Messina Fault dip-slip-rate varies between 0 and -9 mm/yr. In this case, the χ^2 minima is reached for a locking depth of 28 km of the subduction interface (i.e., 81 km down-dip width), with a dip-slip-rate of the Messina Fault of -2.5 mm/yr. It is worth noting that in both cases, the block-modeling inferred Messina Fault slip-rate is smaller than the slip-rate obtained from optimal inversion of the local horizontal velocities in the previous section.

4.3 Crati Valley Fault

In the light of the increased availability of GPS data in the study area, the same approach described above for the Messina Straits, was applied to study the inter-seismic strain accumulation across the Crati Valley (fig. 4.2), a region where the data coverage, during the previous phase of the work was not sufficient for local analysis.

4.3.1 Tectonic setting

The Crati Valley fault extends along the N-S direction for about 40 km and separates the Catena Costiera mountain range from the sedimentary basin of the Crati Valley (figs. 4.9 and 4.10). The N-S trending Crati basin represents the most prominent structural feature associated with the postorogenic extensional tectonics in north Calabria (*Cifelli et al.*, 2007). Its structural architecture is defined by an overall half-graben geometry, bounded to the west by eastward dipping ($60° - 80°$), N-S striking extensional faults, bordering the Coastal Range at its eastern side. In plan view, the border faults show a composite pattern, consisting of subordinate NE-SW and NW-SE striking fault segments. In particular, in the northwestern sector of the Crati basin, the fault array shows a complex pattern of interfering, nearly orthogonal NE-SW and NW-SE striking extensional fault strands. The boundary of the Crati basin is given by the ENE-WSW oriented Pollino fault, which separates the Crati basin from the Pollino structure, which forms the southern part of the southern Apennines thrust belt. In the central and southern Crati basin, two main normal fault systems have been recognized: a major northwest dipping NE-SW striking extensional fault systems and a N-S striking high-angle, conjugate extensional fault arrays. The greater amount of extension in the early stages of basin formation was primarily accommodated by westward dipping NE-SW low-angle extensional faults. Conversely, the N-S striking extensional fault systems overprinted this deformation pattern reconstructed from the Miocene deposits, and it is characterized by high-angle faults (Cifelli et al., 2007).

The present fault system is represented by three main fault segments, starting from the north: Fagnano Castello fault, S. Marco Argentano-S. Fili fault and Montalto Uffugo-Rende fault (fig. 4.9). The fault planes dip steeply towards the east and develop at the base of the mountain range (*Tortorici et al.*, 1995). The major

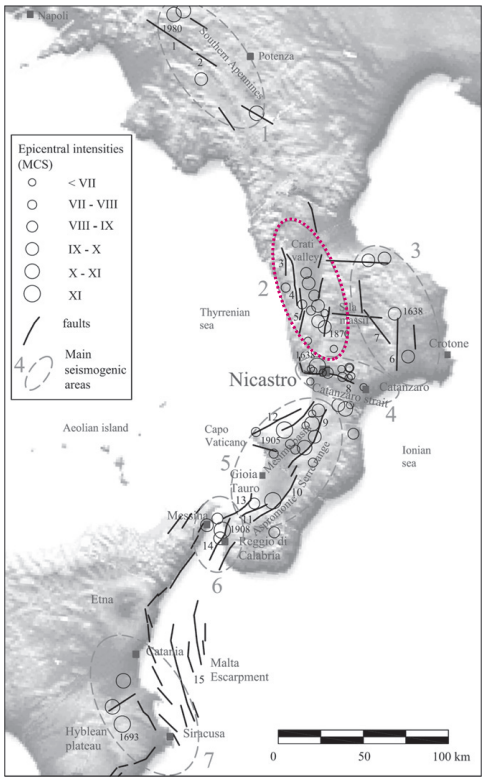

Figure 4.9: *Shaded relief of Southern Italy with principal historical seismic events felt in Nicastro and main seismogenic sources in the region. We report only those of interest of this thesis. 4, S. Marco Argentano-S. Fili; 5, Montalto Uffugo-Rende; 6, Marchesato. From* (Pagliaroli & Lanzo, 2008).

historical event associated to this area is the 1870 Cosenza earthquake (I_0 = IX-X MCS and M_S = 6.3) that may be related to the activity of Montalto Uffugo-Rende fault. Focal mechanisms of the main instrumental events in the area show a clear estentional tectonic all along the eastern Calabrian coast (fig. 4.10) (*Cifelli et al.*, 2007).

4.3.2 Strain accumulation analysis

GPS data show that an extentional velocity gradient of about 2 mm/yr is accomodated across the Crati Basin and Sila Massif. Velocity vectors from GPS stations lying in this region undergo a clockwise rotation of about 30° from ∼N-ward to NE-ward moving from west to east (fig. 4.3).

Again, assuming that all the observed velocity gradient is due to the strain accumulation on a singole fault, we use an elastic dislocation model approach to invert velocities from 10 GPS stations wich form a transect extending about perpendicular to the Crati Valley. We constrain the fault strike to be normal to the maximun strain rate direction (∼N-S, fig. 2.7) and, using a constrained, non-linear

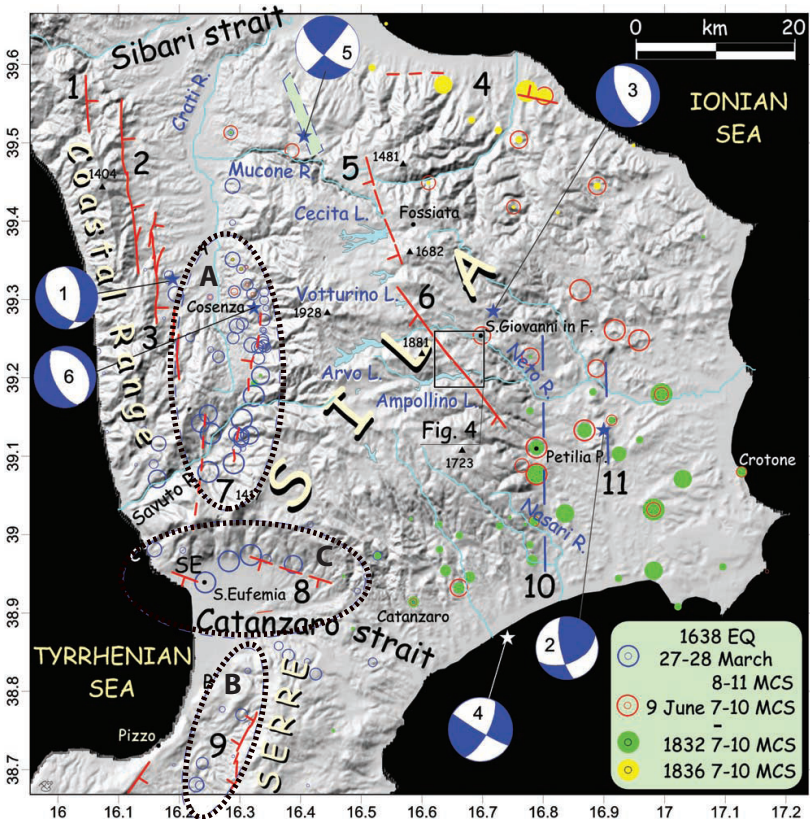

Figure 4.10: *Shaded relief of northern Calabria. HIDD of 1638 events is shown together with that of 1832 and 1836 (modified from* Boschi et al. (2000) *and* Monachesi & Stucchi, (1998)*, respectively) (intensities proportional to dimension of circles; see symbols in legend). Dashed ellipses A-C show tentatively the epicentral areas of the three main shocks occurred between 27 and 28 March 1638. Blue stars are the location of the main instrumental events (ML = 4-4.5) with related focal mechanisms (1, 20 February 1980, ML = 4.3; 2, 24 January 1990, ML = 4.5; 3, 24 April 1991, ML = 3.9; 4, 26 March 1994, ML = 4.1; 5, 27 April 1996, ML = 4.0; 6, 18 October 2001, MW = 4.4). Red lines are the primary, possibly active faults of the region. From* (Galli & Bosi, 2003).

optimization algorithm, invert for the other fault plane geometric parameters and slip-rates.

We realize 5000 random resamples with replacement of the original dataset to estimate the 95% confidence interval associated with the inverted parameters using the bootstrap percentile method. We run 5000 optimal inversions and find the modeled parameters distributions shown in figure 4.14. The figure also shows the values of 95% confidence level lower and upper bounds and mean and optimal values of every parameter. The same parameters are listed in the table 4.2.

The observed velocity gradient accros the Crati Valley seem to be quite well modeled by a $60.1^{-3.1}_{+2.1}{}^{\circ}$ W-dipping normal fault, locked at $6.1^{-4.3}_{+4.8}$ depth, and an extentional dip-slip-rate of $3.8^{-1.6}_{+2.0}$ mm/yr and a right-lateral slip-rate of $0.3^{-0.2}_{+0.3}$ mm/yr. Figure 4.12 shows observed velocities relative to the station CETR and the

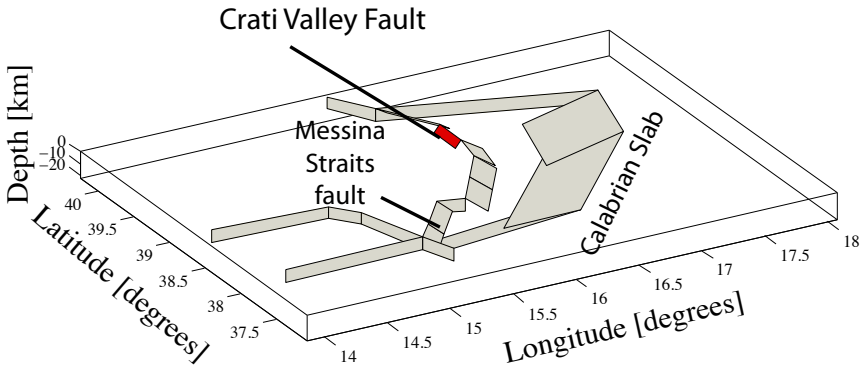

Figure 4.11: *3D block model used in the second part of the work to study the Crati Valley fault system.*

modeled velocity gradients from the inverted fault parameters. We can conclude that a good fit is reached in the western portion of the profile, while bigger residuals interest the area from the Sila Massif to the eastern coast. A possible explanation is the presence of another structure boarding the eastern side of the Sila Massif, the so-called Marchesato fault, a normal structure that some authors describe as possible still active (*Moretti*, 1999, *Pagliaroli & Lanzo*, 2007). We tried to add this structure into the model and the fit was significantly improved. However, because of the small number of data, the model parameters are not well constrained and we cannot discriminate among different solutions.

As for the Messina Straits, to investigate if the observed velocity gradient across the Crati Valley and Sila Massif could be affected by the elastic contribution from nearby active structures we use a block model approach (*Mead & Loveless*, 2009). The study of this structure, was not included in the purpouses of the first section of the work, so it was not modeled at the best. Now, based on available informations (i.e. *Cifelli et al.*, 2007; *Monaco & Tortorici*, 2000) we slightly modify the block geometry previously used. We replace the two segments north of the western Calabrian normal Fault system (CAL1) with three smaller segments, the central one of wich, represents the Crati Valley fault (fig 4.11). We parametrize the Crati Valley fault using the parameters value obtained from the previous local inversion (tab. 4.2). All the other faults are parametrized as in the Messina Straits experiment.

Again we realize sets of test varying the locked portion of the western Calabrian normal Fault system (CAL1) (fig 4.6, 1) and the Tindari-Giardini Fault system (TGF) from 0 to 20 km and of the Calabrian subduction interface (Sl1, Sl2, and Sl3) from 0 to 40 km. We run all the tests while accounting for both the end-member kinematic boundary conditions along the Ionian-Calabria plate contact,

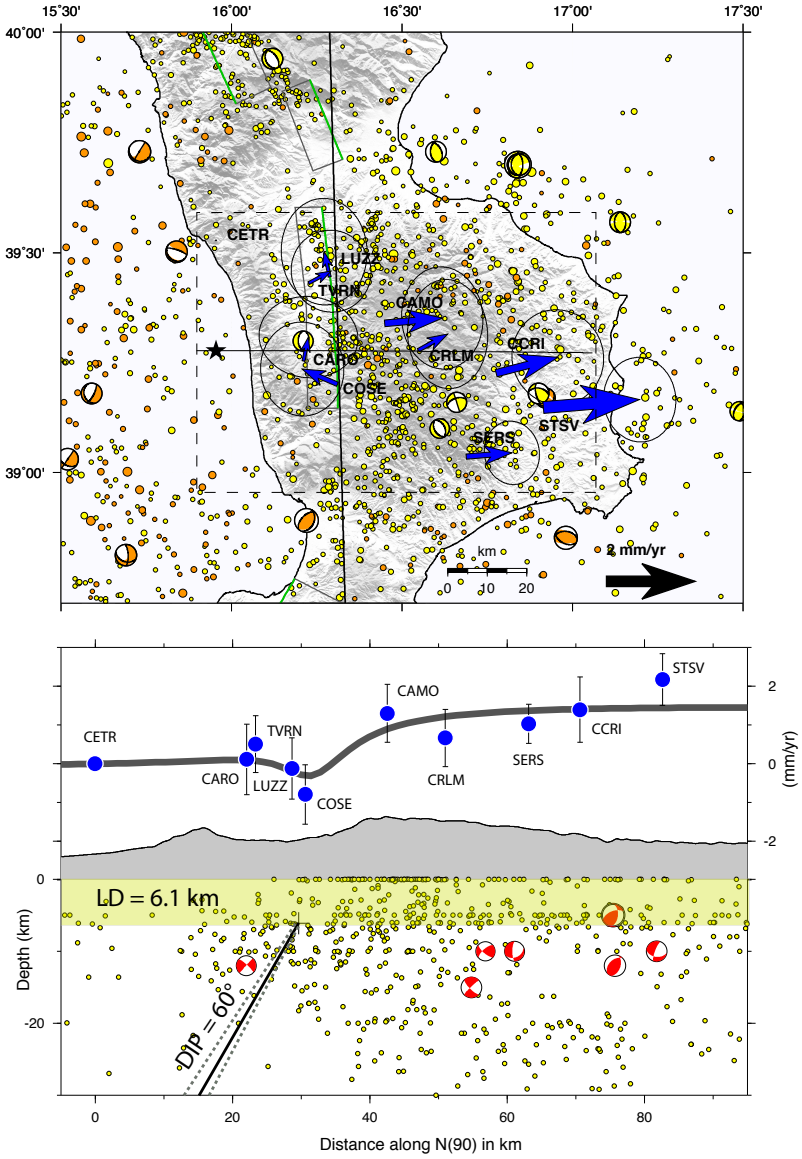

Figure 4.12: *As in the fig. 4.4. Horizontal observed velocities are w.r.t. station CETR and the cross section is N-S oriented.*

that is considering the Ionian block as part of Nubia and as part of the Apulian microplate.

Looking at the χ^2 and slip-rate variation we find no significant variation of the Crati Valley fault slip-rates changing the degree of coupling of the Tindari-Giardini and western Calabria fault systems for both the analyzed boundary conditions. Conversely, we find that changing the locking width of the subduction interface has a large impact on the model χ^2 statistics and on the Crati Valley fault slip-rates (fig. 4.13). The slip-rate value varies between ∼-3 and ∼-9 mm/yr and between -3 and∼

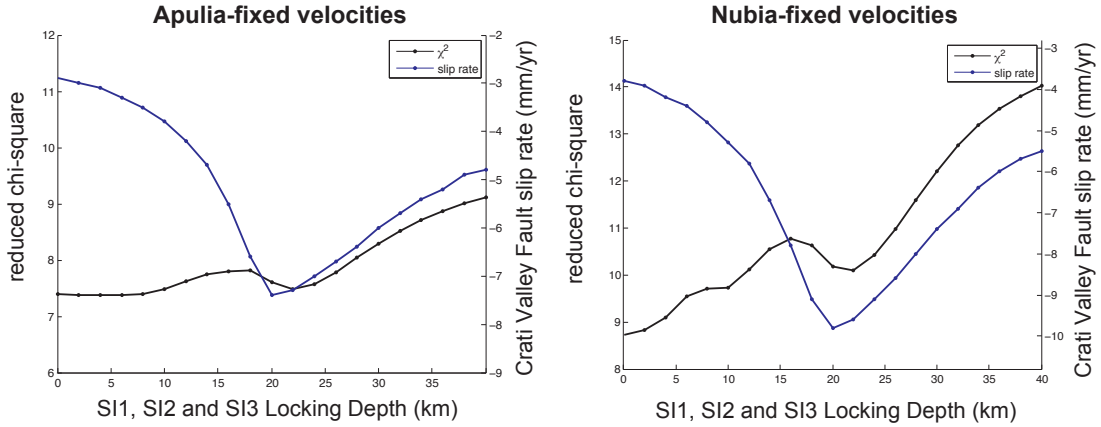

Figure 4.13: *Plots of the variation in the reduced chi-square values (black lines) and Crati Valley Fault dip slip-rates (blue lines; negative values correspond to extension) obtained from the block-modeling by varying the locking depths of the Calabrian subduction interface from 0 to 40 km. (Left) Results obtained using Apulia-fixed velocities (fig. 4.6). (Right) Results obtained using Nubia-fixed velocities (see fig. 4.7).*

-7 mm/yr assuming Nubia fixed and Apulia fixed velocities, respectively. Unlike what found previously, model χ^2 statistic shows that the model that best fits the new GPS data is a model with subduction zone minimal locking depth corrispondig to a dip-slip-rate of ∼-3 mm/yr for both the kinematic boundary conditions.

4.4 Discussion and conclusion

We use data from permanent GPS networks and a smaller aperture non-permanent GPS network to study the kinematics and active strain accumulation in the area affected by the destructive 1908 Messina-Reggio Calabria, Mw = 7.1, earthquake and across the Crati Valley. GPS velocities define a well constrained kinematic pattern (fig. 4.3), where, in a fixed Eurasian reference frame, stations located in Sicily move NW-ward at an average rate of ∼4.5 mm/yr, whereas stations in Calabria move NE-ward at average rates of ∼3.2 mm/yr. Faster N-ward motion rates are observed in NE-Sicily, whereas across the Peloritani Mountains and the Messina Straits velocities rotate from N-ward to NE-ward, and this trend continues along Calabria. In northern Calabria, GPS data show that an extentional velocity gradient of about 2 mm/yr is accomodated across the Crati Valley and Sila Massif. Velocity vectors from GPS stations lying in this region undergo a clockwise rotation of about 30° from ∼N-ward to NE-ward moving from west to east.

Assuming that the observed velocity gradient across the Messina Straits and

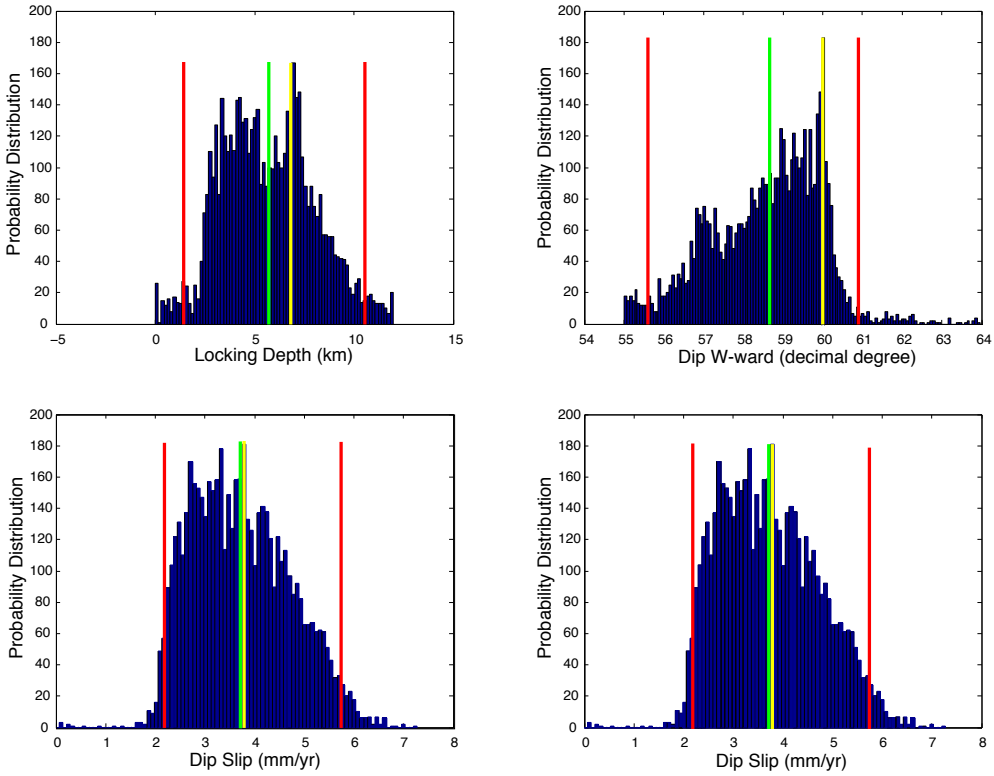

Figure 4.14: *Histograms of modeled Crati Valley fault parameters from 5000 bootstrap resamples of the data. Red lines mark values of 95% confidence level lower and upper bounds computed using the bootstrap percentile method. Green and yellow lines mark mean and optimal values of every parameter. The same parameters are listed in the tables* **??**.

Crati Valley (figs. 4.4 and 4.12) is due to slip on a single planar dislocation locked above a certain depth and that all strain that accumulates interseismically is elastic, we develop a simple dislocation model of the deformation. We use a non-linear constrained optimization algorithm to invert for the fault locking depth, dip, upper-edge location and slip-rate, constraining the fault strike to be normal to the estimated extensional deformation. We find that the observed velocity gradient across the Messina Straits can be explained by a single $30.1^{-0.7}_{+1.1}{}^{\circ}$ SE-dipping normal fault, locked at $7.6^{-2.9}_{+4.6}$ depth, and a dip-slip-rate of $-3.5^{-1.3}_{+2.0}$ mm/yr and a right-lateral slip-rate of $1.6^{-0.2}_{+0.3}$ mm/yr. While the observed velocities across the Crati Valley seem to be well modeled by a $60.1^{-3.1}_{+2.1}{}^{\circ}$ W-dipping normal fault, locked at $6.1^{-4.3}_{+4.8}$ depth, and an extentional dip-slip-rate of $3.8^{-1.6}_{+2.0}$ mm/yr and a right-lateral slip-rate of $0.3^{-0.2}_{+0.3}$ mm/yr. Uncertainties associated with the modeled fault plane geometry and slip-rates have been evaluated adopting a bootstrap approach (figs. 4.5 and 4.14).

The results of our local dislocation analysis across the Straits provide some clues about the geometry and kinematics of the fault responsible for the 1908 Messina-

	LD (km)	**D W-ward** (°)	**SS** (mm/yr)	**DS** (mm/yr)
Optimal model	6.1	60.1	0.3	3.8
Bootstrap	$5.7^{-4.3}_{+4.8}$	$58.7^{-3.1}_{+2.1}$	$0.3^{-0.2}_{+0.3}$	$3.8^{-1.6}_{+2.0}$

Table 4.2: *The upper row shows the values of optimally inverted model parameters estimated with the non-linear inversion algorithm. LD = locking depth, D= dip, SS = strike slip, DS = dip slip. The bottom rows show the mean values, obtained by running inversion with 5000 bootstrap re-samples of the original data, with 95% confidence level interval, estimated using the bootstrap percentile method* (Arnadottir & Segall, 1994).

Reggio Calabria earthquake. The continuation of the modeled fault plane (see fig. 4.4) in the upper 7-8 km agrees rather well with the NE-SW oriented gently SE-ward dipping fault plane proposed by several authors as the fault segment that ruptured during the Messina earthquake (see *Pino et al.*, (2009) for a summary). Recent compilations of geological and tectonic data (DISS) suggest a long-term geological slip-rate of 1-2 mm/yr, which is consistent with the interseismic slip-rate derived in our analysis. The discrepancy, in fact, stands still within the 95% confidence bounds provided by our bootstrap analysis of model uncertainties (table 4.1).

In order to frame the observed local deformation features within the present-day microplate kinematics, we use an elastic block-modeling approach that, taking into account both crustal blocks rotations and elastic strains at block-bounding faults, allows to investigate the impact of elastic strain contributes from other nearby active faults onto the velocity gradient measured across the Messina Straits and Crati Basin. We develop a block geometry allowing the Tyrrhenian, Sicily and NE-Sicily, Calabria, and Apulia blocks to move independently, or partially independently, with respect to a fixed Ionian block that is moving either with the Nubian or Apulian plate. Using Nubia-fixed or Apulia-fixed velocities (figs. 4.6 and 4.7) allows us to account for both end-members kinematics along the Sicily-Calabria plate boundary (e.g., *D'Agostino et al.*, 2008; *Serpelloni et al.*, 2007).

Both models match the horizontal velocity data quite well and suggest that the elastic contribution of the Tindari-Giardini fault system and the western Calabria normal fault system on the inverted slip-rates of the Messina Straits and Crati Valley faults, is minimal or negligible. In contrast, both models predict elastic strain accumulation on the subduction interface, offshore Calabria, and show that the inferred slip-rates on the two analyzed structures are strongly impacted by the assumed locking width of the Calabrian subduction thrust, increasing the uncertainties of fault slip-rates estimated from geodetic data.

Chapter 5

Central Mediterranean kinematic analysis from elastic block modeling and statistical tests

5.1 Introduction

In the ligth of a new and increased GPS data availability we run some statistical tests with the aim to investigate the present day kinematics of plates and microplates composing the central Mediterranean region. A detailed kinematic analysis was behind the goals of the previous stage of the work. We use GPS velocities and block modeling approach because, although determining the angular velocity of a rigid block on a sphere is usually sufficient to study plate kinematics, the short interval spanned by GPS observations and proximity of some stations to the block boundaries require us to consider the effects of interseismic elastic strain accumulation (*Murray & Segall*, 2001).

Geological and seismic data suggest a fragmentation of the central Mediterranean region in several microplates and GPS velocities indicate their independent motion from Eurasian and Nubian blocks.

We propose five different block models, making move independently, the Adriatic, Calabrian and Sicilian plates, and compare them by performing F-ratio tests (*Gordon et al.*, 1987) on the model χ^2_ν (chi square per degrees of freedom).

5.2 Previous works

Many different hypotheses have been made in the previous works about the kinematic of microplates lying in the central Mediterranean area within the Africa-Eurasia collision zone. However, because of the complexity of active deformation in the area and of the lack of any clear decoupling fracture marking the transition between the Nubia and Eurasian plates, the issue is still debated and a general consensus has not yet been reached.

The tectonic evolution of the central Mediterranean was profoundly influenced by Adria, a block of continental lithosphere underlying Italy, Sicily, and the Dinarides, that behaved as a tectonic indenter during convergence between Africa and Europe (*Channell & Horvath*, 1976). Many authors focused their investigations

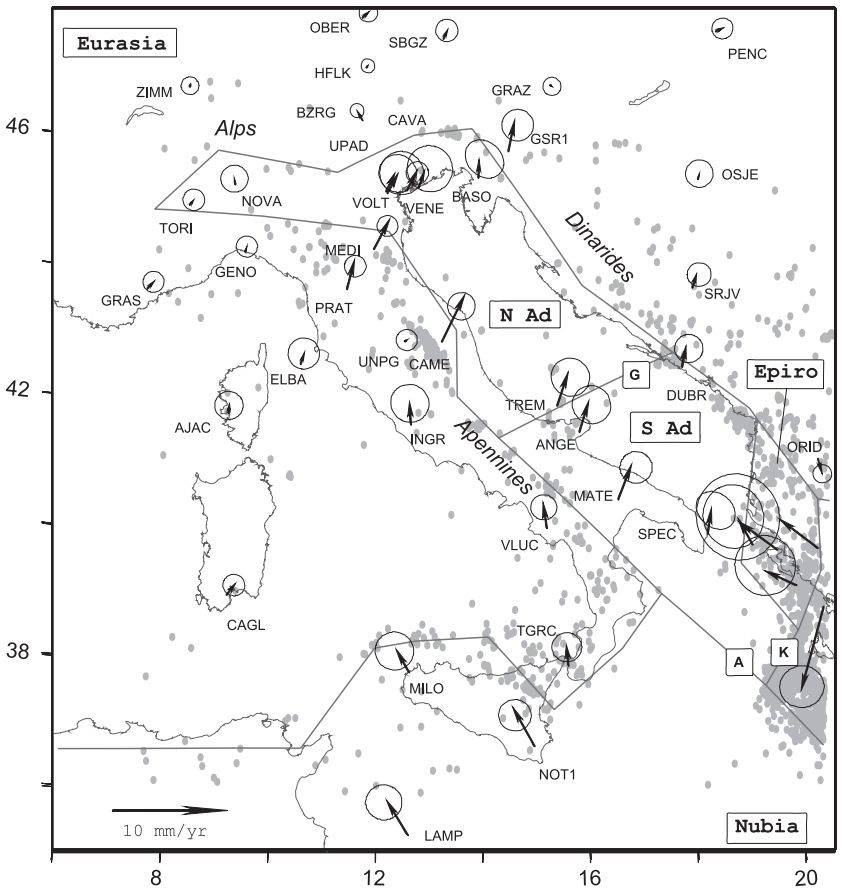

Figure 5.1: *Location of the segments (solid lines) and blocks used to model the Adriatic region. (N Ad) North Adria, (S Ad) South Adria. (G) Gargano-Dubrovnik fault zone; (K) Kefallinia fault zone; (A) Apulia escarpment. From* (Battaglia et al., 2004).

on the Adriatic block kinematics proposing two opposite points of view: Adria as a promontory of Africa and as an independent microplate between Nubia and Eurasia.

Geomagnetic data averaged over several Myr, *Sn* shear wave propagation observations (*Mantovani et al.*, 1990, *Channell*, 1996; *Mele*, 2001), the reconstruction of past relative plate positions (*Dewey et al.*, 1989; *Mazzoli & Helman*, 1994; *Wortmann et al.*, 2001; *Rosenbaum et al.*, 2002) and the absence of differential paleomagnetic rotations (*Channell*, 1996; *Rosenbaum et al.*, 2004) have been used as arguments to support the first hypotesis.

Whereas seismological and space geodetic studies now converge in the definition of the Adriatic region as moving independently relative to both Eurasia and Africa. *Calais et al.*, (2002) and *Battaglia et al.*, (2004) have shown that the velocities of GPS sites within the Adriatic region are consistent with a counterclockwise rigid rotation relative to Eurasia about a pole located in the Po Valley. *Calais et al.*, (2002),

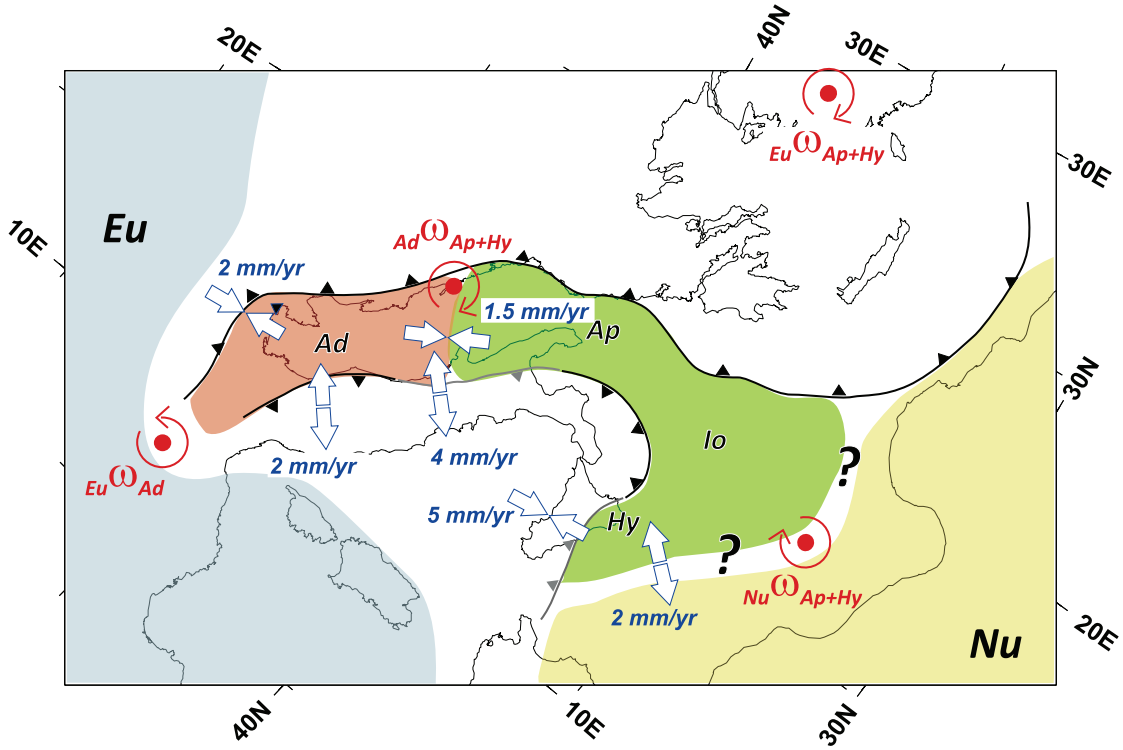

Figure 5.2: *Seismotectonic sketch of the microplate subdivision of the Adriatic Promontory. The Po Valley and the northern Adriatic Sea define the Adria microplate (Ad, in brown), while the Apulia Promontory, the Ionian Sea, and the Hyblean Plateau define an additional single microplate (Ap+Io+Hy, in green). Converging and diverging arrows represent regional directions of shortening and extension, respectively, with labeled predicted deformation rates. The yellow and light blue regions represent the geographical extent of the Nubia and Eurasia plates, respectively. Black lines with triangles show active subduction/collision zones, while gray ones indicate inactive subduction/collision. From* (D'Agostino et al., 2008).

Oldow et al., (2002) and *Battaglia et al.*, (2004) also propose a separation between the northern and the southern Adriatic region along a tectonic structure known as the Gargano-Dubrovnik line (fig. 5.1). However, because the Adriatic-Africa transition is not marked by any clear decoupling fracture or by any interruption of lithological facies along the marginal belts (Apennines-Maghrebides and Dinarides-Hellenides) (*Mantovani et al.*, 1990), substantial uncertainty remains regarding the southward extent of Adria and its southern boundary with Nubia. *Battaglia et al.*, (2004) and *Serpelloni et al.*, (2005), place the boundary along the Apulia Escarpment while other authors resolve the need of a direct boundary between Adria and Nubia suggesting that Apulia forms a single microplate with the Ionian Sea and possibly

with the Hyblean Plateau (*D'agostino et al.*, 2008) (fig. 5.2) or considering diffuse deformation in the Ionian Sea (*Goes et al.*, 2004).

GPS velocities charaterizing the stations lying in the Sicilian and Calabrian domains have been differently interpreted by different authors. Eurasia and Nubia-fixed residual velocities in Calabria suggest to *D'Agostino & Selvaggi*, (2004) the presence of an intermediate crustal block which can be interpreted as a forearc sliver or as an independent Ionian block while no independent motion is expected from their model for the Sicilian region. Conversely *Serpelloni et al.*, (2007) hypotize a microplate like behaviour of Pelagian-Sicily region, in agreement with the presence of a decoupling zone corresponding to the distributed deformation between Tunisia and Sicily. They, also, interpret the SE-ward displacements of Calabrian stations with respect to Nubia as evidence that convergence is still occurring or, alternatively, that the Ionian basin may be presently moving independently, or partially independently, from the Nubian plate. Supporting the latter hypothesis, the NE-ward drift of Calabrian stations with respect to Eurasia has been interpreted by *Goes et al.*, (2004) in the framework of recent plate reorganization, causing the Calabrian and Ionian domains to be coupled and driven E-ward by the Hellenic slab pull. In the light of a denser GPS velocity field *D'Agostino et al.*, (2011), extending the analysis of *D'Agostino et al.,* (2008), suggest that the subaerial portions of the Apulian-Ionian-Hyblean foreland do not behave in a homogeneous kinematic way but are fragmented in different crustal blocks independent of the Nubia plate. Moreover they statistically argue that the Apulian and Hyblean blocks cannot be regarded as belonging to the same microplate.

5.3 Microplates geometries

Loocking at the horizontal GPS velocity fields shown in the figures 5.4 and 5.5 we can see residual velocities of a few mm/yr within all our modeled microplates (much faster velocities charaterize the hellenic domain) both, in the Eurasian and Nubian reference frame. We read that as an evidence of independent motion. GPS velocities also show distinct motion for the individual microplates.

Moving from south to north we can observe a sudden change, charaterizing both magnitude and direction, in the velocity field with mean motion of 5 mm/yr ∼NNW-ward (Eurasia fixed) and 3 mm/yr ∼NE-ward (Nubia fixed) in the Sicilian domain and 3 mm/yr ∼NE-ward (Eurasia fixed) and 4 mm/yr ∼ESE-ward (Nubia fixed) in Calabria. A clear change is also visible crossing the Appennine chain. The western block motion is representative of the Thirrenyan crust kinematics and the GPS stations lying on it are about uniformely moving with a mean rate of 2.5 mm/yr ∼NNE-ward and 5 mm/yr ∼SE-ward w.r.t. Eurasia and Nubia, respectively. Region east of Appenines, instead, seems to be kinematically fragmented in several blocks. A velocity gradient is observed moving from the Po Valley to the Apulian block along the Adriatic region with velocities increasing and rotating from N-ward

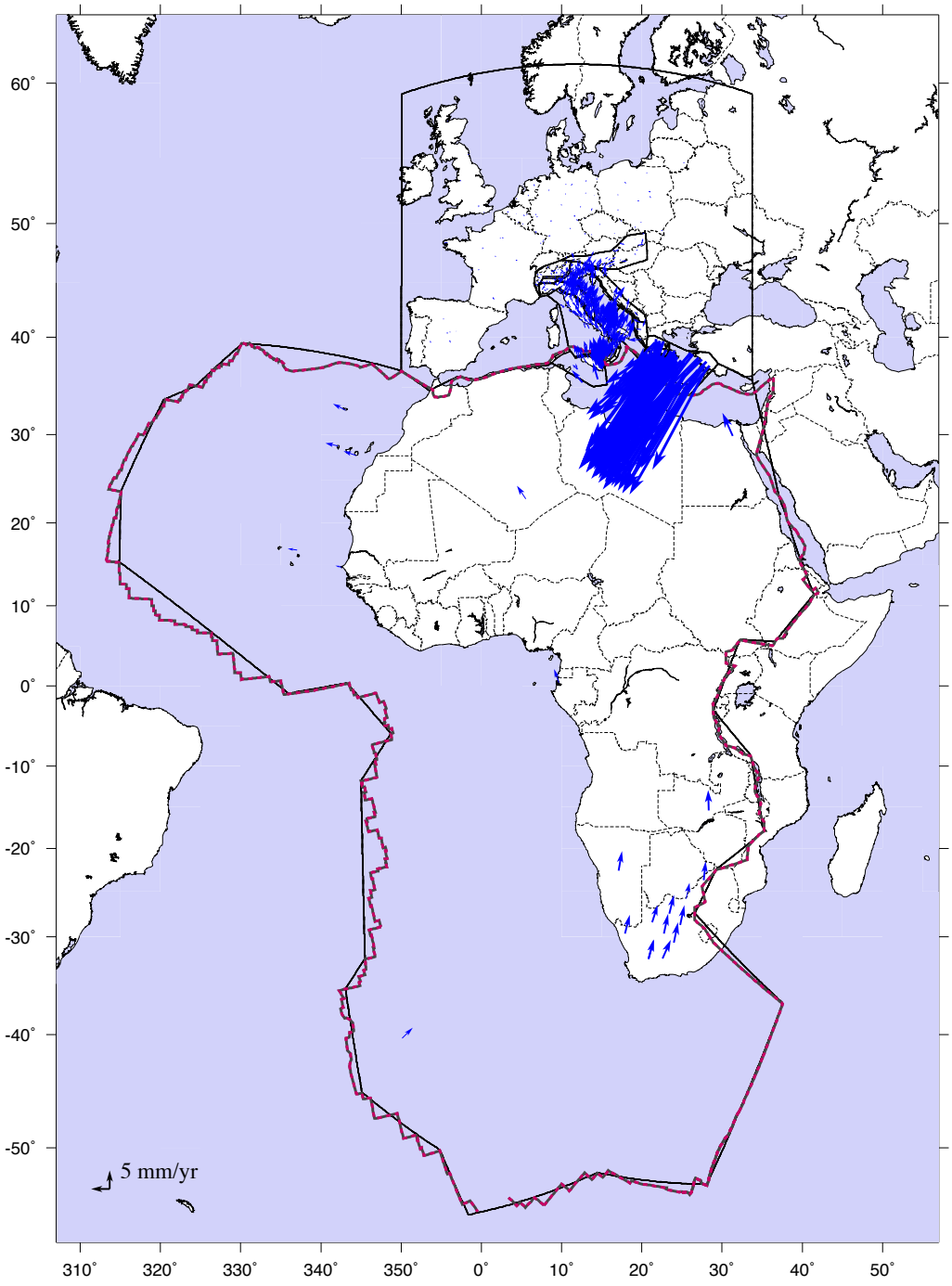

Figure 5.3: *Eurasia (blue) and Nubia (red) fixed horizontal GPS velocity vectors. The dottet pink line shows the Nubia Plate model from* Bird et al., (2003)

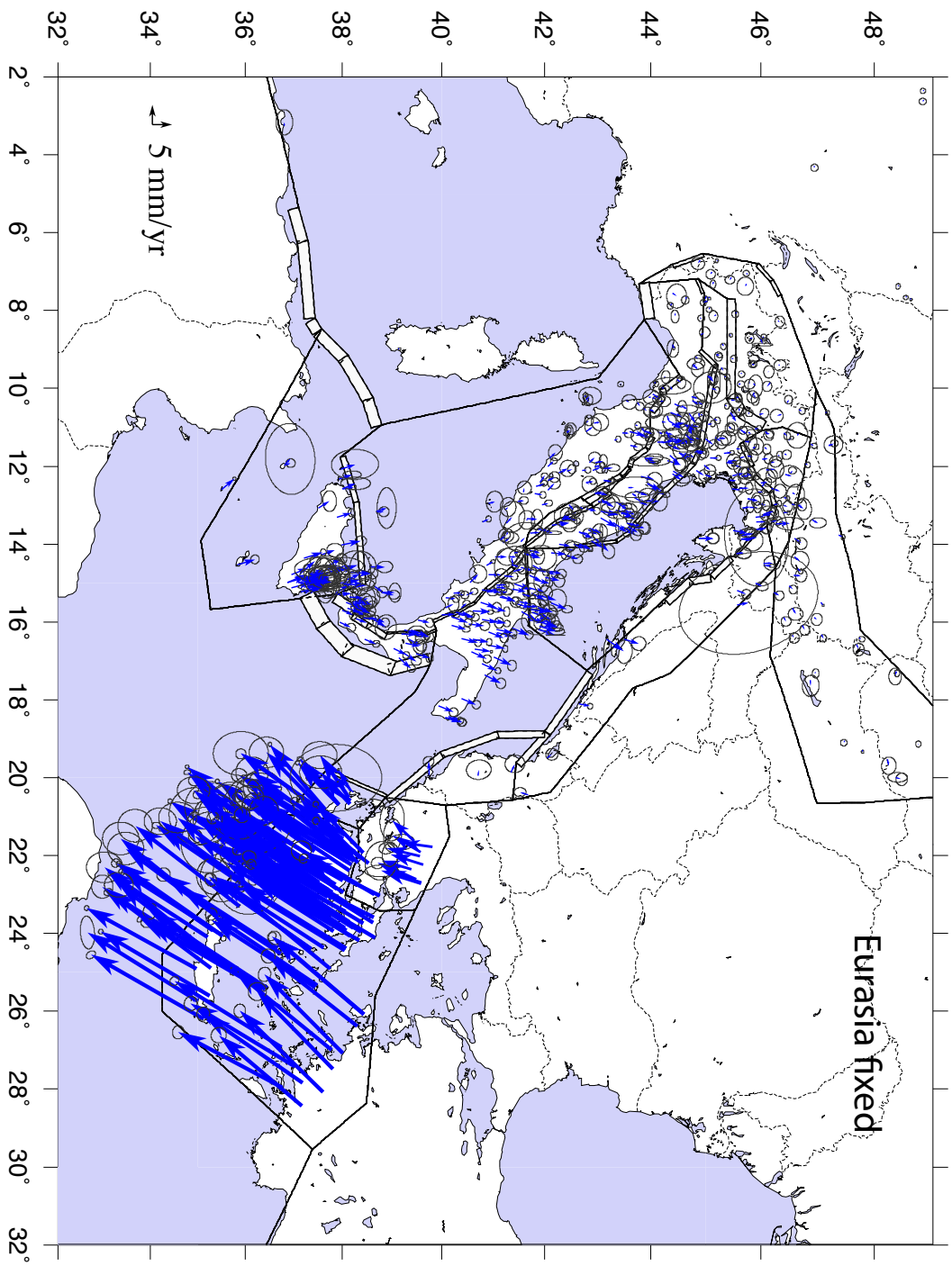

Figure 5.4: *Eurasia fixed horizontal GPS velocity vectors and 95% confidence error ellipses.*

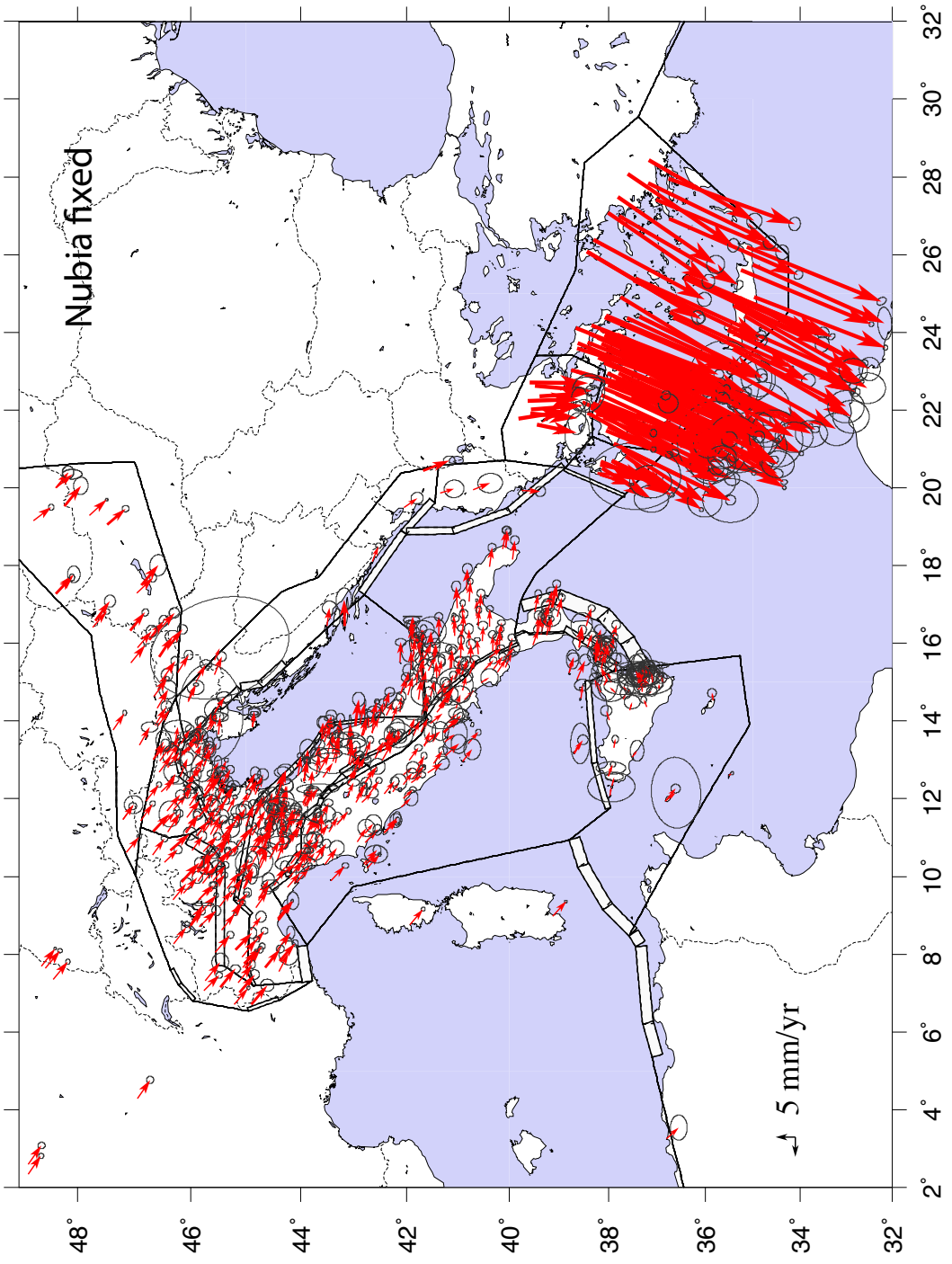

Figure 5.5: *Nubia fixed horizontal GPS velocity vectors and 95% confidence error ellipses.*

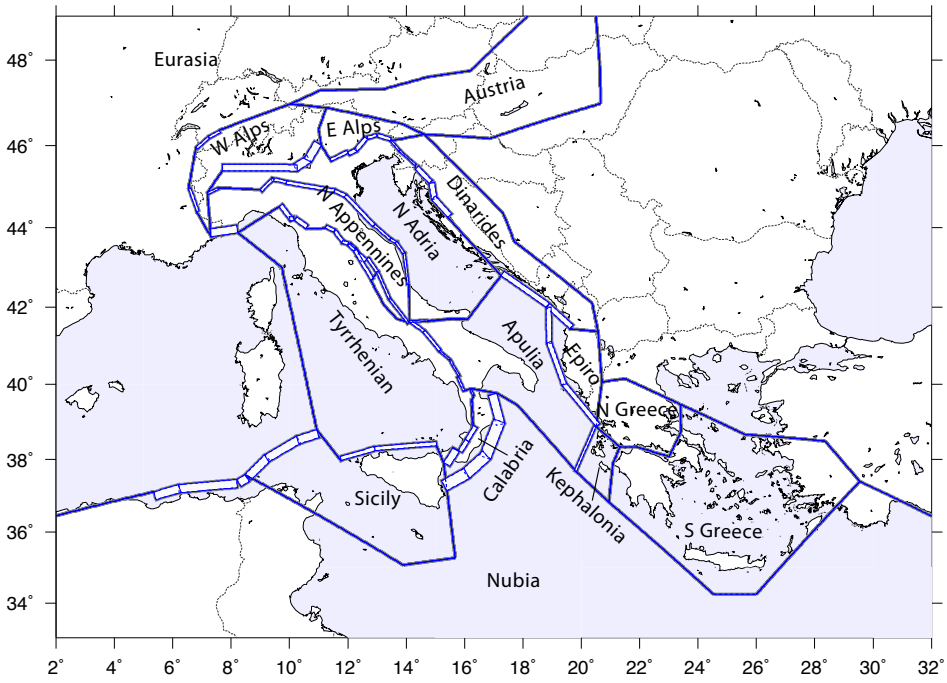

Figure 5.6: *Schemathic representation of all the tested blocks with names. Surface projections of the fault planes are also shown.*

to ∼NE-ward in the Eurasian reference frame and decreasing and rotating from ∼SE-ward to E-ward in the Nubian reference frame.

On the base of the above GPS velocity field analysis and using as reference the informations from the DISS database we draw and test five different block geometries for the central Mediterranean region (fig. 5.6-5.9).

All the tested models assume as independent blocks the Eurasian, Nubian, Aegean, Epiro, Dinarides, Austria, Western and Eastern Alps, Northern Appenines and Tyrrhenian plates. The Eurasian block boundaries do not trace tectonic lineaments, this block just performs the motion of the stable Eurasian plate (fig. 5.3). The Nubian block is, instead, drawn by tracing the plate boundaries from *Bird et al.*, (2003). All the boundaries of this two main plates are assumed to be vertical and locked above 15 km. The central Mediterranean plate boundaries are parameterized by using dip and locking depth values from the DISS. The only exception is the Aegean region that has been modeled as in *Apel et al.*, [in preparation]. The statistical tests made for the residual minimization suggest to the authors a fragmentation in three smaller microplates (Kephalonia, Northern and Southern Greece) and an almost uncoupled subduction interface. Below report a brief description of all models in order of complexity (please, see fig. 4.2 for the fault system names):

1. The 1th model (fig. 5.7, A), the simplest one, assumes that the African plate stretches like a promontory in the Mediterranean, thus including the Adriatic, Sicilian and Ionian region too.

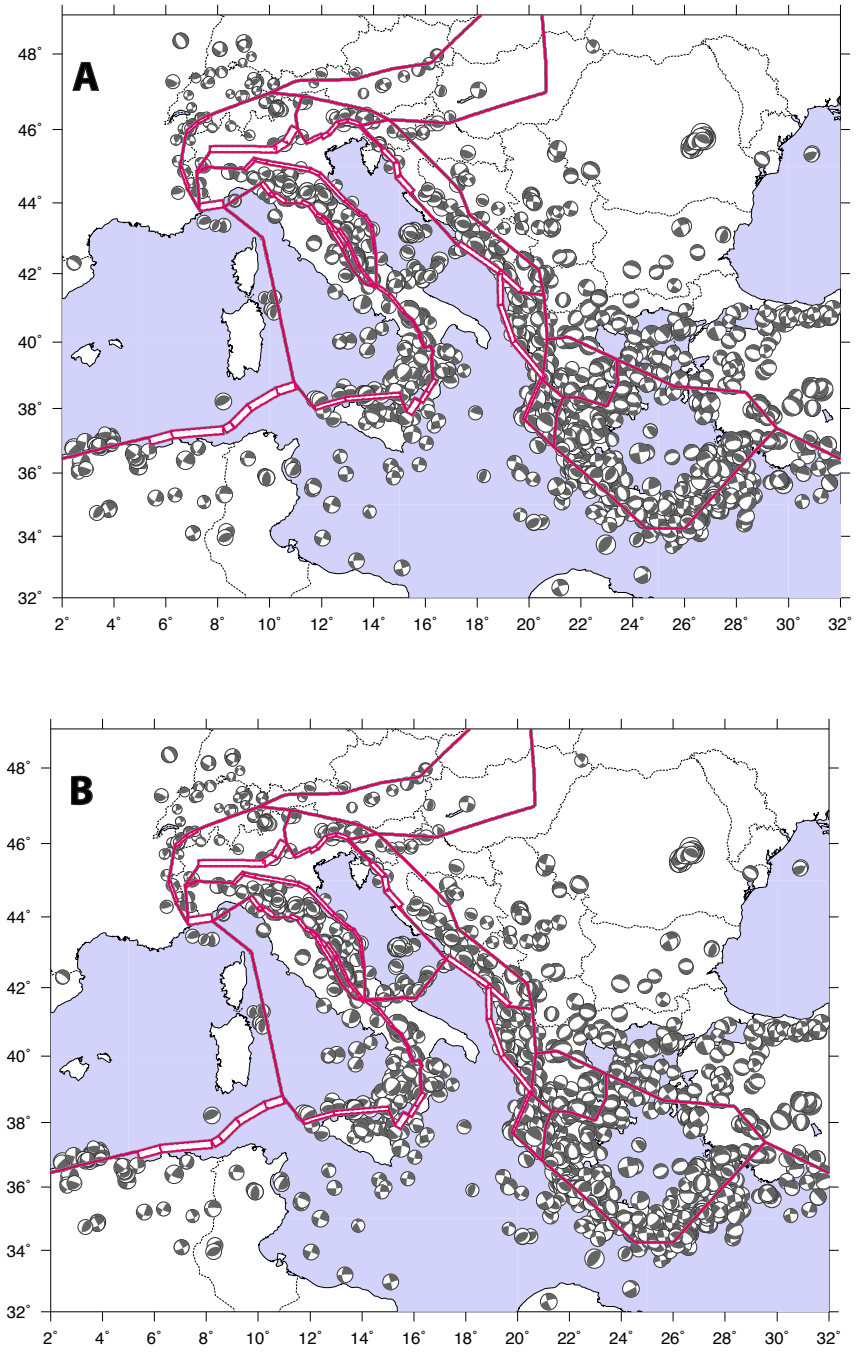

Figure 5.7: *Model 1 (A): the African plate stretches like a promontory in the Mediterranean. Sicily, Adriatic and Ionian Sea elong to Nubia. Model 2 (B): Northern Adriatic is independent from Nubia. As in the following figures, focal solutions are also shown. The blue lines are the block boundaries.*

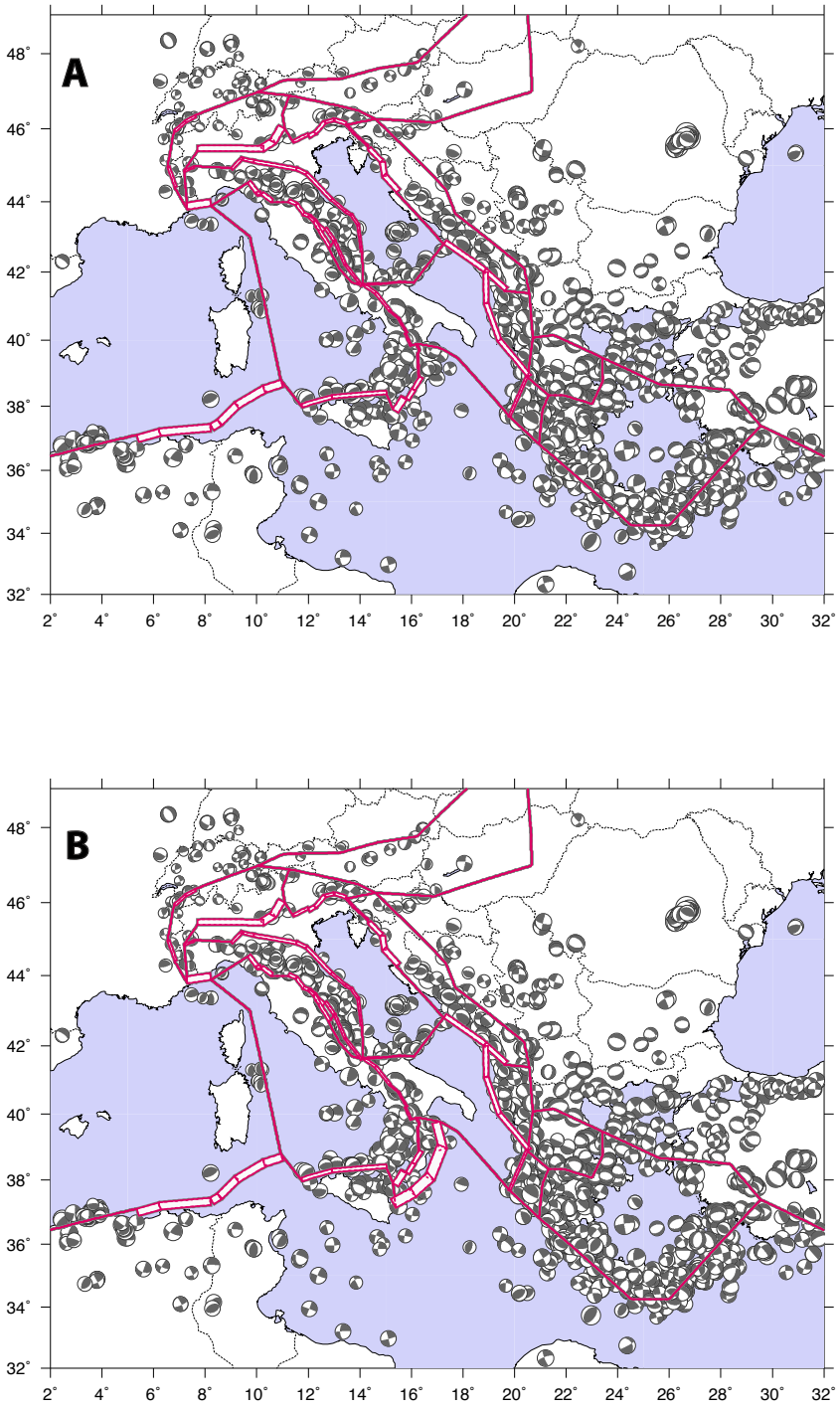

Figure 5.8: *Model 3 (A): Adriatic plate divided into two blocks, both independent from Nubia. Model 4 (B): Adriatic and Calabrian Arc independent from Nubia.*

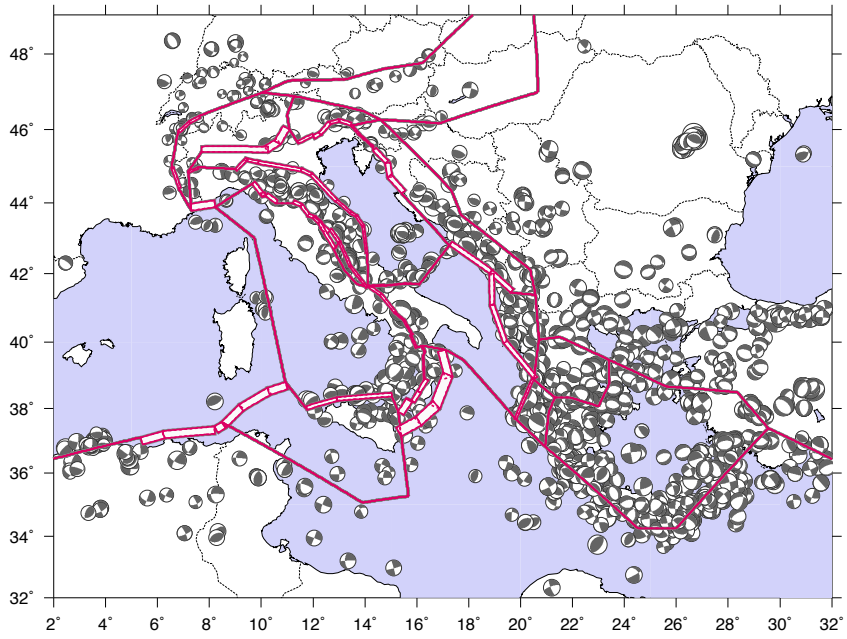

Figure 5.9: *Model 5: the last model assume independent motion for the Adriatic, Calabrian and Sicilian blocks.*

2. The 2th model (fig. 5.7, B) separates the northern part of the Adriatic region from the Nubia plate through the Gargano-Dubrovnik fault at wich the focal mechanisms assing an compressive behavior NW-SE oriented.

3. The 3th model (fig. 5.8, A) separates the Apulian block from Nubia. The boundary between southern Adriatic and the Ionian Sea coincides with the Apulian Escarpment. However, as already note, this tectonic lineament is not cleary imaged by seismicity. This could be due to the relatively high heat flow in the area or to the fact that this lineament is partially covered by the soft sediments of the Calabrian wedge that could imply aseismic deformations (*Battaglia et al.*, 2004).

4. With the 4th model (fig. 5.8, B) we assumes that also the Calabrian region has a microplate behavior, separate from the Ionian and Nubian plates through a tectonic lineament coincident with the convergent boundary generated by subduction, NW-ward oriented, of the Ionian lithosphere below the Tyrrhenian basin.

5. The 5th and last tested model (fig. 5.9) assumes the independence of Sicily from Nubia. The boundaries of this microplates are: (North) the compressive margin extending $\sim$ E-W offshore the northern coast of Sicily wich continues to the west with the Tell-Atlas system, a contractional belt that runs from Morocco to Tunisia. (East) the Tindari-Giardini fault and the Malta Escarpement, both charaterized by transcurrent behavior. (South-West) a tectonic lineament extending through the Sicily Channel where focal mechanisms clearly show a right lateral motion $\sim$NW-SE

oriented.

5.4 Statistical tests

5.4.1 Chi-Squared Statistics

As geodetic data alone are not able to discriminate between n and $n+1$ plate models we use statistical tests to investigate about our proposed models. To test which one, among the analized geometries, is the optimal one we use the χ^2 and $\chi^2_\nu = \chi^2/DOF$ statistics:

$$\chi^2 = \sum_{c=1}^{\#data} \left(\frac{v_c^{model} - v_c^{data}}{\sigma_c} \right)^2 \tag{5.1}$$

$$\chi^2_\nu = \frac{\chi^2}{\#data - \#model\ parameters} \tag{5.2}$$

where v_c^{model} and v_c^{data} are the predected and observed velocity components, and σ_c is the 1σ uncertainty for each component of the input GPS velocities. The number of degrees of freedom (DOF) is defined by: $\#data$, the number of GPS components used as input data (east and north components for each station) and $\#model\ parameters$, the number of model parameters that we solve for in the inversion (3 per block - pole of rotation latitude and longitude and rotation rate). The statistics indicate how well the model fit the data within their uncertainty bounds. Lower values of χ^2 indicate better fit to the data. χ^2 can be calculated for a single data component at a single station, for sites within an individual block, or for the entire model. Increasing the number model parameters inevitably leads to better fits and lower total χ^2. Dividing by the number of degrees of freedom (DOF) helps us to compare our model where we solve for a different number of parameters, but χ^2_ν ignores all correlations between parameters. Because these correlations change as model geometry changes, caution should be exercised in making strictly quantitative comparisons of models using χ^2_ν alone. Nonetheless, the statistics provide a basis for qualitative comparisons. For uncorrelated parameters, a χ^2_ν of 1 indicates that on average all the predicted velocities are consistent with the 1σ standard deviation of the input data.

5.4.2 *F* Test

If a N data set is well fitted by two different models, with r parameters ($N - r$ degrees of freedom) and p parameters ($N - p$ degrees of freedom), rispectively, with $p > r$, then the second one should lead to a better data fitting. To verify that the χ^2 reduction is not due only to the largest number of parameters of the second model compared to the first we use the *F test*.

Model #	Blocks	DOF	χ^2_ν	F_e	F_t ($F_{0.01}$)
1	15	1512	7.4	–	–
2	16	1509	4.9	246	3.78
3	17	1506	4.7	27.7	3.78
4	18	1503	4.4	30.0	3.78
5	19	1500	4.3	11.8	3.78

Table 5.1: *Table shows, for each model: degrees of freedom (DOF), χ^2_ν, experimental (F_e) and theorethical (F_t) F values. Every model was compared with the previous one (with one block less, then three more degrees of freedom).*

In the case of two model with r and p parameters, respectively, then the statistic F has the expression (*Stein & Gordon.*, 1984):

$$F = \frac{\left[\chi^2(r) - \chi^2(p)\right]/(p-r)}{\chi^2_\nu(p)} \tag{5.3}$$

This statistic is F distributed with $\nu_1 = p-r$ and $\nu_2 = N-p$ degrees of freedom. The test examines the probability $P_F(F, \nu_1, \nu_2)$ of finding an F value grater than the observed value F for a random sample with ν_1 and ν_2 degrees of freedom. In the particular case examined in this work we compare couples of models with p and $p+1$ blocks to test if there was actually an improvement in the data fitting. The model with p blocks has $3(p-1)$ parameters and $N-3p+3$ degrees of freedom while the model with $p+1$ blocks has $3p$ parameters and $N-3p$ degrees of freedom, so the statistic F:

$$F = \frac{\chi^2(p\ blocks) - \chi^2(p+1\ blocks)/3}{\chi^2(p+1\ blocks)/(N-3p)} \tag{5.4}$$

is tested using the probability $P_F(F, \nu_1, \nu_2)$ with $\nu_1 = 3$ and $\nu_2 = N-3p$.

5.5 Results and conclusions

We proposed five different plate models realized varying the kinematic configuration of the central Mediterranean region. All proposed models were compared in order of complexity by using the χ^2 and F-ratio statistics. Blocks lying on the Italian pensinsula and sorrounding area were parametrized with locking depth and dip values from the DISS database. The Aegean region blocks were parametrized as in *Apel et al.*, [in preparation]. The Eurasian and Nubian plate boundaries are assumed to be vertical and locked above 15 km. By using an elastic block model approach, we invert horizontal velocities from 770 GPS stations lying within the outer margins of our blocks. To model the motion of the Eurasian and Nubian plates we selected only the stations used during the data analysis stage to estimate the Euler rotation vectors.

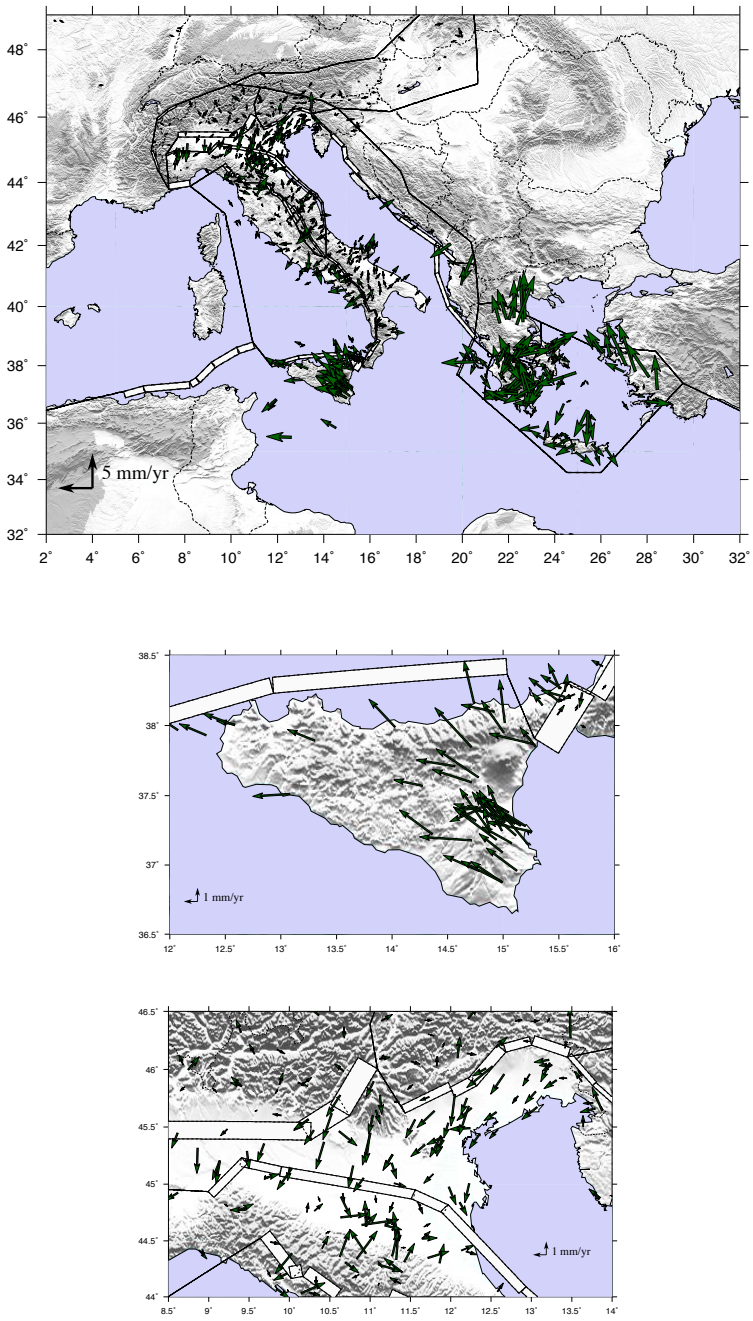

Figure 5.10: *Residual (measured minus modeled) velocity vectors from the 15-blocks model (# 1). The two small figures show a zoom for the Sicilian and Northern Adriatic domains, where the most significant improvment in fitting of the data is achieved by adding four additional blocks (compare with fig. 5.11).*

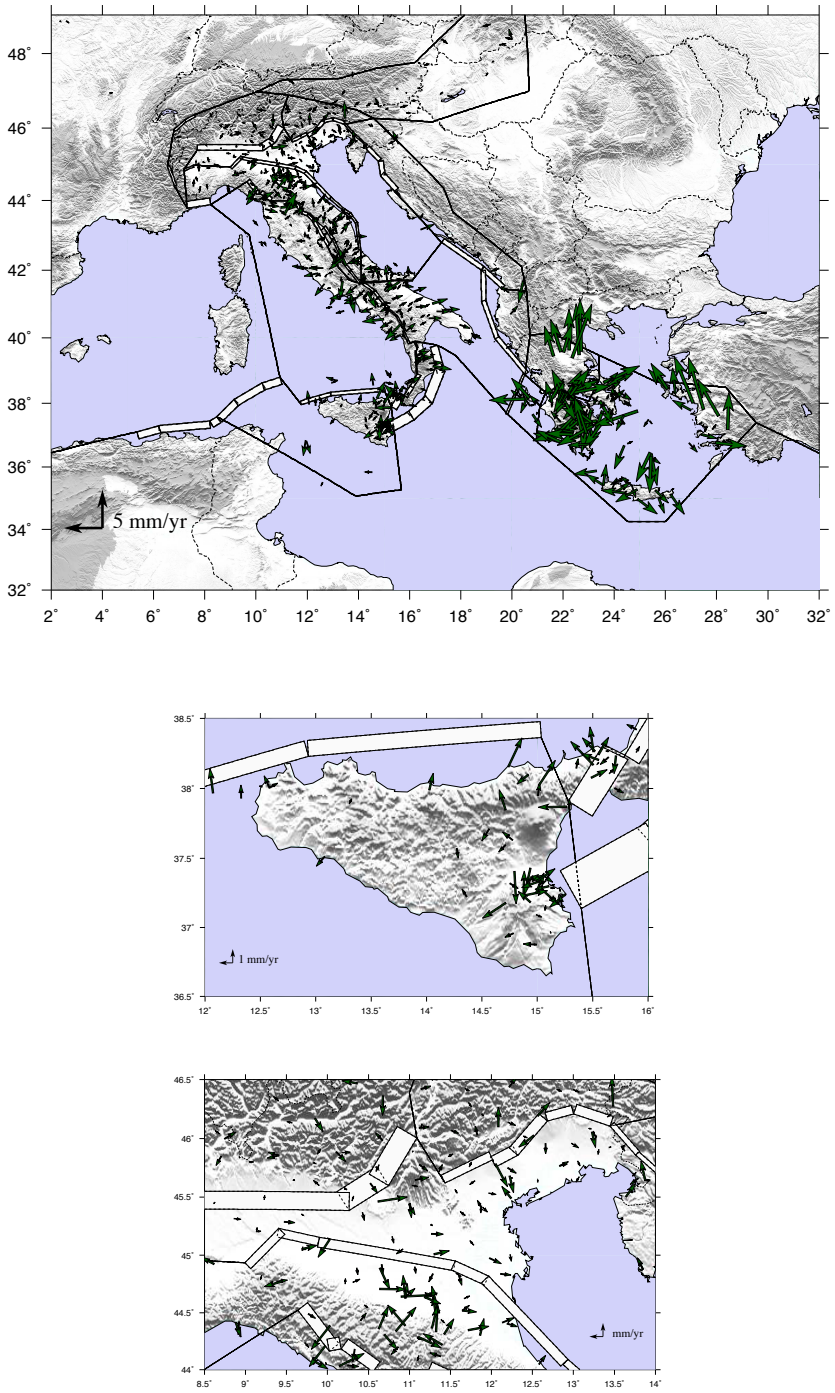

Figure 5.11: *Residual (measured minus modeled) velocity vectors from the 19-blocks model (up). Central and low figures as in the fig. 5.10.*

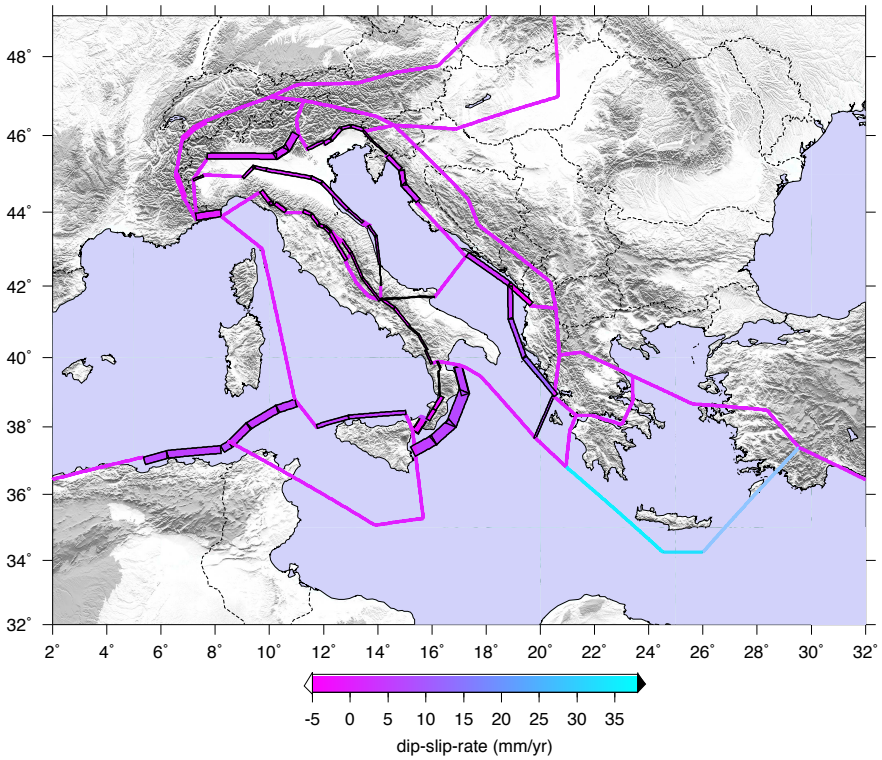

Figure 5.12: *Best model (# 5) predicted fault dip-slip rates and kinematics for the central Mediterranean region. Violet segments indicate slip-rate* < 10 *mm/yr, blue ones indicate slip-rates of a few cm/yr.*

All the resutls are presented in table 5.1. Table shows, for each model, plates number, degrees of freedom, χ^2_ν value, experimental (F_e) and theoretical (F_t) F vaules. F values shown in the table are from test realized comparing couples of models with p and $p+1$ blocks (every model with respect to the previous) using the equation 5.4.

By comparing the χ^2_ν values we conclude that the most likely model, with $\chi^2_\nu = 4.35$, is the model number five (fig. 5.9) that assumes independent motion for: the Adriadic Sea separate into two microplates along the Gargano-Dubrovnik lineament, the Calabrian and Sicilian blocks.

We sistematically compare experimental and tabulated F-values for couples of models with p and $p+1$ blocks, so with $\nu_1 = 3$ and $\nu_2 = N - 3p$. Table 5.1 shows that the experimental F-values are ever bigger than the theoretical $F_{0.01} = 3.78$ (corrisponding to $P_F(F, \nu_1, \nu_2)$ for a probability of 1%) (*Stein & Gordon.*, 1984). Then, found that the best model is the 19-blocks one (with a $\chi^2_\nu = 4.3$) we can say that there is only a 1% risk that the improvement in fit is due purely to chance.

Figures 5.10 and 5.11 show the residual velocities obtained from 15 and 19-blocks model inversion, respectively. A significant improvement in fit to the data is

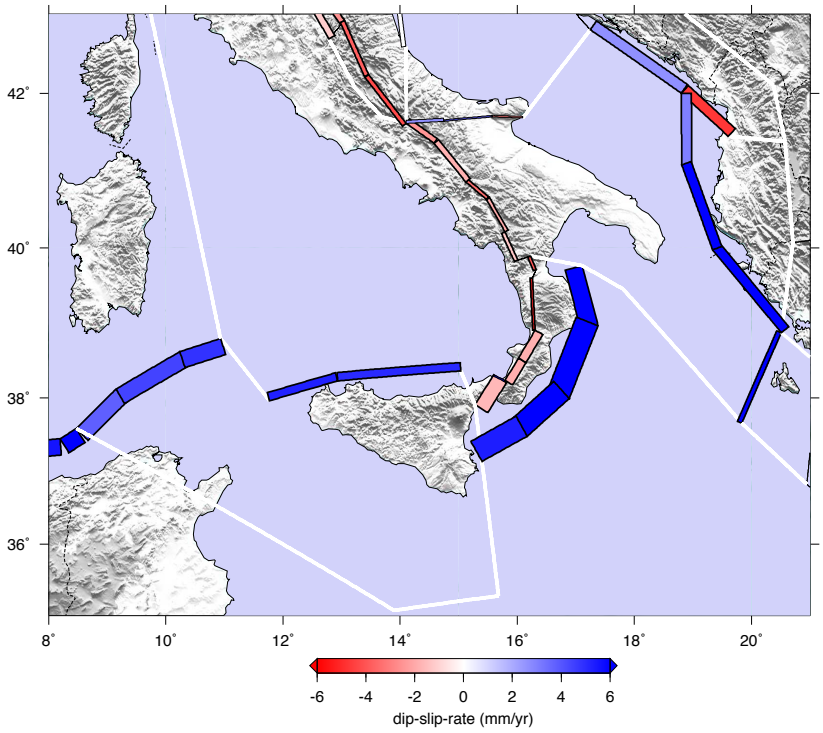

Figure 5.13: *Best model (# 5) predicted fault dip-slip rates and kinematics. Zoom for the Sicilian and Calabrian Arc area. Blue = compression, red = extension.*

achieved by adding four additional blocks in the Central Mediterranean region with a reduction of about 30% of mean residual magnitude. Clear improvements are observable, in particular, for all the stations lying in the Northern Adriatic microplate when allowed it to move independently from Nubia. A significant reduction affects also the stations in the Iblean region, eastern Sicily. Best fitting model displays very small residuals with a mean residual magnitude of 1.1 mm/yr. 54% of the residuals is smaller than the uncertainty associated with the observed velocities. Bigger residuals affect the Hellenic area but this region is moving at a rate of a few centimeters per year, significantly faster than the Italian peninsula and sorroundings areas, so the residual velocities are still small compared to the observed ones.
Figs. 5.12 and 5.13 show block-bounding fault dip slip-rates predicted by the 19-blocks model. According with the available geological and seismological data, the model predicts compression for the Calabrian Slab interface, as well as, for the northern boundary of Sicilian block and along its extension off-shore the northern coast of Africa. A compressional behavior is also observed all along the eastern margin of the Adriatic block while extension charaterizes the Appennine chain from the Messina Straits to the north (fig. 5.13). Again, it is clear the presence of two different kinematic regimes characterizing the central Mediterranean region, with slip-rates lower than 1 cm/yr, and the Hellenic arc where we find slip-rates of a few

cm per year (fig. 5.12).

Chapter 6

Estimation of geometric fault parameters

6.1 Modeling approach

In the previous stage of the work (chapter 5) we explored the kinematics of the central Mediterranean microplates. Performed statistical tests suggested us the block geometry that best fits the observed velocities. Now, within this kinematic framework, we try to expand our knowledge about the Calabrian Slab interface geometry. For this purpose we use again a combined approach of elastic block modeling and chi-squared statistics.

Observed interseismic surface velocities are a sum of a rotational component due to the crustal block rotation plus an elastic component due to the strain accumulation on active faults (assuming rigid blocks). Is worth to note that same velocity fields can be generated from structures with different geometries as they are the result of a combination of dip angle and locking depth values. Shallower dipping segments require bigger locking depth (so less slip) to produce similar magnitudes of elastic deformation at the surface then more steeply dipping segments.

We run suites of block model inversions by varying the dip and locking depth exploring ranges of geometries that minimize the misfit to the observed data. For each variation we invert the horizontal GPS velocities for poles of rotation and slip rates constrained by our prescribed block locations and plate boundary fault geometry. We assume homogenous parameters for all the segments composing the analyzed structures (same dip and locking depth).

Before applying the described approach to the Calabrian Slab interface we test it on other tectonically simpler zones with better data coverage lying in the Italian peninsula: the Irpinia, Mattinata, Friuli and Southern Tyrrhenian fault systems.

It is clear that individually varying the geometric parameters of these relatively small fault systems does not impact, or just slightly, the model χ^2. So, to evaluate the misfit reduction to the data, we compute the reduced χ^2 (χ^2_ν) just taking the stations lying close to the analyzed structure. To select the GPS stations to use we follow a three step approach: 1) compute the horizontal elastic component of the velocity field on a regular $d \times d$ grid with $d = (1/8)^\circ \simeq 13$km parametrizing the fault segments with minimum realistic dip and locking depth values (maximum inferred deformation field) 2) extract only the stations that are less than $d/2$ from a point of the grid with a velocity lower than mean uncertainty on the observed CGPS velocities 3) compute a local reduced χ^2 using only the selected stations.

6.1.1 Test 1: Mattinata Fault system

Mattinata Fault system is a composite source straddles the full length of the Gargano Promontory, and belonging to the oblique to right-lateral strike-slip system that affects the central and southern Adriatic foreland. Field evidence and recent seismological data have shed light on a complex structural arrangement made of shallower (within the uppermost ca. 12 km) faults that affect the ground surface and that were associated to some historical earthquakes, and of deeper (down to ca. 25 km) structures that may have caused the recent M_w ca. 5.0 instrumental events. Geological and seismological data (e.g., *Guidoboni et al.*, 2007; *Di Bucci et al.*, 2006; *Billi et al.*, 2007) suggest a near-vertical structure $\sim 80° - 90°$N-dipping and ∼E-W striking.

We parametrize this structure with three segments, ∼E-W striking and test a reasonable set of fault system parameters which include dip from 40°N to 40°S and a locking depth from 0 to 50 km. The local reduced chi-squared, computed taking only the selected stations (fig. 6.1, A), is contoured and shown in figure 6.1, B as a function of the Mattinata fault system dip and locking depth. As shown in the figure, even if the χ^2 statistic is not able to give us a definite answer regarding the fault locking depth that best fits the GPS data (with a reduced $\chi^2 \simeq 2.6$ for a locking depth renging between 20 and 50 km), it clearly indicates a sub-vertical structure modeled by three 80°N-dipping segments. The inferred parameter values agree rather well with the seismological and geological informations from the literature. Fig. 6.1, C shows the residual velocities obtained from our preferred model.

6.1.2 Test 2: Irpinia Fault system

This composite source straddles a stretch of the southern Apennines between the Irpinia and Basilicata areas, across the high Sele river and, S-ward, the high Agri river valleys. It forms the southern core sector of the high-angle, NE-dipping, large normal fault system of the southern Apennines. This complex structure was the locus of some of the strongest seismic events that ever hit Italy during historical times, including the multiple $M_w = 6.9$ November, 23 1980 Irpinia-Lucania earthquake (*Pantosti & Valensise*, 1990).

The Irpinia fault system is parametrized by three ∼NW-SE striking segments for which we assume equal dip and locking depth values. We run suites of block model inversions by varying the two geometric parameters between 20 and 80 degress (dip) and 0 and 20 km (locking depth). Again, residual velocities from the GPS stations, selected on the basis of the estimated horizontal velocity field (fig. 6.2, A) are note able to identify a well defined χ^2_ν minimum. The model that best fits the GPS velocities is characterized by a dip angle between ~ 50 and 70 degrees and a locking depth between ~ 8 and 20 km with an abslute minimum corresponding to 50° and 10 km, respectively (fig. 6.2, B). In the fig. 6.2, C residual velocities corresponding to the best model are shown.

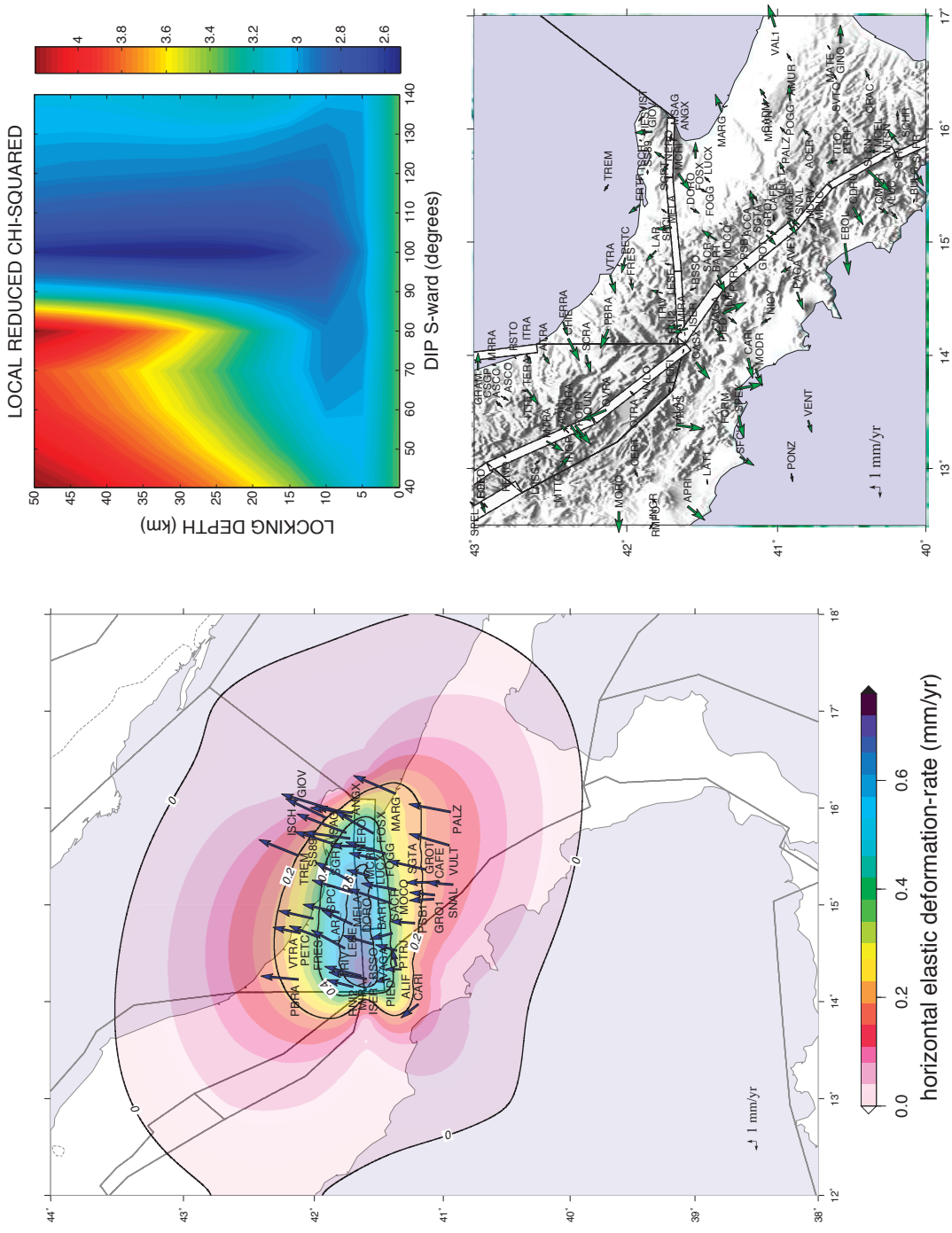

Figure 6.1: *Mattinata fault system: (A) Selected GPS stations on the base of the estimated horizontal velocity field from a three 60°N dipping and 30 km depth segments (see text for explanation). (B) Local reduced chi-squared misfit statistic for the selected GPS stations given the variable fault parameters. The χ^2_ν statistic is shown as a function of the fault segments dip and locking depth. Best fitting models are one with the smallest reduced chi-squared. (C) Residual velocities corresponding to the best model obtained.*

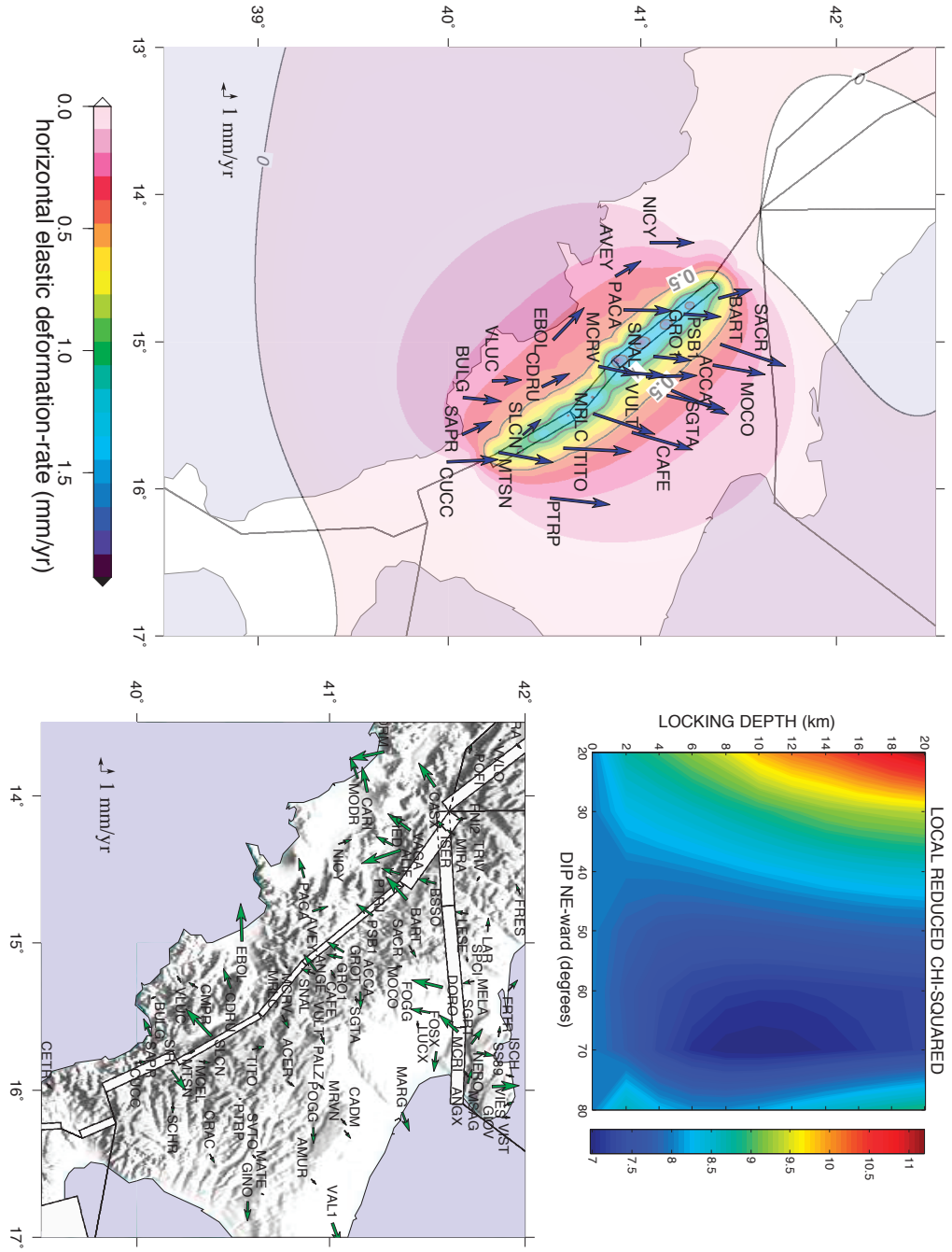

Figure 6.2: *Irpinia fault system: (A) Selected GPS stations on the base of the estimated horizontal velocity field from a three* $60°$ *NE dipping and 30 km depth segments. (B) and (C) as in fig. 6.1.*

6.1.3 Test 3: Friuli Fault system

The Friuli Fault system is a composite structure made of some smaller faults which differ in the hanging wall structural elevations (between western and eastern sectors), and in the strike direction (*Galadini et al.*, 2005). The two main sources that make up the system are the Montebelluna-Montereale and Maniago-Sequals faults. Both these structures belong to the overall thrust system of the eastern Southalpine Chain that borders the Veneto-Friuli plain in north-eastern Italy and continue onto the Italy-Slovenia border. These fronts are S- to SE-verging fault systems and are thought to accommodate the ∼N-S convergence between Africa (the Adriatic microplate here) and Europe. Historical and instrumental catalogues (*Boschi et al.,* 2000; *Pondrelli et al.*, 2006) show a remarkable concentration of damaging and destructive earthquakes over the entire region and adjoining composite sources. In particular, the area was affected by the well known 1976 Friuli seismic sequence.

We investigate the Friuli Fault system geometry by parametrizing it with two segments ∼SW-NE striking. On the basis of the available informations we test a reasonable set of fault system parameters by varying the locking depth and dip values between 0 and 50 km and 20 and 80 degrees, respectively. Contrary to previous tests, the inferred χ^2 statistic gives us clear informations about the fault locking depth that best fits the observed data but it does not define a best dip angle with a small variation of the reduced χ^2 value (fig. 6.3, B). Anyway the absolute χ^2_ν minimum corresponds to a 70° dipping and 10 km locked fault. The fig. 6.3, C shows the inferred residual velocities from this optimal model.

6.1.4 Test 4: Southern Tyrrhenian

An E-W narrow contraction belt runs from the Sicily Channel to the Eolian Islands, about 50 km off the northern Sicily coast. This belt is thought to accommodate 4-5 mm/y of the Africa-Europe convergence (*D'Agostino & Selvaggi*, 2004; *Serpelloni et al.*, 2005). In the past 30 years several events with $M > 5$ originated in this area, including the M_w 5.9 Palermo earthquake of 2002 (*Goes et al.*, 2004; *Pondrelli et al.*, 2004; *Vannucci et al.*, 2004). They are mostly shallow compressional earthquakes with NNW-SSE P-axe. This contraction trend is consistent with the plate motion vectors derived from GPS data. Recent interpretations of the submerged structures in this area by *D'Agostino & Selvaggi*, 2004 and *Goes et al.*, 2004 hypothesized active back-thrusting in the Southern Tyrrhenian Sea between 0.8 and 0.5 My. However, the available data are not sufficient to constrain the direction of dip of the major faults. The north-dipping planes are preferred by many authors because they are consistent with known pre-existing structures.

Because of the uncertainties about the dipping direction we invert sets of model making the dip angle vary from 20°S to 20°N, while the locking depth ranges between 0 and 50 km. Despite the location and the poor data coverage (fig. 6.4, A) the χ^2 statistic is able to identify well defined fault geometric parameters (fig. 6.4, B) indicating, as structure that bast fits the observed data, a ∼ 50°S dipping fault

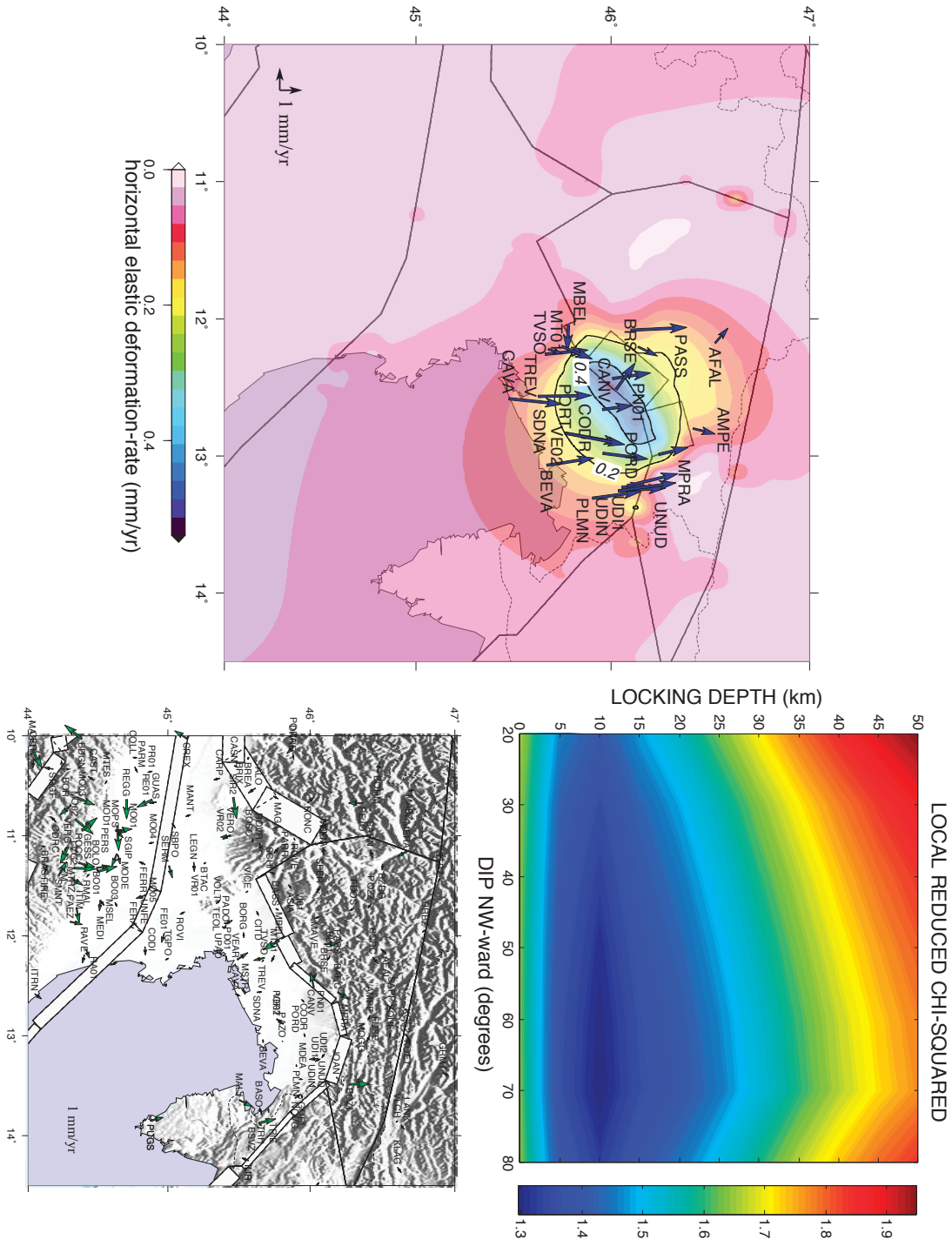

Figure 6.3: *Friuli fault system: (A) Selected GPS stations on the base of the estimated horizontal velocity field from a three* $50°N$ *dipping and 20 km depth segments. (B) and (C) as in fig. 6.1.*

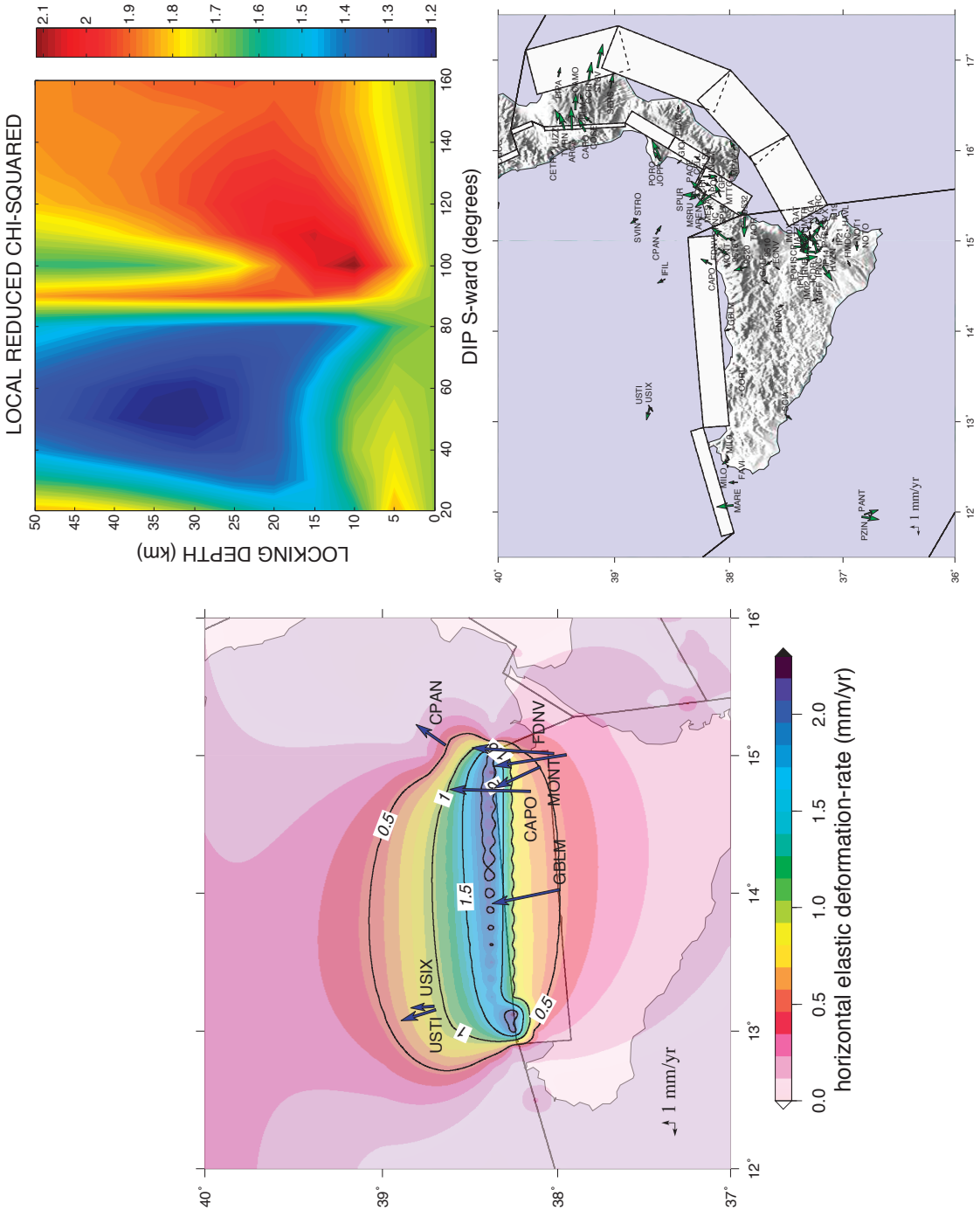

Figure 6.4: *Southern Tyrrhenian fault system: (A) Selected GPS stations on the base of the estimated horizontal velocity field from a three 40° S dipping and 20 km depth segments. (B) and (C) as in fig. 6.1.*

locked at a depth of ∼30-35 km. It's worth noting that, even if the investigated structure lies offshore, the presence of Ustica and the Eolian Islands guarante the presence of data on both sides of the track, and then a sufficient coverage.

6.2 Modeling of the Calabrian subduction interface

The Calabrian Arc subduction zone has been extensively described and investigated in the previous chapters of this thesis (paragraphs 1.4.2 and 2.3.1). However, thanks to the bigger availability of GPS data and in the light of the central Mediterranean plates model, statistically defined in a previous stage of the work (chapter 5), we try to improve our geometric modeling of the Calabrian Slab interface.

We apply the above described approach by first: selecting the GPS stations to use to compute the local χ^2_ν on the base of the estimated horizontal velocity field predicted by a model with four 20°NW-dipping and 20 km locked segments (fig. 6.5, A). Then we run suites of model inversions by varying the dip and locking depth between 10 and 80 degrees and 0 and 70 km, respectively. Fig. 6.5, B shows us that the χ^2 statistic is not able to give as any information about the optimal geometric parameters of the Calabrian Slab interface. This could be due to the geographical position of the structure, offshore the eastern coast of the Calabrian region. The lack of islands in the Ionian Sea, infact, makes the data distribution one-sided with respect to the trench. Moreover seems evident that using the only horizontal GPS velocities is not enough for such a multiparametric modeling.

6.2.1 Vertical velocities: a new constrain

The vertical GPS velocity field (fig. 6.8) on the Calabrian region shows uplift all along the eastern coast with a mean rate of ~ 1 mm/yr. Uplift propagates westward decreasing up to an average rate of a few tenths of a millimeter along the western coast where local subsidence is also observed in the Crati and Gioia-Tauro Basins and across the Messina Straits, probably generated by the presence of active faults (e.g., *Jacques et al.*, 2001; *Molin et al.*, 2004; *Monaco & Tortorici*, 2000).

Models of subduction interfaces predict a typical vertical velocity profile with subsidence close to the trench and maximum uplift corresponding with the surface projection of the deep termination of the fault plane locked portion (*Savage*, 1983, *Kanda & Simons*, 2010). Fig. 6.6 shows the vertical and horizontal velocity profiles generated by a partially locked subduction interface modeled on the basis of the back slip theory of *Savage*, (1983).

Analysis carried out so far have shown that the horizontal GPS velocities alone are note able to give us detailed informations about the geometry of the investigated fault systems. At this point we wonder whether the observed vertical velocity field is representative of the Ionian lithosphere subduction and moreover, if insert the vertical velocity component in our model could be a constraint able to provide informations on geometrical and kinematic characteristics. We investigate the question by perform forward models of elastic dislocations.

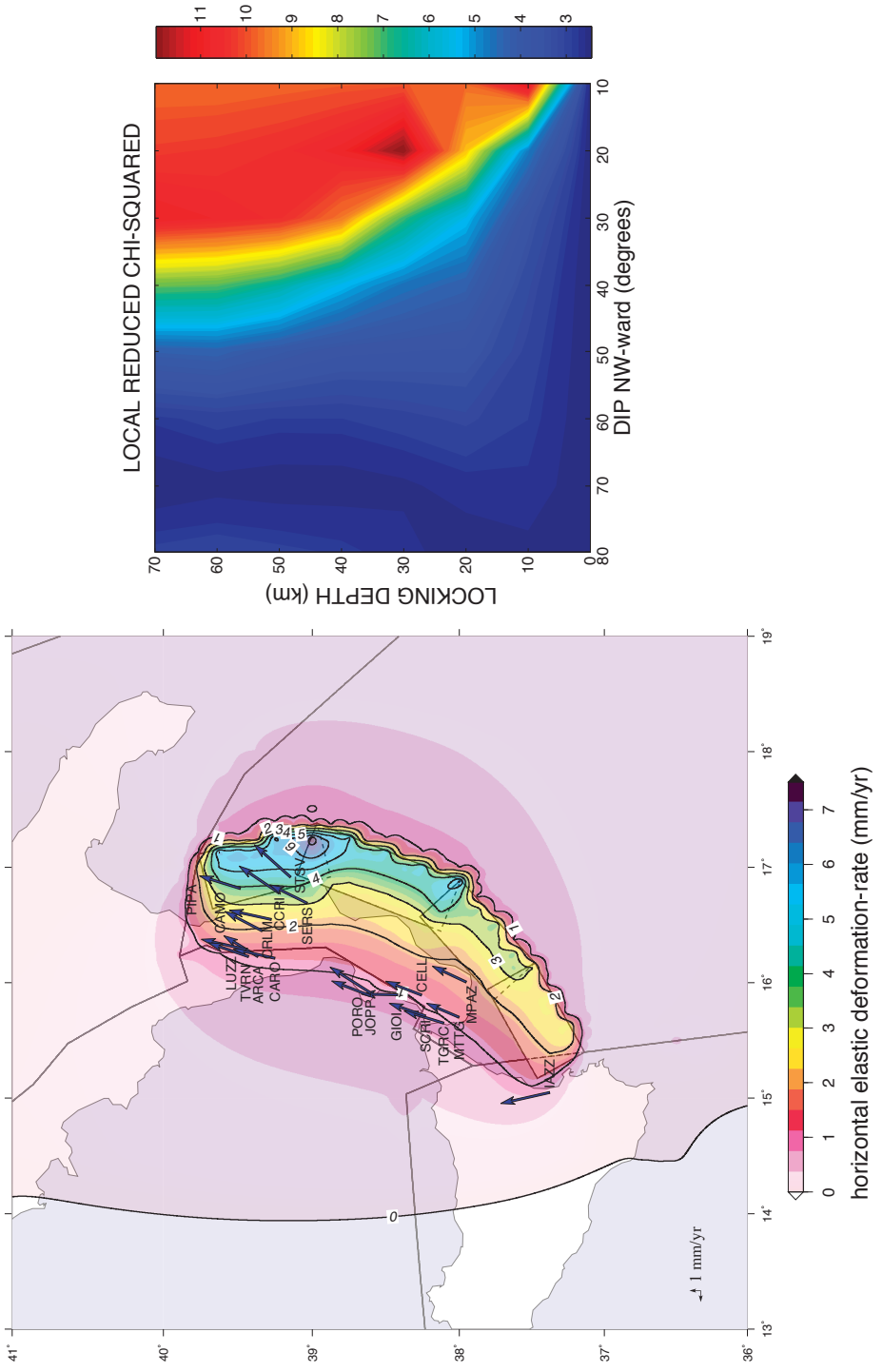

Figure 6.5: *Calabrian subduction interface: (A) Selected GPS stations on the base of the estimated horizontal velocity field from a three* $20°$ *NW dipping and 20 km depth segments. (B) as in fig. 6.1.*

Again, we parametrize the Calabrian Slab interface with four segments as in the optimal microplates model obtained from our kinematic analysis. We estimate the Ionian-Calabrian convergence rate assuming the Ionian block moving as Nubia; the inferred value is 5.5 mm/yr. Then, assuming that all the convergence is accomodated on the subduction interface and that all four segments, composing the geometric model, slip at the same rate we estimate model predicted vertical velocity field by running four forward models, making the locking depth vary from 10 to 40 km while keeping fix all the other parameters (homogenous dip of 30° is also assumed).

Fig. 6.7 shows the trench normal vertical and horizontal profiles of the velocity field obtained from our model of the subduction interface for various locking depths. Comparison with the model of *Kanda & Simons*, (2010) (fig. 6.6) confirms us the correctness of our approach. We compare model vertical velocities with the observed field finding the maximum resolved locking depth to be 25 km. The vertical velocity field from such a model is shown in fig. 6.8 together with velocities from CGPS stations. The maximum estimated uplift, of ∼0.8 mm/yr, is found on land, along the eastern coast of the Calabria region, almost parallel to the trench (contoured by a 0.5 mm/yr isoline in the fig. 6.8). Modeled velocities decrease westward matching the observed field rather well. If we neglect the areas of local subsidence, we can say that to a first approximation, the observed velocity field is in good agreement with the presence of a subduction plane 30°NW dipping and locked at 25 km depth.

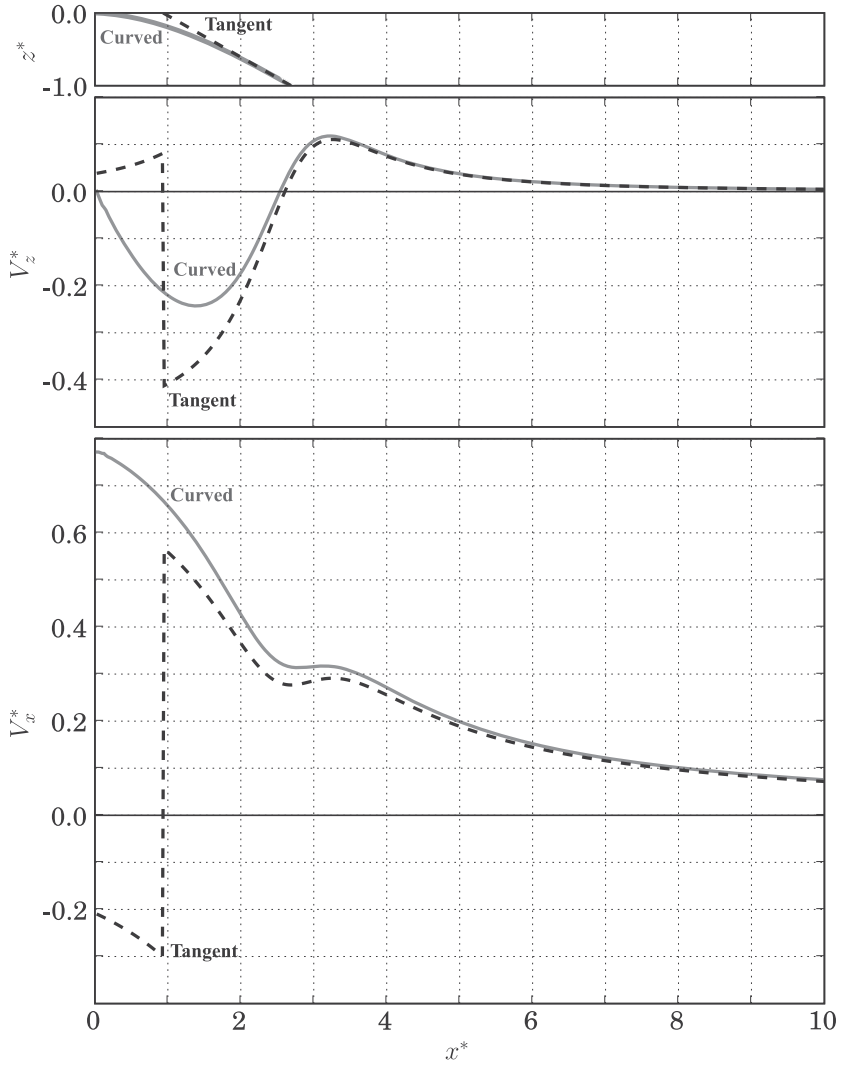

Figure 6.6: *Vertical and horizontal velocity profiles predicted by a backslip model (BSM) of a subduction interface. (top) Faults in cross-sectional view; x* (= x/Dlock) is the dimensionless distance perpendicular to the trench; z*(= z/Dlock) is the dimensionless depth. The origin of the dimensionless x*-z* system is at the location of the trench axis. (middle) Vertical surface velocity profile, Vz*, and (bottom) horizontal surface velocity profile, Vx*, are scaled by the uniform plate convergence velocity, Vp. From* Kanda & Simons, (2010).

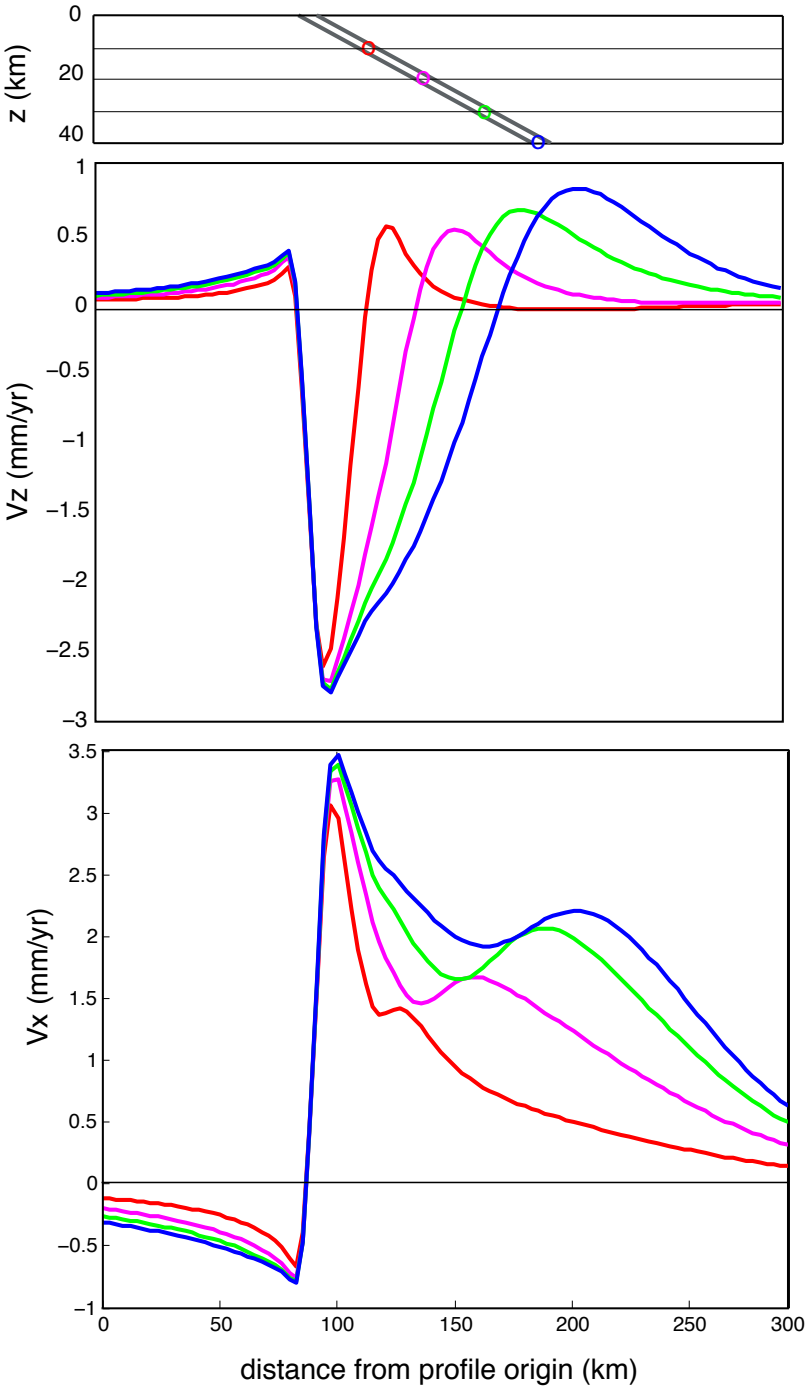

Figure 6.7: *(top): Schematich cross-sectional view of the Calabrian subduction plate. Trench normal profiles of the predicted vertical (middle) and horizontal (bottom) velocity fields for various locking depths (for location see fig. 6.8).*

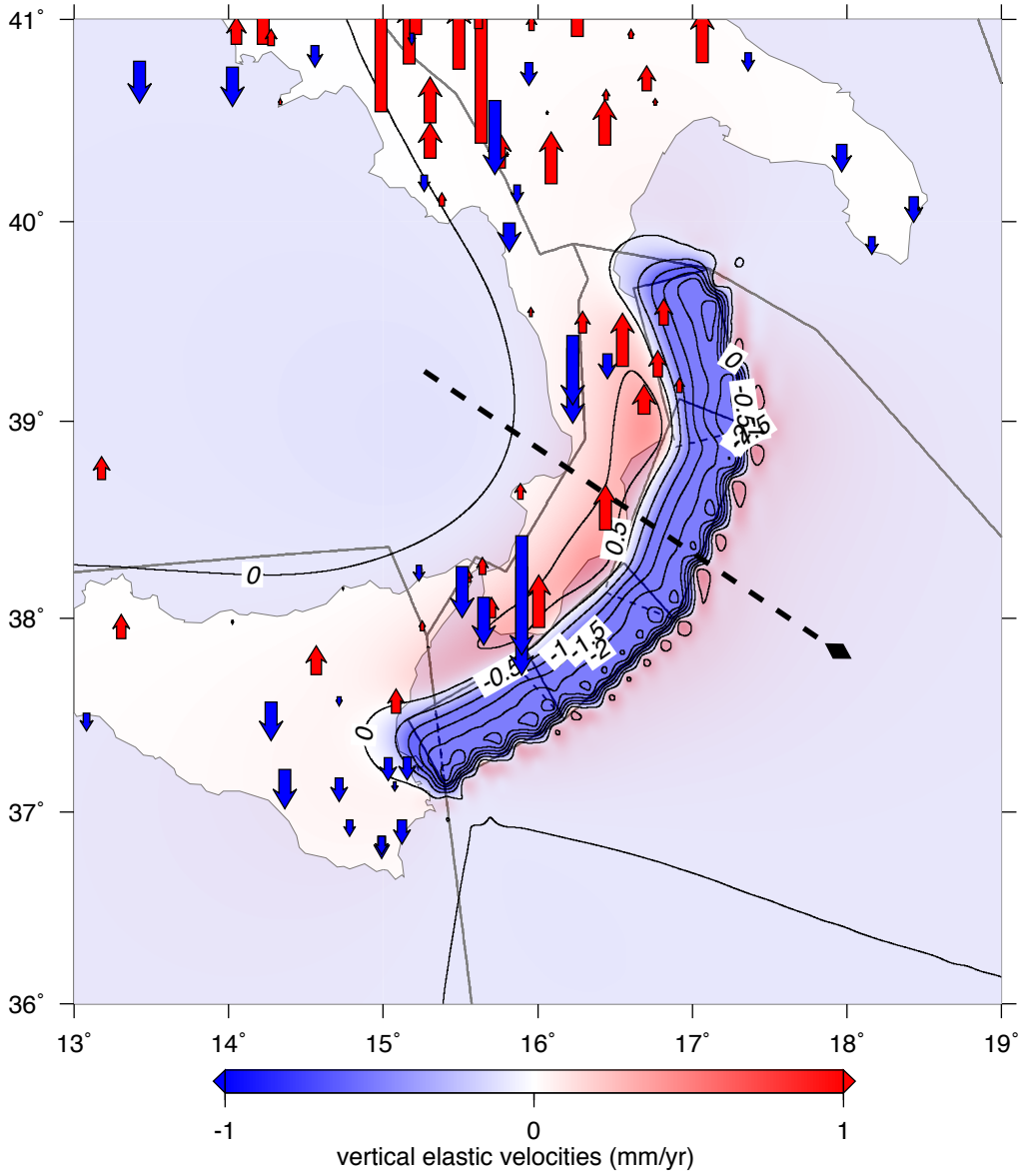

Figure 6.8: *Modeled (contoured) and observed (arrows) GPS vertical velocities. Modeled velocities are generated from a subduction interface parametrized by four* 30° *dipping and 25 km locked segments. Blue: subsidence, red: uplift. Also indicated is the profile along which we project the model vertical velocity field shown in fig. 6.7, Diamond indicate the starting point.*

Conclusions

We use data from about 700 permanent and non-permanent GPS stations lying in the EuroMediterranen region to perform local scale studies about the strain accumulation on active structures (the Messina Straits and Crati Valley faults) and to investigate the present-day behavior of the the Calabrian subduction within the central Mediterranean-scale plates kinematics.

While a general consensus has been reached about the Mediterranean geodynamic evolution dominated by the eastward migration of the Appennine-Calabrian subduction zone (*Malinverno & Ryan*, 1986; *Faccenna et al.*, 2004; *Gvirtzman & Nur*, 2001) debate is still open about the present-day kinematics of the plates and microplates lying in the region. Coexistence of lithospheric blocks with different structural and kinematic features and characterized by different geodynamic processes, including subduction, backarc spreading, rifting, thrusting, normal and strike-slip faulting combined with typical microplates mean velocities lower than 5 mm/yr made the general understanding of the central Mediterranean kinematics, a challenging problem.

Seismological, geological and GPS data (e.g. *Pondrelli et al.*, 2004; *Vannucci et al.*, 2004; *Serpelloni et al.*, 2007) clearly depict the Sicily-Calabrian Arc region as a key area to understand where the Nubia-Eurasia convergence is now accomodated.

In particular, debate is still open about the current behavior of the Calabrian Subduction zone. Although GPS data seem to suggest that the subduction process is stopped (*Serpelloni et al.*, 2007) big uncertainties still remain about the coupling degree of the Ionian lithosphere. The lack of instrumentally recorded thrust earthquakes suggests the presence of a fault plane locked portion (*Gutscher et al.*, 2006). However, depending on the stress conditions, subduction zones, can vary to being fully coupled to almost enterely decoupled with important conseguences in the seismic hazard assignement. Stress conditions on a fault plane are a balance between geological conditions (water content, pore pressure, material properties) and lithostatic load (*Scholz*, 1998). It is evident that knowing the boundary kinematic conditions within which to frame the study of a subduction zone is one of the main keys.

The study region also hosts a big number of active faults that were the locus of some of the strongest earthquakes that struck the Italian Pensinsula in the last centuries (e.g. M_w 7.1 December 28, 1908 Messina-Reggio Calabria, maximum M_w 7 1783 Calabrian seismic sequence, M_w $\sim$7 27 March and 9 June, 1638 Catanzaro events). We focused our study on the Messina Straits and Crati Valley faults, two structures that are probably accumulating strain during the interseismic phase. GPS data show, infact, horizontal velocity gradients accros both these structures with $\sim$3 mm/yr of NW-SE extension and $\sim$2 mm/yr of about E-W extension accommodated across the Messina Straits and the Crati Valley, respectively.

We first perform a local scale study trying to explain the observed velocity gra-

dients as due to single faults accumulating strain. We use a non-linear constrained optimization algorithm to invert for the fault locking depth, dip, upper-edge location and slip-rate, constraining the fault strike to be normal to the estimated extensional deformation. We find that the observed velocity gradient across the Messina Straits can be explained by a single $30.1^{-0.7^\circ}_{+1.1}$ SE-dipping normal fault, locked at $7.6^{-2.9}_{+4.6}$ depth, and a dip-slip-rate of $-3.5^{-1.3}_{+2.0}$ mm/yr and a right-lateral slip-rate of $1.6^{-0.2}_{+0.3}$ mm/yr. While the observed velocities across the Crati Valley seem to be well modeled by a $60.1^{-3.1^\circ}_{+2.1}$ W-dipping normal fault, locked at $6.1^{-4.3}_{+4.8}$ depth, and an extentional dip-slip-rate of $3.8^{-1.6}_{+2.0}$ mm/yr and a right-lateral slip-rate of $0.3^{-0.2}_{+0.3}$ mm/yr. Uncertainties associated with the modeled fault plane geometry and slip-rates have been evaluated adopting a bootstrap approach.

In order to frame the observed local deformation features within the present-day microplate kinematics, we use an elastic block-modeling approach that, taking into account both crustal blocks rotations and elastic strains at block-bounding faults, allows to investigate the impact of elastic strain contributes from other nearby active faults onto the velocity gradient measured across the Messina Straits and Crati Basin. We develop a block geometry allowing the Tyrrhenian, Sicily and NE-Sicily, Calabria, and Apulia blocks to move independently, or partially independently, with respect to a fixed Ionian block that is moving either with the Nubian or Apulian plate. Using Nubia-fixed or Apulia-fixed velocities allows us to account for both end-members kinematics along the Sicily-Calabria plate boundary (e.g., *D'Agostino et al.*, 2008; *Serpelloni et al.*, 2007).

Both models match the horizontal velocity data quite well and suggest that the elastic contribution of the Tindari-Giardini fault system and the western Calabria normal fault system on the inverted slip-rates of the Messina Straits and Crati Valley faults, is minimal or negligible. In contrast, both models predict elastic strain accumulation on the subduction interface, offshore Calabria, and show that the inferred slip-rates on the two analyzed structures are strongly impacted by the assumed locking width of the Calabrian subduction thrust, increasing the uncertainties of fault slip-rates estimated from geodetic data.

In the light of a new and denser GPS velocity field we investigate the central Mediterranean microplates kinematics. On the basis of the focal mechanismis and seismological, geodetical and geological, and with reference to the DISS database, we draw five microplate models.

All the tested models assume as independent blocks the Eurasian, Nubian, Aegean, Epiro, Dinarides, Austria, Western and Eastern Alps, Northern Appenines and Tyrrhenian plates. The Nubian block is drawn by tracing the plate boundaries from *Bird et al.*, (2003) while the Eurasian block just performs the motion of the stable Eurasian plate. All the boundaries of this two main plates are assumed to be vertical and locked above 15 km. The central Mediterranean plate boundaries are parameterized by using dip and locking depth values from the DISS. The only exception is the Aegean region that has been modeled as in *Apel et al.*, (in preparation).

All proposed models were compared in order of complexity by using the χ^2 and

F-ratio statistics (*Gordon et al.*, 1987). According with the conclusions of many recent works (e.g., *Serpelloni et al.*, 2007), we argue that the most likely model, with $\chi^2_\nu = 4.35$, is a 19-blocks model that assumes independent motion for: the Adriadic Sea separate into two microplates along the Gargano-Dubrovnik lineament and the Calabrian block. Our preferred model also predicts a microplate like behaviour of the Sicilian block.

Within these kinematic boundary conditions we further investigate the Calabrian Slab interface geometry using a combined approach of block modeling and χ^2_ν statistic. We shape the central Mediterranean microplates as in our inferred optimal kinematic model and then simplify it assuming no locking (i.e. no elastic strain contribution) for all the block bounding faults except the one under study.

As the observed velocities around active structures are related to a combinations of dip, locking depth and slip-rates on the fault plane we realize suites of inversions estimating the model χ^2_ν while simultaneously varying dip and locking depth between realistic values. Before apply the described approach to the Slab interface we test it on some simpler active structures lying in the Italian Peninsula: the Mattinata, Irpinia, Friuli and Southern Tyrrhenian Fault systems. Since the model χ^2 is not impacted, or just slightly, by variation of geometric parameters of such small structures, we compute a local reduced χ^2_ν using the residual velocities only from the GPS stations lying close to the investigated fault. We select the stations to use on the basis of the predicted horizontal velocity field. Even if our tests turned out to be not able to clearly indicate optimal dip and locking depth values, leaving undeterminated one of two parameters, however, our results at a first approximation ever rather agree with the avaible information about the study structures.

Almost no information is obtained by applying the same approach to the Slab interface. We argue that the particular geography of the structure, offshore the eastern coast of Calabria, the few GPS stations in Calabria and the lack of stations in the Ionian Sea make the modeling of this structure hard to realize. Moreover, our (no) results lead us to conclude that the horizontal velocities alone are not sufficient to constrain the geometry of such a subduction zone when using a multiparametric inversion approach and that more data are needed.

GPS vertical velocity field in the Calabria region shows that, except some areas of local subsidence related to the presence of active faults, uplift is the dominanting trend in the region. Maximum rates of about 1 mm/yr are observed along the eastern coast. Velocities decreas westward to reach minimum values of a few tenths of a millimeter along the eastern coast. Such a pattern rather agrees with the characteristic vertical velocity profile generated by a partially locked trhust fault plane (e.g., *Kanda & Simons*, 2010, *Savage*, 1983). Convergence along a locked subduction zone, infact, produces a very predictable deformation signal in the upper crust that we further explore by realizing forward models of elastic dislocations.

Parametrizing the Calabrian Slab interface with four 30°NW dipping segments, and assuming an homogeneous slip-rate of 5.5 mm/yr (Calabrian-Ionian convergence-rate) we perform four forward model of elastic dislocations to estimate the predicted vertical velocity fields for variable locking depths between 10 and 40 km.

Comparison with the observed field suggest a maximum resolved locking depth of 25 km. The region of correspondent maximum uplift extends along the eastern coast of the Calabria region. Modeled velocities decrease westward matching the observed field rather well. If we neglect the areas of local subsidence, we can say that to a first approximation, the observed velocity field is in good agreement with the presence of a subduction plane 30°NW dipping and locked at 25 km depth.

Evaluating the present-day Sicily and Calabrian Arc region kinematics and understanding which active structures are accumulating strain during the interseismic phase are certainly fundamental tasks for estimating the seismic hazard of this area. However, the particular geography of the region (i.e. the distribution of land and seas), the few GPS stations in Calabria and the lack of stations in the Ionian Sea, leave some uncertainties. In particular, the kinematics of the Ionian basin is a key information missing to define the kinematics of the Ionian-Calabria-Tyrrhenian subduction system, since the absence of GPS stations (no islands are present here) and the few focal solutions in the Calabrian wedge do not provide a well defined pattern of deformation.

The analysis carried out so far suggest us that new constrains are needed and that the horizontal GPS velocities alone are not able to figure out the complexity of this region. Since convergence along a locked subduction zone, produces a typical vertical displacement in the upper crust, inserting the vertical velocities in our models is certainly a major constraint which should be taken into consideration in future works.

Appendix A

A non-linear optmization algorithm and a confidence interval estimation

A nonlinear optimization algorithm is used in this work to seek a set of nine fault parameters (fault length, width, depth, dip, strike, location, strike slip and dip slip) that minimizes the weighted residual sum of squares (RSS), $\Phi(\xi) = \mathbf{r}^T \sum^{-1} \mathbf{r}$. Here $\mathbf{r}$ is the residual vector, the difference between the oserved an predicted data, and $\sum$ is the data covariance matrix. This problem is nonlinear since the predicted surface displacements are nonlinear functions of the fault geometry.

We use a quasi-Newton method wich is effective when the first and second derivatives of the function $\Phi(\xi)$ are not simply computed analitically. Quasi-Newton methods require only that $\Phi(\xi)$ be at least twice continuosly differentiable. In the quasi-Newton method, as in Newton's method, a quadratic model of the objective function $\Phi(\xi)$ is constructed by taking the first three terms of Taylor series expansion about a point ξ_k:

$$\Phi_{k+1} \approx \Phi_k + \nabla\Phi_k^T \delta\xi_k + \frac{1}{2}\delta\xi_k^T H_k \delta\xi_k \tag{A.1}$$

where $\Phi_k = \Phi(\xi_k)$, $\nabla\Phi_k = \nabla\Phi(\xi_k)$ is the gradient of Φ, $H_k = H(\xi_k)$ is the Hessian of Φ, and $\delta\xi_k = \xi_{k+1} - \xi_k$. Since Φ is a stationary point at the minimum of equation A.1,

$$\frac{\partial\Phi_{k+1}}{\partial\delta\xi_k} = 0 \tag{A.2}$$

Hence the quadratic function is minimized as a function of $\delta\xi_k$ by solving Newton's equation

$$H_k \delta\xi_k = -\nabla\Phi_l \tag{A.3}$$

The curvature of Φ along $\delta\xi$ is given by $\delta\xi^T H_k \delta\xi$, which can be approximated using only first-order information:

$$\delta\xi^T H_k \delta\xi \approx (\nabla\Phi_{k+1} - \nabla\Phi_k)^T \delta\xi \tag{A.4}$$

We compute $\nabla\Phi(\xi)$ numerically using a finite difference approximation. The algorithm works in the following manner: the values of $\Phi(\xi_0)$ and $\nabla\Phi(\xi_0)$ are calculated for a given starting value ξ_0. The next value, ξ_1, is calculated from $\xi_1 = \xi_0 + \delta\xi$,

where $\delta\xi$ is a solution to equation A.3, given $\nabla\Phi(\xi_0)$ and $H(\xi_0)$. The initial value of the Hessian is assumed to be the identity matrix, $H(\xi_0) = I$. After ξ_1 has been computed, a new Hessian approximation $H(\xi_1)$ is estimated by $H(\xi_1) = H(\xi_0) + U_0$ where U_0 is an updating matrix, wich takes into account the new curvature information. The updated Hessian must be symmetric and positive define. Then the next step is calculated. This sequence is repeated until the solution converges to a minimum, that is, until we find $\hat{\xi}$ such that $\Phi(\hat{\xi}) < \Phi(\xi)$ for all $\hat{\xi} \neq \xi$.

This method allows one to specify upper and lower bounds, as well as linear and nonlinear constraints on the variables. For an unconstrained problem the following conditions are necessary at the minimun: (1) the gradient at the minimun is zero ($\nabla\Phi(\hat{\xi}) = 0$) and (2) $H(\hat{\xi})$ is positive define, that is, $s^T H(\hat{\xi}) s > 0$ for all nonzero vectors s. In the case of a constrained problem, condition 1 and 2 hold for all parameters not subject to a constraint. If a parameter is at a bound, the condition for a minimum is that the gradient is directed away from the bound, i.e., that the gradient is positive at a lower bound and negative at an upper bound.

A.1 Confidence intervals estimation: bootstrap method

To asses how well the model is constrained by the data, it is important to estimate confidence intervals for the model parameters. This is not a straightforward procedure when the model is a nonlinear function of the data. We do that using the bootstrap method.

The bootstrap is a procedure that involves choosing random samples with replacement from a data set and analyzing each sample the same way. Sampling with replacement means that every sample is returned to the data set after sampling. So a particular data point from the original data set could appear multiple times in a given bootstrap sample.

The number of elements in each bootstrap sample equals the number of elements in the original data set. A new dataset $d_1^*, \ldots, d_n^*$ is drawn, randomly, from the original one $d_1, \ldots, d_n$. Then the model parameters $\hat{\xi^*}$ are estimated from the resampled data using the quasi-Newton algorithm. The resampling and estimation steps are repeated B times yelding B indipendent estimates of the model parameters. The parameter estimates are then ordered such that $\hat{\xi^*}_{[1]} \leq \ldots \leq \hat{\xi^*}_{[B]}$. The two sided $100\times(1-\alpha)\%$ bootstrap percentile method interval for ξ is $[\hat{\xi^*}_{([\frac{\alpha}{2}B]+1)}, \hat{\xi^*}_{([(1-\frac{\alpha}{2})B]+1)}]$ where $[\frac{\alpha}{2}B]$ denotes the integer part of $\frac{\alpha}{2}B$. The bootstrap is based on the premise that the distribution of $\hat{\xi^*}$ is similar to the unknown distribution of $\hat{\xi}$.

I realized a tool on a MatLab platform to estimate the individual confidence intervals associated with the inverted model parameters of the Messina Straits and Crati Valley Faults. The scripts realizes 5000 random bootstrap resamples of the original dataset (GPS velocities), reestimating, for every resempled dataset, the fault geomeric parameters using the optimization algorithm. Mean parameters values and 95% confidence intervals are computed using the bootstrap percentile method.

The advantage of the bootstrap method is that it does not make assumption

about the error distibution in the data. Rather, the true distribution is build up from the data by resampling. The disadvantage is that it is computazionally intensive and the confidence intervals are only approximated.

References

- Allmendinger, R. W., Loveless, J. P., Pritchard, M. E., and Meade, B., (2009): From decades to epochs: Spanning the gap between geodesy and structural geology of active mountain belts: Journal of Structural Geology, v. 31, p. 1409-1422, doi: 10.1016/j.jsg.2009.08.008.

- Altamimi, Z., Collilieux, X., Legrand, J., Garayt, B., Boucher, C., (2007): ITRF2005: a new release of the International Terrestrial Reference Frame based on time series of station positions and earth orientation parameters. J. Geophys. Res. 112, B09401. doi:10.1029/2007JB004949.

- A. Amoruso, L. Crescentini, and R. Scarpa (2002): Source parameters of the 1908 Messina Straits, Italy, earthquake from geodetic and seismic data. J. Geoph. Res., 107(B4):1-11.

- Apel E., R. Burgmann, E. Serpelloni, *in preparation* Rigid Block Motion, Interseismic Strain, and Seismic Coupling along the Hellenic Subduction Zone.

- Argnani, A. (1990): The Strait of Sicily rift zone: Foreland deformation related to the evolution of a back-arc basin, J. Geodyn., 12, 311-331.

- Argnani, A. & L. Torelli (2001): The Pelagian shelf and its graben system, in PeriTethys Memoir 6: Rift/Wrench Basins and Passive Margins, Mem. Mus. Hist. Nat., 186, 529-544.

- Argnani, A., Serpelloni, E., Bonazzi, C., (2007): Pattern of deformation around the central Aeolian Islands: evidence from multichannel seismics and GPS data. Terra Nova 19, 317-323.Argus, D.F., Gordon, R.G., Demets, C., Stein, S., 1989. Closure of the Africa Eurasia North America Plate motion circuit and tectonics of the Gloria Fault. J. Geophys. Res. 94, 5585-5602.

- Argnani, A., (2009): Evolution of the southern Tyrrhenian slab tear and active tectonics along the western edge of the Tyrrhenian subducted slab. Geol. Soc., London, Spec. Publ. 311, 193-212.

- Arnadottir, T., Segall, P., (1994): The 1989 Loma-Prieta earthquake imaged from inversion of geodetic data. J. Geophys. Res. 99, 21835-21855.

- Battaglia, M., M. Murray, E. Serpelloni and R. Burgmann (2004): The Adriatic region: an independent microplate within the Africa-Eurasia collision zone, Geophys. Res. Lett., 31, L09605, doi:10.1029/2004GL019723.

- Basili, R., Valensise, G., Vannoli, P., Burrato, P., Fracassi, U., Mariano, S., Tiberti, M., Boschi, E., (2008): The Database of Individual Seismogenic Sources (DISS), version 3: summarizing 20 years of research on Italy's earthquake geology. Tectonophysics 453, 20-43.

- Bettinelli, P., Avouac, J. P., Flouzat, M., Jouanne, F., Bollinger, L., Willis, P., & Chitrakar, G. R., (2006): Plate motion of india and interseismic strain in the nepal himalaya from gps and doris measurements, Journal of Geodesy, 80(8-11), 567-589.

- Bergeot, N., M. N. Bouin, M. Diament, B. Pelletier, M. Regnier, S. Calmant, and V. Ballu (2009): Horizontal and vertical interseismic velocity fields in the Vanuatu subduction zone from GPS measurements: Evidence for a central Vanuatu locked zone, J. Geophys. Res., 114, B06405, doi:10.1029/2007JB005249.

- Billi, A., Barberi, G., Faccenna, C., Neri, G., Pepe, F., Sulli, A., (2006): Tectonics and seismicity of the Tindari Fault System, southern Italy: crustal deformations at the transition between ongoing contractional and extensional domains located above the edge of a subducting slab. Tectonics 25 (TC2006). doi:10.1029/2004TC001763.

- Billi, A., R. Gambini, C. Nicolai and F. Storti (2007): Neogene-Quaternary intraforeland transpression along a Mesozoic platform-basin margin: the Gargano fault system, Adria, Italy. Geosphere, 3(1), 1-15, 10.1130/GES00057.1.

- Bird, P. (2003): An updated digital model of plate boundaries, Geochemistry Geophysics Geosystems, 4(3), 1027, doi:10.1029/2001GC000252/

- Bonforte, A., Puglisi, G., (2006): Dynamics of the eastern flank of Mt. Etna volcano (Italy) investigated by a dense GPS network. J. Volcanol. Geoth. Res. 153 (3-4), 357-369.

- Bordoni, P. & Valensise, G., (1998): Deformation of the 125 ka marine terrace in Italy: tectonic implications, in Coastal Tectonics, Geol. Soc. London Spec. Publ., Vol.146, pp.71-110, Stewart, I.S. & Vita Finzi, C., Geological Society, London.

- Boschi E, Guidoboni E, Ferrari G, Valensise G, Gasperini P. Catalogo dei forti terremoti in Italia dal 461 a.C. al 1990-Versione 2. ING e SGA, Bologna, 1997 [in Italian].

- Burgmann, R., Segall, P., Lisowski, M., Svarc, J., (1997): Postseismic strain following the 1989 Loma Prieta earthquake from GPS and leveling measurements. J. Geophys. Res. 102, 4933-4955.

- Burgmann, R., M. G. Kogan, G. M. Steblov, G. Hilley, V. E. Levin, and E. Apel (2005): Interseismic coupling and asperity distribution along the Kamchatka subduction zone, J. Geophys. Res., 110, B07405, doi:10.1029/2005JB003648.

- Calais E., Nocquet J. M., Jouanne F. e Tardy M., (2002): Current strain regime in the Western Alps from continuous Global Positioning System measurements, 1996-2001. Geology, 30 (7), 651-654.

- Calais, E., M. Vergnolle, V. San'kov, A. Luknev, A. Miroshnitchenko, S. Amarjargal, and J. De verche re, (2003): GPS measurements of crustal deformation in the Baikal-Mongolia area (1994-2002): Implications for current kinematics of Asia, J. Geophys. Res., 108, doi:10.1029/2002JB002373.

- Cernobori, L., A. Hirn, J. H. McBride, R. Nicolich, L. Petronio, M. Romanelli, and Streamers/Profiles Working Groups (1996): Crustal image of the Ionian basin and its Calabrian margins, Tectonophysics, 264, 175-189, doi:10.1016/S0040-1951(96)00125-4.

- Channell, J.E.T., & Horvath, F., (1976) The African-Adriatic promontory as a paleogeographical premise for Alpine orogeny and plate movements in the Carpatho-Balkan region: Tectonophysics, v. 35, p. 71-110.

- Chiarabba, C., Jovane, L., DiStefano, R., (2005): A new view of Italian seismicity using 20 years of instrumental recordings. Tectonophysics 395, 251-268.

- Chiarabba, C., P. De Gori, and F. Speranza (2008): The southern Tyrrhenian subduction zone: Deep geome- try, magmatism and Plio-Pleistocene evolution, Earth Planet. Sci. Lett., 268, 408-423, doi:10.1016/j.epsl.2008.01.036.

- Cifelli, F., M. Mattei, and F. Rossetti (2007): Tectonic evolution of arcuate mountain belts on top of a retreating subduction slab: The example of the Calabrian Arc, J. Geophys. Res., 112, B09101, doi:10.1029/2006JB004848.

- Ching, K.-E., R.-J. Rau, K. M. Johnson, J.-C. Lee, and J.-C. Hu (2011): Present-day kinematics of active mountain building in Taiwan from GPS observations during 1995-2005, J. Geophys. Res., 116, B09405, doi:10.1029/2010JB008058.

- D'Agostino, N. & Selvaggi, G. (2004): Crustal motion along the Eurasia-Nubia plate boundary in the Calabrian Arc and Sicily and active extension in the Messina Straits from GPS measurements, J. Geophys. Res., 109, B11 402, doi:10.1029/2004JB002998.

- D'Agostino, N., Avallone, A., Cheloni, D., D'Anastasio, E., Mantenuto, S., Selvaggi, G., (2008). Active tectonics of the Adriatic region from GPS and earthquake slip vectors. J. Geophys. Res. 113, B12413. doi:10.1029/2008JB005860.

- D'Agostino, N., E. D'Anastasio, A. Gervasi, I. Guerra, M. R. Nedimovic, L. Seeber, and M. Steckler (2011): Forearc extension and slow rollback of the Calabrian Arc from GPS measurements, Geophys. Res. Lett., 38, L17304, doi:10.1029/2011GL048270.

- DeMets, C., Gordon, R. G., Argus, D. F. and Stein, S. (1994): Effect of recent revisions to the geomagnetic reversal time scale on estimates of current plate motions, Geophys. Res. Lett., 21, 2191-2194.

- DeMets, C., Gordon, R. G., & Argus, D. F., (2010): Geologically current plate motions, Geophysical Journal International, 181, 1,80.

- Devoti, R., F. Riguzzi, M. Cuffaro, and C. Doglioni (2008): New GPS constraints on the kinematics of the Apennines subduction, Earth Planet. Sci. Lett., 273, 163-174, doi:10.1016/j.epsl.2008.06.031.

- Dewey, J. F., M. L. Helman, E. Turco, D. H. W. Hutton, and S. D. Knott (1989): Kinematics of the western Mediterranean, in Alpine Tectonics, edited by M. P. Coward, D. Dietrich, and R. G. Park, Geol. Soc. Spec. Publ., 45, 265-283.

- Di Bucci, D., A. Ravaglia, S. Seno, G. Toscani, U. Fracassi and G. Valensise (2006): Seismotectonics of the Southern Apennines and Adriatic foreland: Insights on active regional E-W shear zones from analogue modeling. Tectonics, 25, TC4015, 10.1029/2005TC001898.

- Dixon, T.H., Miller, M., Farina, F., Wang, H.Z., Johnson, D., (2000): Present-day motion of the Sierra Nevada block and some tectonic implications for the Basin and Range province, North American Cordillera. Tectonics 19, 1-24.

- Doglioni, C., E. Carminati, and M. Cuffaro (2006): Simple kinematics of subduction zones, Int. Geol. Rev., 48, 479-493, doi:10.2747/0020-6814.48.6.479.

- Doglioni, C., E. Carminati, M. Cuffaro, and D. Scrocca (2007): Subduction kinematics and dynamic constraints, Earth Sci. Rev., 83, 125-175, doi:10.1016/j.earscirev.2007.04.001.

- Dong, D., Herring, T.A., King, R.W., (1998): Estimating regional deformation from a combination of space and terrestrial geodetic data. J. Geodesy. 72, 200-214.

- Dong, D., Fang, P., Bock, Y., Cheng, M.K., Miyazaki, S., (2002): Anatomy of apparent seasonal variations from GPS-derived site psosition time series. J. Geophys. Res. 107 (B4), 2075. doi:10.1029/2001JB000573.

- Faccenna, C., T. W. Becker, F. P. Lucente, L. Jolivet, and F. Rossetti (2001b): History of subduction and back-arc extension in the central Mediterranean, Geophys. J. Int., 145, 809-820.

- Faccenna, C., Piromallo, C., Crespo-Blanc, A., Jolivet, L. and Rossetti, F. (2004): Lateral slab deformation and the origin of the western Mediterranean arcs, Tectonics, 23, TC1012, doi:10.1029/2002TC001488.

- Faccenna, C., L. Civetta, M. D'Antonio, F. Funiciello, L. Margheriti, and C. Piromallo (2005): Constraints on mantle circulation around the deforming Calabrian slab, Geophys. Res. Lett., 32, L06311, doi:10.1029/2004GL021874.

- Ferranti, L., Monaco, C., Antonioli, F., Maschio, L., Kershaw, S., Verrubbi, V., (2007): The contribution of regional uplift and coseismic slip to the vertical crustal motion in the Messina Straits, southern Italy: evidence from raised Late Holocene shorelines. J. Geophys. Res. 112, B06401. doi:10.1029/2006JB004473.

- Floyd, M. A., et al. (2010): A new velocity field for Greece: Implications for the kinematics and dynamics of the Aegean, J. Geophys. Res., 115, B10403, doi:10.1029/2009JB007040.

- Galadini, F., M. E. Poli and A. Zanferrari (2005): Seismogenic sources potentially responsible for earthquakes with M >=6 in the eastern Southern Alps (Thiene-Udine sector, NE Italy). Geophys. J. Int., 161, 739-762.

- Gahalaut, V.K. & Chander, R., (1997): On interseismic elevation changes for great thrust earthquakes in the Nepal Himalaya, Geophys. Res. Lett., 24, 1011-1014.

- Gahalaut, V.K. & Chander, R., (1999): On interseismic elevation changes observed near 75.5uE longitude in the NW Himalaya, Bull. seism. Soc. Am., 89, 837-843.

- Galli, P., and V. Bosi, (2004): Catastrophic 1638 earthquakes in Calabria (southern Italy): New insights from paleoseismological investigation, J. Geophys. Res., 108(B1) doi:10.1029/2001JB001713, 2003.

- Ghisetti F., (1992): Fault parameters in the Messina Strait (southern Italy) and relations with the seismogenic source. Tectonophysics, 210:117-133.

- Goes, S., Giardini, D., Jenny, S., Hollenstein, C., Khale, H. G. & Geiger, A., (2004): A recent tectonic reorganization in the south-central Mediterranean, Earth. Planet. Scie. Lett., 226, 335-345.

- Gordon, R. G., S. Stein, C. DeMets, and D. F. Argus (1987): Statistical tests for closure of plate motion circuits, Geophys. Res. Lett., 14, 587-590.

- Guidoboni, E., G. Ferrari, D. Mariotti, A. Comastri, G. Tarabusi and G. Valensise (2007): CFTI4Med, Catalogue of Strong Earthquakes in Italy (461 B.C.-1997) and Mediterranean Area (760 B.C.-1500). INGV-SGA. Available from http://storing.ingv.it/cfti4med/.

- Gutscher, M. A., Roger, J., Baptista, M. A., Miranda, J. M. & Tinti, S., (2006): Source of the 1693 Catania earthquake and tsunami (southern Italy): new evidence from tsunami modeling of a locked subduction fault plane, Geophys. Res. Lett., 33, L08 309, doi:10.1029/2005GL025442.

- Gvirtzman, Z., and Nur A., (2001): Residual topography, lithospheric structure and sunken slabs in the central Mediterranean. Earth Planet. Scie. Lett., 187, 117-130.

- Herring, T., King, R.W., McClusky, S., (2006): GAMIT Reference Manual, Release 10.3, Department of Earth, Atmospheric, and Planetary Sciences. Massachussetts Institute of Technology.

- Hollenstein, C., Kahle, H.G., Geiger, A., Jenny, S., Goes, S., Giardini, D., (2003): New GPS constraints on the Africa-Eurasia plate boundary zone in southern Italy. Geophys. Res. Lett. 30 (18), 1935. doi:10.1029/2003GL017554.

- Hollenstein, C., M. D. Muller, A. Geiger, and H. G. Kahle (2008): Crustal motion and deformation in Greece from a decade of GPS measurements, 1993-2003, Tectonophysics, 449(1-4), 17-40, doi:10.1016/j.tecto. 2007.12.006.

- Jackson, M. & Bilham, R., 1994. Constraints on Himalaya deformation inferred from vertical velocity fields in Nepal and Tibet, J. geophys. Res., 99, 13 897-13 912.

- Jacques, E., C. Monaco, P. Tapponnier, L. Tortorici, and T. Winter (2001): Faulting and earthquake trigering during the 1783 Calabria seismic sequence, Geophys. J. Int., 147, 499-516.

- Jolivet, L., and C. Faccenna (2000): Mediterranean extension and the Africa-Eurasia collision, Tectonics, 19(6), 1095-1106.

- Kanda, R. V. S., and M. Simons (2010): An elastic plate model for interseismic deformation in subduction zones, J. Geophys. Res., 115, B03405, doi:10.1029/2009JB006611.

- Langbein, J., Johnson, H., (1997): Correlated errors in geodetic time series: implications for time-dependent deformation. J. Geophys. Res. 102, 591-603.

- Larson, K., Burgmann, R., Bilham, R. & Freymueller, J.T., (1999): Kinematics of the India-Eurasia collision zone from GPS measurements, J. geophys. Res., 104, 1077-1093.

- Lundgren, P., Casu, F., Manzo, M., Pepe, A., Berardino, P., Sansosti, E., Lanari, R., (2004): Gravity and magma induced spreading of Mount Etna volcano revealed by satellite radar interferometry. Geophys. Res. Lett. 31 (4). doi:10.1029/2003GL018736.

- Malinverno, A. & Ryan, W. B. F., (1986): Extension in the Tyrrhenian Sea and shortening in the Apennines as result of arc migration driven by sinking in the lithosphere, Tectonics, 5, 227-245.

- Mantovani, E., D. Babbucci, D. Arbarello, and M. Mucciarelli (1990): Deformation pattern in the central Mediterranean and behavior of the African/Adriatic promontory, Tectonophysics, 179, 63-79.

- Mao, A., Harrison, C.G.A. and Dixon, T.H. (1999): Noise in GPS coordinate time series, J. Geophys. Res., 104, 2797-2816.

- Mattei, M., F. Cifelli, and N. D'Agostino (2007): The evolution of the Calabrian Arc: Evidence from paleo-magnetic and GPS observations, Earth Planet. Sci. Lett., 263, 259-274, doi:10.1016/j. epsl.2007.08.034.

- Mattia, M., Palano, M., Bruno, V., Cannavó, F., Bonaccorso, A., Gresta, S., (2008): Tectonic features of the Lipari-Vulcano complex (Aeolian archipelago, Italy) from 10 years (1996-2006) of GPS data. Terra Nova 20 (5), 370-377.

- Mattia, M., Palano, M., Bruno, V., Bruno, V., Cannavó, F., (2009): Crustal motion along the Calabro-Peloritano Arc as imaged by twelve years of measurements on a dense GPS network. Tectonophys 476 (3-4), 528-537.

- Mazzoli, S., and M. Helman (1994): Neogene patterns of relative plate motion of Africa-Europe: Some implications for recent central Mediterranean tectonics, Geol. Rundsch., 83, 464-468.

- McClusky, Reilinger, R., Mahmoud, S., Ben-Sari, D. & Tealeb, A. (2003): GPS constraints on Africa (Nubia) and Arabia plate motions, Geophysical Journal International 155 (1) , 126-138 .

- Meade, B.J. & Bradford Hagar, H. (2005): Block models of crustal motion in suthern California constrained by GPS measurements, J. Geopjys. Res, 110, B03403, doi:10.1029/2004JB003209.

- Meade, B. J., and J. P. Loveless (2009): Block modeling with connected fault network geometries and a linear elastic coupling estimator in spherical coordinates, Bulletin of the Seismological Society of America, 99, 3124-3139, doi:10.1785/0120090088.

- Mele, G. (2001): The Adriatic lithosphere is a promontory of the Africa Plate; Evidence of a continuous mantle lid in the Ionian Sea from efficient Sn propagation, Geophys. Res. Lett., 28, 431-434.

- Meletti, C., Galadini, F., Valensise, G., Stucchi, M., Basili, R., Barba, S., Vannucci, G., Boschi, E., (2008): A seismic source zone model for the seismic hazard assessment of the Italian territory. Tectonophysics 450, 85-108.

- Minelli, L., and C. Faccenna (2010): Evolution of the Calabrian accretionary wedge (central Mediterranean), Tectonics, 29, TC4004, doi:10.1029/ 2009TC002562.

- Molin, P., Pazzaglia, F.J., Dramis, F., (2004): Geomorphic expression of active tectonics in a rapidly deforming forearc, Sila massif, Calabria, southern Italy. American Journal of Science 304, 559-589.

- Monachesi, G., and M. Stucchi, DOM 4.1 an intensity database of damaging earthquakes in the Italian area, 1998. (Available as http://emidius.itim.mi.cnr.it/DOM/home.html).

- Monaco, C., Tortorici, L., (2000): Active faulting in the Calabrian Arc and eastern Sicily. Journal of Geodynamics 29, 407-424.

- Moretti A., (1999): Faglie attive nella Calabria Settentrionale-Progetto 5.1.2 "Inventario delle faglie attive e dei terremoti ad esse associabili" - GNDT: Aggiornamenti e contributi dalle UR-http://emidius.itim.mi.cnr.it/GNDT/P512/UR_UNICS990623.html.

- Murray, M. H., and P. Segall (2001): Modeling broad scale deformation in northern California and Nevada from plate motions and elastic strain accumulation, Geophys. Res. Lett., 28, -4318.

- Neri, G., Barberi, G., Orecchio, B., Mostaccio, A., (2003): Seismic strain and seismogenic stress regimes in the crust of the southern Tyrrhenian region. Earth Planet. Sci. Lett. 213, 97-112.

- Oldow, J. S., et al. (2002): Active fragmentation of Adria, the north Africa promontory, central Mediterranean orogen, Geology, 30, 779-782.

- Oleskevich, D., R. D. Hyndman, and K. Wang (1999): The updip and downdip limits of subduction earthquakes: Thermal and structural models of Cascadia, south Alaska, S.W. Japan, and Chile, J. Geophys. Res., 104, 14,965-14,991.

- Okada, Y., (1985): Surface deformation due to shear and tensile faults in a half-space. B. Seismol. Soc. Am. 75, 1135-1154.

- Okada, Y., (1992): Internal deformation due to shear and tensile faults in a half space, Bull. seism. Soc. Am., 82, 1018-1040.

- Pagliaroli A., Lanzo G. (2008): Selection of real accelerograms for the seismic response analysis of the historical town of Nicastro (Southern Italy) during the March 1638 Calabria earthquake. Engineering Structures, Special Issue on "Seismic reliability, analysis and protection of historic buildings and heritage sites", 30, 2211-2222. ISSN: 0141-0296. doi:10.1016/j.engstruct.2007.06.002.

- Pantosti, D., and G. Valensise (1990): Faulting Mechanism and Complexity of the November 23, 1980, Campania-Lucania Earthquake, Inferred From Surface Observations, J. Geophys. Res., 95(B10), 15,319-15,341, doi:10.1029/JB095iB10p15319.

- Patacca, E., and P. Scandone (2004): The Plio-Pleistocene thrust belt foredeep system in the southern Apennines and Sicily (Italy), in Geology of Italy: Special Volume of the Italian Geological Society for the IGC 32 Florence 2004, edited by S. Crescenti et al., pp. 93-129, Soc. Geol. It., Rome.

- Pacheco, J. F., L. R. Sykes, and C. H. Scholz (1993): Nature of seismic coupling along simple plate boundaries of the subduction type, J. Geophys. Res., 98, 14,133-14,159.

- Pepe, F., Sulli, A., Bertotti, G., Catalano, R., (2005): Structural highs formation and their relationship to sedimentary basins in the north Sicily continental margin (southern Tyrrhenian Sea): implication for the Drepano Thrust Front. Tectonophys 409, 1-18.

- Pino, N.A., Piatanesi, A., Valensise, G., Boschi, E., (2009): The 28 December 1908 Messina Straits earthquake (M(w)7.1): a great earthquake throughout a century of seismology. Seismol. Res. Lett. 80, 243-259.

- Piromallo, C., Morelli, A., (2003): P wave tomography of the mantle under the Alpine-Mediterranean area. J. Geophys. Res. 108 (B2), 2065. doi:10.1029/2002JB001757.

- Pondrelli, S., Piromallo, C. and Serpelloni, E. (2004b): Convergence vs. Retreat in Southern Tyrrhenian Sea: insights from kinematics, Geophys. Res. Lett., 31, L0661, doi:10.1029/2003GL019223.

- Pondrelli, S., S. Salimbeni, G. Ekstrm, A. Morelli, P. Gasperini, and G. Vannucci (2006): The Italian CMT data set from 1977 to the present, Phys. Earth Planet. Inter., 159, 286-303, doi:10.1016/j.pepi.2006.07.008.

- Reilinger, R., et al. (2006): GPS constraints on continental deformation in the Africa-Arabia-Eurasia continental collision zone and implications for the dynamics of plate interactions, J. Geophys. Res., 111, B05411, doi:10.1029/2005JB004051.

- Rosenau, M., and O. Oncken (2009): Fore-arc deformation controls frequency-size distribution of megathrust earthquakes in subduction zones, J. Geophys. Res., 114, B10311, doi:10.1029/2009JB006359.

- Rosenbaum, G., Lister, G.S., Duboz, C., (2002): Relative motions of Africa, Iberia and Europe during Alpine orogeny. Tectonophysics 359, 117-129.

- Rosenbaum, G., G. S. Lister, and C. Duboz (2004): The Mesozoic and Cenozoic motion of Adria (central Mediterranean): A review of constraints and limitations, Geodin. Acta, 17, 125-139.

- Rossi, S., and R. Sartori (1981): A seismic reflection study of the external Calabrian Arc in the northern Ionian Sea (eastern Mediterranean), Mar. Geophys. Res., 4, 403-426, doi:10.1007/BF00286036.

- Savage, J.C., Burford, R.O., (1970): Accumulation of tectonic strain in California. B. Seismol. Soc. Am. 60, 1877-1896.

- Savage, J.C., Burford, R.O., (1973): Geodetic determination of relative plate motion in central California. Journal of Geophysical Research 78, 832-845.

- Savage, J. C. (1983): A dislocation model of strain accumulation and release at a subduction zone, J. Geophys. Res., 88, 4984-4996, doi:10.1029/JB088iB06p04984.

- Schellart WP, Freeman J, Stegman DR, Moresi L, May D (2007): Evolution and diversity of subduction zones controlled by slab width. Nature 446: doi:10.1038/nature05615.

- Scholz, C. H. (1998): Earthquakes and friction laws, Nature, 391, 37-42.

- Sella, G., T. H. Dixon, and A. Mao (2002): REVEL: A model for recent plate velocities from space geodesy, J. Geophys. Res., 107(B4), 2081, doi:10.1029/2000JB000033.

- Selvaggi, G., and A. Amato (1992): Subcrustal earthquakes in the northern Appennines (Italy): Evidence for a still active subduction?, Geophys. Res. Lett., 19, 2127-2130.

- Selvaggi, G. & Chiarabba, C. (1995): Seismicity and P-wave velocity image of the southern Tyrrhenian subduction zone, Geophys. J. Int, 121, 818-826.

- Serpelloni, E., Anzidei, M., Baldi, P., Casula, G. and Galvani, A., (2005a): Crustal velocity and strain-rate fields in Italy and surrounding regions: new results from the analysis of permanent and non-permanent GPS networks, Geophy. J. Int., 161(3), 861-880. doi:10.1111/j.1365-246X.2005.02618.x.

- Serpelloni, E., Battaglia, M., Murray, M., Burgmann, R., Casula, G., Anzidei, M. and Baldi, P. (2005b): Block modeling of GPS velocities in Italy and surrounding regions and kinematics of the Adriatic microplate, Geophys. Res. Abs., 7, 05808.

- Serpelloni, E., Casula, G., Galvani, A., Anzidei, M., Baldi, P., (2006): Data analysis of permanent GPS networks in Italy and surrounding regions: application of a distributed processing approach. Ann. Geophys.-Italy 49, 897-928.

- Serpelloni, E., G. Vannucci, S. Pondrelli, A. Argnani, G. Casula, M. Anzidei, P. Baldi and P. Gasperini (2007): Kinematics of the Western Africa-Eurasia plate boundary from focal mechanisms and GPS data, Geophys. J. Int. doi:10.1111/j.1365-246X.2007.03367.

- Shen, Z.-K., Jackson, D.D., Kagan, Y.Y., 2007. Implications of geodetic strain rate for future earthquakes, with a five-year forecast of M5 earthquakes in Southern California. Seismol. Res. Lett. 78, 116-120.

- Simoes, M., J. P. Avouac, R. Cattin, and P. Henry (2004): The Sumatra subduction zone: A case for a locked fault zone extending into the mantle, J. Geophys. Res., 109, B10402, doi:10.1029/2003JB002958.

- Song, T. R. A., and M. Simons (2003): Large trench-parallel gravity variations predict seismogenic behavior in subduction zones, Science, 301, 630-633, doi:10.1126/science.1085557.

- Stein, S. & Gordon, R. (1984): Statistical test of additional plate boundaries from plate motion inversion. Earth Planet. Sci. Lett, 69, 401-412.

- Thatcher, W., (1995): Microplate versus continuum descriptions of active tectonic deformation. Journal of Geophysical Research 100, 3885-3894.

- Thatcher, W., (2007): Microplate model for the present-day deformation of Tibet. Journal of Geophysical Research 112, B01401. doi:10.1029/2005JB004244.

- Tichelaar, B. W., and L. J. Ruff (1993): Depth of seismic coupling along subduction zones, J. Geophys. Res., 98, 2017-2037.

- Tortorici, L., C. Monaco, C. Tansi, and O. Cocina (1995): Recent and active tectonics in the Calabrian Arc (southern Italy), Tectonophysics, 243, 37-55.

- Vergne, J., R. Cattin, and J. P. Avouac (2001): On the use of dislocations to model interseismic strain and stress build-up at intracontinental thrust faults, Geophys. J. Int., 147, 155-162, doi:10.1046/j.1365-246X. 2001.00524.x.

- Vannucci G., Pondrelli S., Argnani A., Morelli A., Gasperini P. and Boschi E. (2004): An Atlas of Mediterranean Seismicity. Annali di Geofisica, suppl. vol. 47, 247-306.

- Wells, R. E., R. J. Blakely, Y. Sugiyama, D. W. Scholl, and P. A. Dinterman (2003): Basin-centered asperities in great subduction zone earthquakes: A link between slip, subsidence, and subduction erosion?, J. Geophys. Res., 108(B10), 2507, doi:10.1029/2002JB002072.

- Westaway, R., (1993): Quaternary uplift of southern Italy, J. Geophys. Res., 97, 15 437-15 464.

- Williams, S.D.P. (2003a): The effect of coloured noise on the uncertainties of rates estimated from geodetic time series. J. Geod., 76, 483-494, doi:10.1007/s00190-002-0283-4.

- Williams, S.D.P., Bock, Y., Fang, P., Jamason, P., Nikolaidis, R.M., Prawirodirdjo, L., Miller, M., Johnson, D.J., (2004): Error analysis of continuous GPS position time series. J. Geophys. Res. 109, B03412. doi:10.1029/2003JB002741.

- Wortel, M.J.R., Spakman, W., (2000): Subduction and slab detachment in the Mediterranean-Carpathian region. Science 290 (5498), 1910-1917.

- Wortmann, U. G., H. Weissert, H. Funk, and J. Hauck (2001): Alpine plate kinematics revisited: The Adria problem, Tectonics, 20, 134-147, doi:10.1029/2000TC900029.

- Zhang, J. (1996): Continuous GPS measurements of crustal deformation in southern California, Ph.D. dissertation, Univ. of Calif., San Diego.

- Zhang, J., Y. Bock, H. Johnson, P. Fang, S. Williams, J. Genrich, S. Wdowinski and J. Behr (1997): Southern California permanent GPS Geodetic Array: Error analysis of daily position estimates and site velocities, J. Geophys. Res., 102, 18,035 - 18,055.